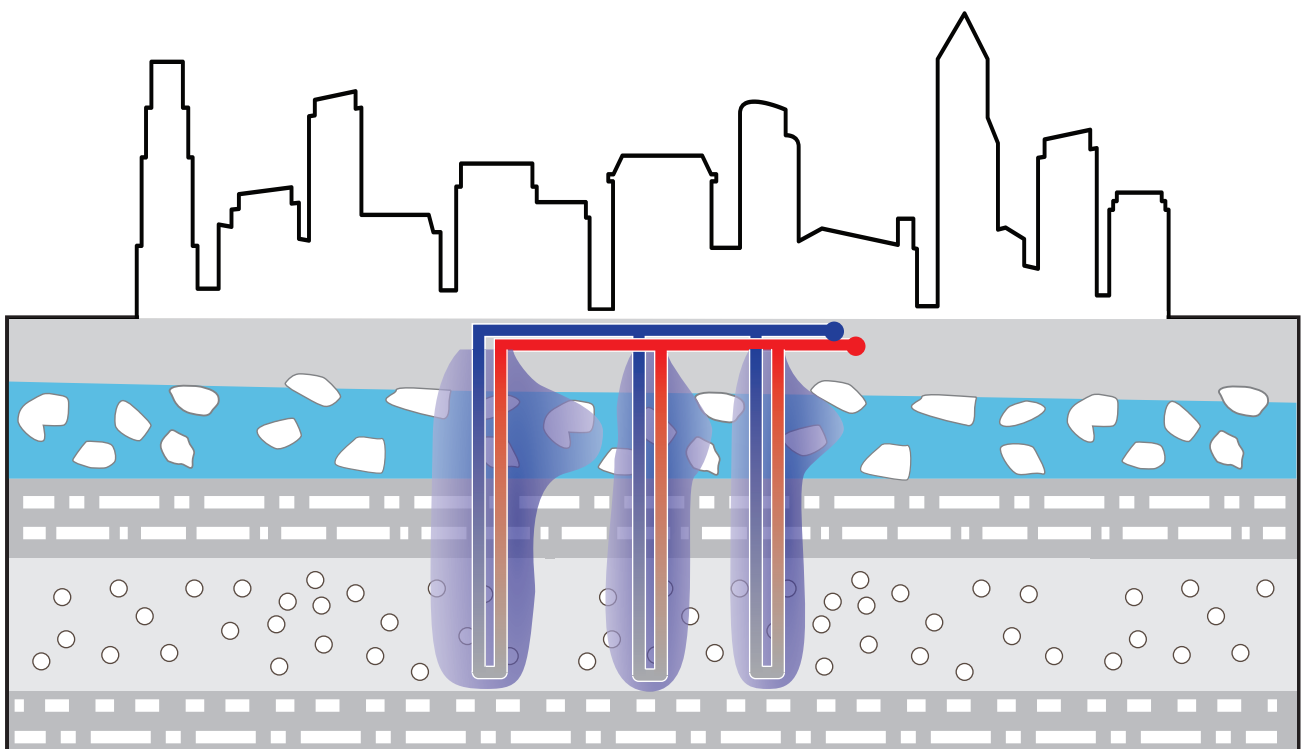




MARTIN-LUTHER-UNIVERSITÄT
HALLE-WITTENBERG

Doctoral Thesis

Towards Sustainable Shallow Geothermal Systems: Combined Simulation-Optimization of Borehole Heat Exchanger Fields under Uncertainty



Hesam SOLTAN MOHAMMADI

**Towards
Sustainable Shallow Geothermal Systems:
Combined Simulation-Optimization of
Borehole Heat Exchanger Fields under Uncertainty**

Dissertation

**zur Erlangung des
Doktorgrades der Naturwissenschaften (Dr. rer. nat)**

der
Naturwissenschaftlichen Fakultät III
Agrar- und Ernährungswissenschaften,
Geowissenschaften und Informatik
der Martin-Luther-Universität Halle-Wittenberg

vorgelegt von
Hesam Soltan Mohammadi

Tag der Verteidigung: 27. Februar 2025

Deutscher Titel:

*Hin zu einem nachhaltigen Betrieb oberflächennaher geothermischer Systeme:
Kombinierte Simulations-Optimierung von Erdwärmesondenfeldern unter Unsicherheit*

Begutachtung:

Prof. Dr. Peter Bayer

PD. Dr. Kathrin Menberg

Abstract

Borehole heat exchangers (BHEs) are a cornerstone of shallow geothermal energy systems, enabling efficient thermal exchange with the subsurface. However, in densely configured BHE fields, uncontrolled heat extraction or injection can lead to thermal imbalances in the ground, jeopardizing system performance and regulatory compliance. These issues are further compounded by uncertainty in the characterization of subsurface properties, fluctuations in predefined energy demand, imprecise description of the governing thermal processes, and failure to account for their transient behavior. As a result, flexible planning tools and more inclusive management strategies are needed to mitigate these issues in BHE fields.

To address these challenges, this doctoral dissertation introduces an integrated framework that combines simulation, optimization, and uncertainty quantification methods to enhance the thermal performance and sustainability of BHE fields throughout their operational lifetime.

The core of the presented work is the development of a flexible framework that combines simulation and optimization methods to identify optimal load balancing plans among BHEs. The development of the framework is initiated by accounting for uncertainties in temperature predictions and uncertainty in energy demand. A sequential optimization strategy that incorporates monthly temperature measurements enables adaptive load distribution among BHEs, minimizing the maximum temperature changes throughout the entire operational lifetime of the BHE field. Case studies with two different field configurations—five and 26 BHEs—demonstrate the effectiveness of this approach, achieving reductions in thermal anomalies of 2.9 K and 8.9 K, respectively, over 15 years of operation and highlighting its potential for strategic load management.

To further address uncertainties in dynamic (hydro)geological conditions, an existing semi-analytical modeling method (Moving Finite Line Source, MFLS) is modified to include transient groundwater velocity. Validated against numerical simulations under different groundwater flow fluctuation patterns and BHE configurations, the model shows a maximum mean absolute error of 0.18 K over ten years of operation. When embedded in a calibration-optimization framework, this method reduces temperature variations by 10%, illustrating the advantages of accounting for temporal variability and parameter estimation in more reliable energy management.

As the next step, this work extends the modeling of BHE systems from a deterministic to a stochastic approach. A Bayesian inference framework is introduced to improve long-term temperature predictions under complex subsurface settings, demonstrated in a case with three layers, each having distinct material properties and groundwater velocities. The proposed methodology employs an affine invariant ensemble sampler to estimate nine highly correlated

subsurface parameters and their associated uncertainties during the monitoring and operation of the BHE field. Comparison with a numerical model, along with extensive statistical analysis of the applied Markov Chain Monte Carlo-based sampler's performance, demonstrates that the proposed approach reduces prediction uncertainty by more than 90 % over a five-year simulation horizon, when temperatures are measured and assimilated for 32 months using the MFLS with anisotropy model. These advancements, through data assimilation techniques, enhance the applicability of analytical models for reliability-based planning and decision-making in BHE systems.

All the procedures developed in the presented study enable the integration of efficient analytical modeling tools, dynamic optimization, and Bayesian learning to support the long-term viability of closed-loop geothermal systems and promote dynamic planning in BHE system operations. This study offers a more robust approach that minimizes extreme thermal changes in the subsurface while flexibly addressing different sources of uncertainty. Future research should focus on implementing the developed methodology using real measurements from BHE fields in various (hydro)geological and operational settings.

Zusammenfassung

Erdwärmesonden (EWS) sind ein zentraler Bestandteil oberflächennaher geothermischer Systeme, die einen effizienten Wärmeaustausch mit dem Untergrund gewährleisten. In dicht beieinanderliegenden EWS-Feldern kann jedoch eine unkontrollierte Wärmeentnahme oder -einspeisung zu thermischen Ungleichgewichten im Boden führen, die sowohl die Systemleistung beeinträchtigen als auch die Einhaltung von Vorschriften gefährden. Diese Herausforderungen werden weiter verschärft durch Unsicherheiten in der Bestimmung der Untergrundbedingungen, Schwankungen in dem prognostizierten Energiebedarf, ungenaue Modellierungen der zugrunde liegenden thermischen Prozesse, sowie das Versäumnis, deren transienten Eigenschaften zu berücksichtigen. Infolgedessen sind flexible Planungsansätze und umfassendere Managementstrategien notwendig, um diesen Herausforderungen in EWS-Feldern zu begegnen. Aus diesem Grund wird in dieser Dissertation ein integrierter Ansatz vorgestellt, der Simulation, Optimierung und Unsicherheitsquantifizierung kombiniert, um die thermische Leistung und Nachhaltigkeit von EWS-Feldern über ihre gesamte Betriebsdauer zu verbessern.

Der Kern dieser Arbeit liegt in der Entwicklung eines flexiblen Ansatzes, der Simulation und Optimierung kombiniert, um die optimale Verteilung der Wärmeentnahme für die EWS zu ermitteln. Die Entwicklung der Methodik basiert auf der Berücksichtigung von Unsicherheiten, sowohl in den Temperaturprognosen als auch in dem zu erwartenden Energiebedarf. Eine sequenzielle Optimierungsstrategie, die monatliche Temperaturmessungen berücksichtigt, ermöglicht eine adaptive Verteilung der Wärmeentnahme zwischen den EWS und minimiert die maximalen Temperaturänderungen über die gesamte Betriebsdauer des EWS-Feldes. Fallstudien mit zwei unterschiedlichen Feldkonfigurationen – fünf und 26 EWS – belegen die Wirksamkeit dieses Ansatzes, indem sie eine Reduktion der thermischen Anomalien um 2,9 K bzw. 8,9 K über eine Betriebsdauer von 15 Jahren erzielen und somit das Potenzial für ein strategisches Wärmemanagement aufzeigen.

Um zusätzliche Unsicherheiten in transienten (hydro)geologischen Bedingungen zu berücksichtigen, wird eine bestehende semianalytische Modellierungsmethode (Moving Finite Line Source, MFLS) angepasst, um instationäre Grundwasserflussraten zu integrieren. Durch die Validierung mit numerischen Simulationen unter verschiedenen Szenarien von Grundwasserströmungsschwankungen und EWS-Konfigurationen erzielt das Modell einen mittleren absoluten Fehler von maximal 0,18 K über einen Zeitraum von zehn Betriebsjahren. Im Rahmen eines Kalibrierungs- und Optimierungsprozesses verringert die Methodik die Temperaturschwankungen um 10 % und verdeutlicht die Vorteile der Berücksichtigung zeitlicher Schwankungen sowie der präzisen Parameterschätzung für eine zuverlässigere Energiemanagementstrategie.

Im nächsten Schritt erweitert diese Arbeit die Modellierung von EWS-Systemen von einem deterministischen auf einen stochastischen Ansatz. Ein Bayessches Inferenzverfahren wird eingeführt, um langfristige Temperaturprognosen unter komplexen Untergrundbedingungen zu optimieren. Dies wird anhand eines Fallbeispiels mit drei Schichten veranschaulicht, die jeweils unterschiedliche Materialeigenschaften und Grundwasserströmungsgeschwindigkeiten aufweisen. Die vorgestellte Methode verwendet einen Affine Invariant Ensemble Sampler zur Schätzung von neun stark korrelierten Untergrundparametern und den damit verbundenen Unsicherheiten während der Überwachung und des Betriebs des EWS-Feldes. Der Vergleich mit einem numerischen Modell, sowie eine umfassende statistische Analyse der Leistung des Markov-Chain-Monte-Carlo-basierten Samplers, zeigen, dass der vorgeschlagene Ansatz die Vorhersageunsicherheit über einen fünfjährigen Simulationszeitraum um mehr als 90 % reduziert, wenn Temperaturmessungen in das Modell integriert und über 32 Monate hinweg mithilfe des MFLS mit Anisotropie Modells assimiliert werden. Durch den Einsatz von Data-assimilationstechniken erweitern diese Fortschritte die Anwendbarkeit analytischer Modelle und ermöglichen eine zuverlässigkeitsbasierte Planung sowie fundierte Entscheidungsfindung in EWS-Systemen.

Alle in dieser Studie entwickelten Methoden ermöglichen die effiziente Integration analytischer Modellierungsverfahren, dynamischer Optimierung und Bayesschen Lernens, um die langfristige Rentabilität geothermischer Systeme zu gewährleisten und die dynamische Planung des EWS-Betriebs zu unterstützen. Diese Studie bietet einen robusteren Ansatz, der extreme thermische Veränderungen im Untergrund reduziert und gleichzeitig flexibel auf unterschiedliche Unsicherheitsquellen reagiert. Zukünftige Forschungen sollten sich darauf konzentrieren, die entwickelte Methodik unter Verwendung realer Messdaten aus EWS-Feldern in unterschiedlichen (hydro)geologischen und betrieblichen Kontexten umzusetzen.

Publications

This doctoral thesis is structured as a cumulative dissertation and synthesizes the following three peer-reviewed publications:

Chapter 2 has been published as Soltan Mohammadi, H., Ringel, L. M., de Paly, M., and Bayer, P. (2024). Sequential long-term optimization of shallow geothermal systems under descriptive uncertainty and dynamic variation of heating demand. *Geothermics* (121), 103021.

<https://doi.org/10.1016/j.geothermics.2024.103021>.

Chapter 3 has been published as Soltan Mohammadi, H., Ringel, L. M., Bott, C., and Bayer, P. (2024). Adaptive management of borehole heat exchanger fields under transient groundwater flow conditions. *Renewable Energy* (234), 121060.

<https://doi.org/10.1016/j.renene.2024.121060>.

Chapter 4 has been published as Soltan Mohammadi, H., Ringel, L. M., Bott, C., Erol, S., and Bayer, P. (2025). Bayesian uncertainty quantification in temperature simulation of borehole heat exchanger fields for geothermal energy supply. *Applied Thermal Engineering* (265), 125210.

<https://doi.org/10.1016/j.applthermaleng.2024.125210>.

Authorship contribution statement

In all three peer-reviewed publications included in this cumulative doctoral dissertation, Hesam Soltan Mohammadi is the first, corresponding, and leading author with the most contribution throughout the research process—from conceptualization and methodology to the visualization of results, investigation and data analysis, drafting and finalizing the manuscript, and handling revisions. The detailed author contributions in each publication, according to the Contributor Roles Taxonomy (CRediT)(Brand et al., 2015), are as follows:

Soltan Mohammadi et al. (2024a), **Chapter 2**: Conceptualization: H.S.M, M.d.P, and P.B; Funding acquisition: P.B; Investigation: H.S.M; Methodology: H.S.M, L.M.R, and P.B; Software: H.S.M, L.M.R, and M.d.P; Supervision: P.B; Visualization: H.S.M; Writing – original draft: H.S.M; Writing – review & editing: H.S.M, L.M.R, M.d.P, and P.B.

Soltan Mohammadi et al. (2024b), **Chapter 3**: Conceptualization: H.S.M, L.M.R, and P.B; Data curation: H.S.M; Formal analysis: H.S.M and L.M.R; Funding acquisition: P.B; Investigation: H.S.M, L.M.R, and C.B; Methodology: H.S.M, L.M.R, and P.B; Software: H.S.M; Supervision: P.B; Project administration: P.B; Validation: H.S.M, L.M.R, and C.B; Visualization: H.S.M and C.B; Writing – original draft: H.S.M; Writing – review & editing: H.S.M, L.M.R, C.B, and P.B.

Soltan Mohammadi et al. (2025), **Chapter 4**: Conceptualization: H.S.M, L.M.R, and P.B; Data curation: H.S.M; Formal analysis: H.S.M; Funding acquisition: P.B; Investigation: H.S.M, L.M.R, and C.B; Methodology: H.S.M, L.M.R, S.E, and P.B; Software: H.S.M, C.B., and S.E; Supervision: P.B; Project administration: P.B; Validation: H.S.M and L.M.R; Visualization: H.S.M and C.B; Writing – original draft: H.S.M; Writing – review & editing: H.S.M, L.M.R, C.B, S.E, and P.B.

H.S.M: Hesam Soltan Mohammadi, **M.d.P**: Michael de Paly, **P.B**: Peter Bayer, **L.M.R**: Lisa Maria Ringel, **C.B**: Christoph Bott, **S.E**: Selçuk Erol

Acknowledgments

First and foremost, I would like to express my deepest appreciation to Peter Bayer for the opportunity to work under his supervision over the past (almost) five years. My journey began during the strict COVID-19 pandemic lockdown, a time when international travel was severely restricted. Yet, I was fortunate to be one of the few able to take to the skies and make my way to Germany, all with Peter's unwavering support.

Over the years, Peter has been a constant source of motivation and encouragement. There were many moments when I felt on the verge of giving up, as things were not progressing as smoothly as I had hoped. However, Peter's patience and steady-state optimism kept me moving forward. I am deeply grateful for the flexible boundary conditions he provided, his constant support, and the freedom he gave me to pursue my own research while helping me grow as an independent researcher.

Next, I would like to thank my co-authors for their invaluable contributions to my research, particularly Lisa Ringel and Christoph Bott, who generously took unlimited time to listen to my problems and help me find solutions. Without their support, this work would not have been possible.

A special thanks to Hannes Hemmerle for his insightful ideas and for sharing his creativity, particularly in helping to improve some of the graphics in my work.

Lukas Römhild is the next person I am truly grateful to. His willingness to review parts of my work, proofread my German emails and texts, and share coffee breaks with me, along with the lasting friendship we have built outside the office, have made my years in Halle (Saale) truly unforgettable.

I am also grateful to all the other members of the working group of Applied Geology—Andreas Englert, Anika Thomas, David Hoffmann, Dominik Müller, Florian Fritz, Guanyu Yuan, Hannah Gebhardt, Jenny Weise, Julia Becher, Laura Meyer, Maxi Noethen, and Wolfgang Gossel—whose camaraderie and support made the office feel like home.

My thanks are also extended to Anne Ballhaus, Daniela Rothe, and Marie Petzold from our secretariat, who helped me navigate complicated bureaucratic procedures.

I would like to acknowledge Ryan Pearson, our native English-speaking student assistant, for always being there to proofread my work under time pressure and on short notice. His dedication is greatly appreciated.

Next, I want to thank my parents—Eti and Nosrat—whose support has been a constant source of strength, no matter how far apart we are or what I am doing, whether I am succeeding or struggling. Their belief in me, even in times when I doubted myself, has been immeasurable. Merci Maman, Merci Baba!

And my deepest thanks go to my partner, whose presence, patience, kindness, and support through all the ups and downs of the past years have been invaluable and beyond words. You are truly großartig—danke, Wiebke!

Finally, I would like to acknowledge the financial support of the German Research Foundation (Deutsche Forschungsgemeinschaft, DFG) under grant number BA2850/7-1, which made this research possible.

Contents

Abstract	v
Zusammenfassung	vii
Publications	ix
Authorship contribution statement	xi
Acknowledgments	xiii
Nomenclature	xxi
1 Introduction	3
1.1 Borehole heat exchanger (BHE)	4
1.2 Modeling of BHEs	5
1.3 Uncertainty in BHE systems	6
1.4 Optimization of BHEs	7
1.5 Bayesian inference for modeling BHEs	8
1.6 Objectives and scope of this thesis	9
1.6.1 Main objectives	9
1.6.2 Scope and limitations	9
2 Sequential optimization of BHE fields under uncertainty	13
2.1 Introduction	13
2.2 Methodology	16
2.2.1 Simulation of a borehole heat exchanger field	16
2.2.2 Optimization objective	17
2.2.3 Sequential optimization procedure	18
2.2.4 Parameter settings of case studies	19
2.3 Results and discussion	23
2.3.1 Maximum temperature change profiles	23
2.3.2 Optimal load patterns	26
2.3.3 Sensitivity analysis on the variability of heating demand	28
2.4 Conclusions and outlook	30
3 Adaptive management of BHE fields considering transient groundwater flow	33
3.1 Introduction	33

3.2	Methodology	36
3.2.1	Simulation of a borehole heat exchanger field	36
3.2.2	Optimization-calibration procedure	38
3.2.3	Model setup	40
3.3	Results and discussion	43
3.3.1	Single borehole heat exchanger	43
3.3.2	Multiple borehole heat exchangers	45
3.3.3	Optimal load balancing	46
3.4	Conclusions and outlook	49
4	Bayesian inference for stochastic modeling of BHE fields	53
4.1	Introduction	53
4.2	Methodology	57
4.2.1	Forward modeling	57
4.2.2	Inverse modeling	61
4.2.3	Model setup for the demonstration case	62
4.2.4	Implementation of the inversion procedure	66
4.3	Results and discussion	68
4.3.1	Statistical analysis of MCMC sampling	68
4.3.2	Evaluation of the posterior samples	73
4.3.3	Simulated temperature changes	75
4.4	Conclusions and outlook	78
5	Conclusions and future work	81
5.1	Summary and conclusions	81
5.2	Outlook	83
	Appendix	87
	A. Supplementary material for Chapter 4	87
	References	95
	Curriculum vitae	111
	Declaration	115

List of Figures

1.1	Various configurations of borehole heat exchangers in vertical systems.	4
2.1	Conceptual diagram of the sequential optimization.	15
2.2	Flowchart of the sequential optimization.	20
2.3	Geometric layout of two BHEs fields.	21
2.4	Original monthly heat demand profile and the corresponding excess load.	22
2.5	Maximum temperature change using single-step and sequential optimization.	24
2.6	Temperature change of each BHE using single-step and sequential optimization.	25
2.7	Optimal load patterns using single-step and sequential optimization.	27
2.8	Original heat demand profile with the corresponding uncertainty range.	29
2.9	Maximum temperature change using different uncertainty ranges in heating demand using single-step and sequential optimization.	29
3.1	Conceptual flowchart of the adaptive optimization of loads in BHE fields.	41
3.2	Layout of the fields with one BHE and multiple BHEs.	41
3.3	Monthly heat demand profile for two BHE fields.	42
3.4	Different fluctuation patterns of groundwater velocity over ten years of operation.	44
3.5	Temperature changes of single BHE using different groundwater flow patterns.	45
3.6	Temperature changes of multiple BHEs using different groundwater flow patterns.	47
3.7	Optimal load patterns using single-step and adaptive optimization.	48
3.8	Comparison of the monthly calibrated groundwater flow velocity obtained by adaptive optimization with the true pattern.	48
3.9	2D top-view of the heat plume around BHEs using adaptive optimization.	49
4.1	Conceptual framework of the Bayesian method for stochastic predictions of temperature changes.	57
4.2	Illustration of the composite model approach for a single BHE.	58
4.3	Schematic illustration of the affine invariant ensemble MCMC sampler approach.	62
4.4	3D view of the numerical model with three layers and groundwater flow.	63
4.5	Reference monthly temperature changes along the depth.	65
4.6	Reference average heat extraction rate of BHEs in different layers.	66
4.7	Validation of the numerical results against the forward model at five time-steps.	67
4.8	Trace plots of model samples for nine parameters at five time-steps.	70
4.9	Autocorrelation of the nine model parameters at five time-steps.	71
4.10	Violin plots of the nine model parameters at five time-steps.	72

4.11	Pair plots of unknown model parameters within the first layer at month six.	74
4.12	Comparison of simulated and observed temperature changes at month 60 over the depth, using inferred model parameters from selected time-steps.	75
4.13	Comparison of the RMSE and the range of temperature change predictions at month 60, based on the model samples from selected time-steps.	76
4.14	Comparison of the 95% confidence interval, mean, and median of predicted temperature changes with observed temperature changes at a depth of 10 m.	77
A.1	Validation of the forward solver (MFLSA) with numerical results over depth.	87
A.2	Validation of the forward solver (MFLSA) with numerical results over time.	88
A.3	Pair plots of all nine parameters at month 6.	89
A.4	Pair plots of all nine parameters at month 12.	90
A.5	Pair plots of all nine parameters at month 24.	91
A.6	Pair plots of all nine parameters at month 36.	92
A.7	Pair plots of all nine parameters at month 48.	93

List of Tables

2.1	Parameter specifications for case studies.	22
3.1	Parameter specifications for case studies.	42
4.1	Reference model parameters for different layer.	64

Nomenclature

Abbreviations

2D	Two-dimensional
3D	Three-dimensional
AIES	Affine invariant ensemble sampler
BHE	Borehole heat exchanger
DU	Descriptive uncertainty
FLS	Finite line source
GSHP	Ground source heat pump
GW	Groundwater
GSF	Groundwater flow
HDPE	High-density polyethylene
LP	Linear programming
MAE	Mean absolute error
MCMC	Markov Chain Monte Carlo
MFLS	Moving finite line source
MFLSA	Moving finite line source with anisotropy
PDF	Probability density function
RMSE	Root mean square error
TRT	Thermal response test

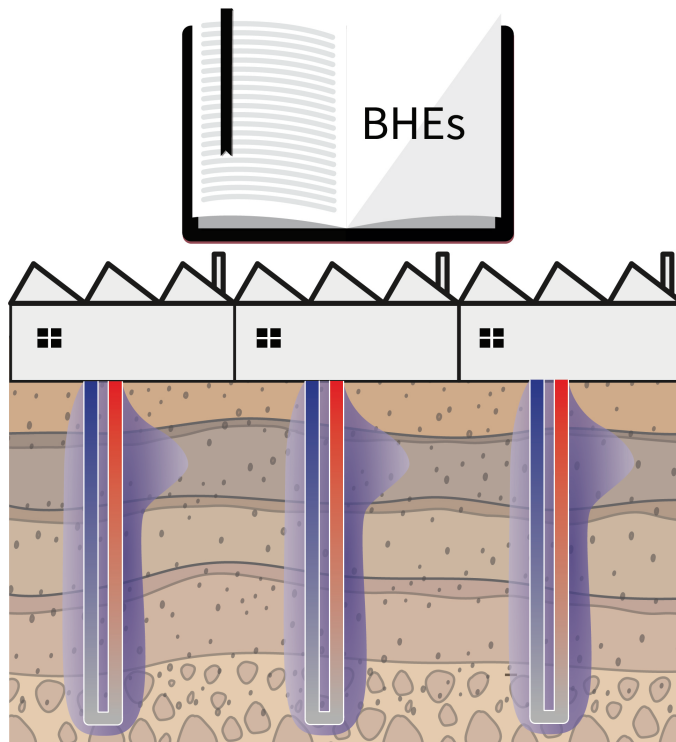
Symbols

A	Acceptance probability
a	Affine invariant step size
c	Specific heat capacity ($\text{Jkg}^{-1}\text{K}^{-1}$)
d	Measured data
E	Energy demand
\mathbf{e}	All-ones vector
erfc	Complementary error function
F	Forward model
Fo	Fourier number
H	Characteristic length (m)
k	Counter index for the number of BHEs
L	Length of borehole (m)
l	Counter index for the number of time-steps
ℓ	Log-likelihood
m	Counter index for optimization time-steps
$N(0, 1)$	Standard normal distribution (mean = 0, variance = 1)
N_{BHE}	Number of BHEs
N_t	Number of time-steps
$N_{t_{\text{opt}}}$	Number of optimization time-steps
n	Porosity
Pé	Péclet number
p	Probability distribution function
\mathbf{q}	Heat extraction/injection rate vector (Wm^{-1})
q	Heat extraction/injection rate (Wm^{-1})
r	Distance to the BHE axis (m)
S	Field domain
s	Random sample from a probability distribution
T	Temperature ($^{\circ}\text{C}$)
t	Time (s)
$U(0, 1)$	Uniform distribution between 0 and 1
u	Darcy velocity (ms^{-1})
v_a	Seepage velocity (ms^{-1})
vhc	Volumetric heat capacity ($\text{Jm}^{-3}\text{K}^{-1}$)
v_T	Heat transport velocity (ms^{-1})
w	Weighting factor
x	Coordinate in x-direction (m)
y	Coordinate in y-direction (m)
z	Coordinate in z-direction (m)

α	Thermal diffusivity (m^2s^{-1})
α_l	Longitudinal dispersivity (m)
α_t	Transversal dispersivity (m)
$\Delta\mathbf{T}$	Temperature change vector (K)
ΔT	Temperature change (K)
ζ	Affine invariant step size
Θ	Parameter of interest
λ	Thermal conductivity ($\text{Wm}^{-1}\text{K}^{-1}$)
ρ	Density (kgm^{-3})
σ	Standard deviation
τ	Auxiliary variable
$\boldsymbol{\omega}$	Thermal response coefficient vector
ω	Thermal response coefficient

Chapter 1

Introduction



1 Introduction

Ground source heat pump (GSHP) systems are currently the most widely used geothermal technology worldwide (Figueira et al., 2024; Lund and Toth, 2021). The growth in the number of GSHP systems, particularly over the past two decades, has been accompanied by extensive research efforts to support reliable planning, design, and operation of these systems. A key component of GSHP systems is the use of heat exchangers installed in the ground, enabling the extraction or injection of heat (Cui et al., 2024). These ground heat exchangers operate within narrow temperature ranges and supply energy to an aboveground heat pump, which is connected to a building's heating and/or cooling system. GSHP systems commonly use borehole heat exchangers (BHEs), where a heat carrier fluid circulates through closed tubes within boreholes. Depending on energy demands, these systems may use either a single BHE or an array of BHEs arranged in borehole fields.

The ground offers a compelling energy source for several reasons. Geothermal energy is widely available, and by drilling boreholes to depths ranging from tens to hundreds of meters, substantial volumes of the ground can be accessed for various applications, such as heating and cooling (Walch et al., 2022), energy storage (Shah et al., 2024), and integration with other energy systems (Olabi et al., 2020). Compared to air-source heat pumps, the ground provides much higher energy density and far less temperature variability for GSHP systems (Aprianti et al., 2021; Violante et al., 2022). However, heat transport in the ground is generally slower, primarily governed by conduction, and can be accompanied by coupled processes such as advection due to groundwater flow (Abesser et al., 2023).

The slow thermal transport in the ground is a critical aspect for the long-term operation of BHEs (Gebhardt et al., 2024). Over decades, imbalanced energy extraction or injection leads to the gradual development of thermal anomalies—areas of altered ground temperature that grow in size and intensity. These anomalies often result in a gradual decline in overall system efficiency (Cai et al., 2022; Chen et al., 2021). Thermal regeneration of the ground is similarly slow, with recovery times comparable to or even exceeding the operational lifespan of the system (Hein et al., 2016).

To address these concerns, precautionary regulations restrict the extent of induced ground temperature changes and the excessive spread of thermal anomalies in the subsurface (Hähnlein et al., 2010). These restrictions are not only aimed at addressing the long recovery times but also at preserving soil and groundwater ecosystems (Blum et al., 2021; Soltani et al., 2021). Hence, such measures help prevent conflicts between neighboring systems, ensuring that adjacent installations do not extremely interfere with each other (Fasci, 2023; Hähnlein et al., 2013). Especially in Central European cities and cold climates, concerns about

the thermal overuse of urban ground are increasing (Noethen et al., 2023a). As a result, there is a rising demand for improved strategies to regulate and control shallow geothermal development (Adebayo et al., 2024; Gheysari et al., 2021; Kirschstein et al., 2024).

1.1 Borehole heat exchanger (BHE)

BHEs are essential components in shallow geothermal energy systems, enabling efficient heating and cooling by harnessing the stable temperature of the subsurface. As part of GSHP technology, these systems tap into the stored thermal energy in the subsurface. BHEs transfer heat between the ground and a fluid that circulates in pipe loops. For closed-loop systems, boreholes are drilled into the ground, and pipes are typically installed horizontally or vertically. In the cold season, the fluid absorbs heat from the ground to warm a building, while in the warm season, it can return heat to the ground to cool the building. Vertical BHEs are typically used in urban areas due to their ability to reach greater depths in the subsurface while requiring less surface area. In terms of technical design, BHEs are commonly configured using U-tube, double U-tube, or coaxial systems (Figure 1.1), each suited to different environmental conditions and system requirements (Aresti et al., 2018). The U-tube BHE is the simplest design, consisting of two pipes bent into a U-shape inside the borehole. One pipe carries the fluid downward, while the other returns it to the surface. The double U-tube BHE design features two U-shaped pipes placed close to each other within the borehole. This setup enhances the system's thermal transfer capacity, making it more efficient in areas with lower ground thermal conductivity. By allowing more fluid to circulate, it improves the system's overall thermal performance. The coaxial BHE design features a smaller pipe inside a larger one, with the heat transfer fluid flowing through both pipes in opposite directions. The choice of BHE design depends on factors such as the type of soil or rock, the depth of the boreholes, the available surface area, and the building's heat demand. The schematic depiction of the various BHE configurations is shown in Figure 1.1, which is taken from (Rees, 2016).

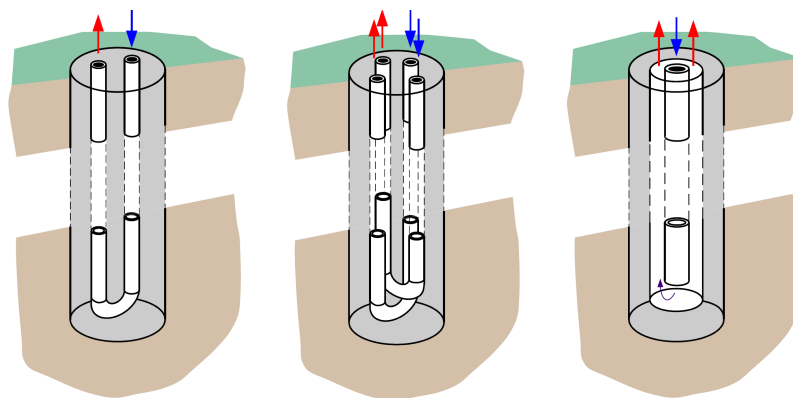


Figure 1.1: Various configurations of borehole heat exchangers in vertical systems (Rees, 2016).

1.2 Modeling of BHEs

A wide variety of models exist for simulating BHEs, and it is not feasible to present them in detail within the scope of this thesis. Therefore, the focus will be on the models most relevant to this work. Eskilson (1987) introduced the concept of *g*-functions, which are dimensionless response functions for heat step impulses. These functions were initially determined through simulations using radially symmetric two-dimensional numerical models. By superimposing *g*-functions, the transient heat extraction/injection at a BHE can be simulated, and the borehole wall temperature, depending on the heat extraction/injection per borehole length, can be calculated. BHE fields can be characterized by *g*-functions derived for specific geometries or by superimposing individual BHE *g*-functions. Planning software, such as the Earth Energy Designer (EED), utilizes a library of various *g*-functions to determine the required BHE properties and suggest the best choice from a set of available options. Over time, the number of *g*-functions and related computational methods has grown, incorporating additional geometries and varying conditions.

Modeling techniques for BHEs generally fall into two main categories: numerical and analytical methods. Numerical modeling platforms offer significant flexibility (Boockmeyer and Bauer, 2016; Casasso and Sethi, 2014; Chen et al., 2022, 2020; Chwieduk, 2021; Gebhardt et al., 2024; Harris et al., 2024; Häfner et al., 2015; Hein et al., 2016; Nguyen et al., 2017; Zhao et al., 2023), though this comes at the cost of relatively high computational demands. The computational expense, data requirements, and time needed to build and calibrate numerical models limit their practical applicability.

To address these limitations, (semi-)analytical models, such as those based on *g*-functions (Eskilson, 1987), offer a convenient way to approximate the thermal response of the subsurface using closed-form solutions (Cui et al., 2024; Li and Lai, 2015). Despite efforts to expand their applicability—by incorporating multi-layer subsurfaces (Guo et al., 2023), accounting for advective heat transfer due to groundwater flow (Erol and François, 2018; Molina-Giraldo et al., 2011), addressing discontinuous and heterogeneous thermal loads (Coen et al., 2021), considering land use and surface conditions (Guo et al., 2024; Rivera et al., 2015), BHE inclination (Lazzarotto, 2016; Lazzarotto and Björk, 2016), and interference between neighboring BHEs (Fascì et al., 2023)—many analytical models still rely on conceptual simplifications that limit their accuracy and broader applicability in realistic settings.

While these models offer specific advantages, as mentioned above, they face challenges in handling combinations of multiple complexities and often rely on simplistic assumptions. For instance, line source solutions (Zeng et al., 2002) typically assume a constant extraction/injection rate along the borehole wall, which can vary across a BHE field. Although this assumption is convenient, it simplifies the system and deviates from Eskilson's original conditions for *g*-functions. To address this, several researchers (Cimmino, 2015, 2016; Chiasson and Elhashmi, 2017) have proposed adjustments to the specific extraction/injection rate per borehole or segment to maintain a constant borehole wall temperature. Such adjustments are particularly important for thermal interactions within borehole fields, as assuming a con-

stant extraction/injection can lead to overestimations in Eskilson's g -functions (Claesson and Javed, 2011; Fasci et al., 2021), and consequently, the temperatures in the field. While these assumptions can be practical in some scenarios, they are not entirely realistic (Cimmino, 2015).

Analytical models are favored thanks to their computational efficiency, but oversimplifications can limit their realism. A potential research direction for further investigation is to combine data-driven approaches with existing efficient analytical models, rather than developing entirely new models with different constraints or simplifications. This synergy should improve model accuracy and applicability by relaxing simplifying assumptions, such as a constant heat extraction rate, to better align with real-world conditions.

1.3 Uncertainty in BHE systems

Understanding the thermal processes in shallow ground is essential for further developing regulations and planning subsurface energy use in urban areas, as well as for the optimal design and operation of GSHP systems. To this end, computer-based simulation tools and model-based planning are continuously advancing, enabling process-based predictions of ground temperature changes and geothermal system performance throughout their lifespan.

However, despite ongoing improvements in modeling techniques, the accuracy of these predictions depends not only on the conceptual maturity of the models but also on the accuracy of the model parameters. Many of these parameters are linked to subsurface conditions, which remain highly variable and difficult to measure directly. In-situ methods such as thermal response tests (TRTs) (Gehlin, 2002), borehole drilling, and hydraulic testing (Lembcke et al., 2016; Wagner et al., 2014) can provide useful data, but they cannot fully capture the complexities and transient dynamic of the subsurface.

Current BHE design guidelines often assume a homogeneous ground medium, ignoring spatial heterogeneity (e.g., VDI (2001)). While this simplification can be reasonable in cases of moderate thermal and hydraulic variation, it becomes problematic when significant heterogeneity is present. In such cases, a complex pattern of overlapping thermal anomalies can emerge (Noethen et al., 2023b,a), making accurate modeling difficult without detailed knowledge of the subsurface—something that is unattainable. This uncertainty, referred to as “descriptive uncertainty”, can be mitigated through field tests and site characterizations, but these investigations are costly. As a result, safety factors are typically used, such as increasing the required borehole length, which increases costs.

When average or expected ground properties are used for design, these values are often uncertain or only applicable to the close vicinity of the measurement point, such as those derived from TRTs. Moreover, uncertain ground properties are not the only challenge to the successful operation of GSHP systems. Other sources of uncertainty, including rough predictions of seasonal energy demand, temperature variability, and climate change, introduce a new category of uncertainty, which we refer to as “predictive uncertainty.” This type of uncertainty extends beyond site characterization or model parameter identification and calls for short-term system integration to account for its impact on long-term performance (Koenigsdorff and van

Trecek, 2006). These various sources of uncertainty, each with its own implications, call for dynamic strategies. Modeling and optimization tools should be capable of accounting for these uncertainties to ensure the long-term sustainability of the systems.

1.4 Optimization of BHEs

BHE field optimization is not commonly incorporated into the design tools used during the planning and operational stages of shallow geothermal systems. Instead, the most common approach involves selecting the best configuration—such as the geometric arrangement and borehole depth—by choosing from a set of predefined options. In some cases, sensitivity analyses are performed to identify optimal configurations (Casasso and Sethi, 2014). However, this approach often fails to account for the complexities of thermal processes in the subsurface, which are inherently slow and gradual. Uncontrolled energy extraction can disrupt this delicate balance, resulting in irreversible and potentially critical thermal anomalies. In the short term, such anomalies reduce the performance of heat pumps, and in the long term, their correction becomes increasingly difficult, often leading to environmental and technical challenges that could jeopardize the continued viability of the system (Cai et al., 2022; Chen et al., 2021).

To mitigate these risks, various optimization strategies have been developed to better distribute heating and cooling demands across individual BHEs within a field. Beck et al. (2010) were pioneers in applying mathematical optimization to BHE fields, focusing on minimizing temperature anomalies through load adjustments. Building on this work, Bayer et al. (2014) proposed improving field performance by taking underperforming BHEs out of operation. Further advancements were made by Hecht-Méndez et al. (2013), incorporating groundwater flow (GWF) into a combined simulation-optimization framework. In several other studies (Cimmino and Bernier, 2014b; Egidi et al., 2023; Noel and Cimmino, 2022; Spitler et al., 2020), optimization frameworks were expanded by mathematically optimizing parameters such as spacing, placement, and borehole length for fields with fixed energy demands. However, these efforts primarily focus on minimizing capital costs and achieving economic efficiency, often at the expense of operational parameters. Moreover, they rely on static, deterministic models that fail to consider the naturally variable and uncertain thermal states of the ground over time, basing solutions on initial predictions alone.

Given the complexity of subsurface thermal evolution and associated uncertainties (Heim et al., 2022), dynamic optimal control strategies provide a more practical solution for real-world applications. These strategies use continuous simulations and real-time feedback to adjust model inputs and optimize solutions (Javadi et al., 2019; Kümpel et al., 2022; Stoffel et al., 2022, 2023). Although advanced control algorithms have been applied to geothermal systems (Ma et al., 2020; Noye et al., 2022), the predictive models often oversimplify the thermal dynamics, hindering accurate representation of subsurface behavior (Heim et al., 2024a; Ikeda et al., 2017).

Therefore, further research is needed on simulation-based frameworks that leverage continuous monitoring during BHE field operations and incorporate new insights as they emerge.

These frameworks should be able to flexibly revise optimal operational plans and address model uncertainties, enabling an adaptive optimal control strategy.

1.5 Bayesian inference for modeling BHEs

Modeling subsurface thermal processes requires input parameters, typically estimated through TRTs (Gehlin, 2002; Spitler and Gehlin, 2015). Optimization methods are often used to estimate key thermal properties, focusing on a limited set of parameters (Dion et al., 2024a,b; Puttige et al., 2020). However, in complex environments, multiple parameters are strongly correlated, making the search for optimal values less effective than understanding their statistical dependencies.

Probabilistic methods, which rely on statistical inference from data, offer a better understanding of parameter distributions compared to traditional calibration methods. Therefore, further exploration of Bayesian approaches potential in BHE field site characterization and modeling.

Bayesian inference is a statistical method used to estimate parameters by updating prior knowledge with measured data (Bolstad and Curran, 2016). It begins with an initial set of assumptions, known as the prior distribution $P(\theta)$, and as new measurements d are made, these assumptions are updated to form a posterior distribution $p(\theta|d)$. This update is made using Bayes' theorem, which is expressed as:

$$p(\theta|d) = \frac{p(d|\theta)p(\theta)}{p(d)}$$

where $p(\theta)$ represents the prior distribution, which contains the initial assumptions or available information about the parameters; $p(d|\theta)$ is the likelihood, or the probability of the data given the parameters; and $p(d)$ is the marginal likelihood, which normalizes the distribution. This process combines prior knowledge with the likelihood of the measured data, indicating how well the model parameters explain the measurements in real time. The result is a refined estimate of the parameters that incorporates both prior knowledge and new data (Scheidt et al., 2018).

While calibration techniques and Bayesian methods have primarily been used to analyze the short-term characterizations of the BHE systems (Choi et al., 2022, 2018b,a; Menberg et al., 2019; Pasquier and Marcotte, 2020; Pasquier et al., 2019; Shoji et al., 2023), their potential as data assimilation tools for long-term BHE field simulations and optimal control strategies remains insufficiently investigated. Given the subsurface's inherent uncertainties, ground properties and operational parameters should be treated as dynamic systems requiring continuous monitoring and updated understanding (Shin et al., 2024). Bayesian inference, specifically, enables probabilistic modeling of BHEs by accounting for a range of parameter values, offering a reliability-based framework for operational decision-making. This approach treats discrepancies between model predictions and actual measurements over time as an inverse problem, allowing for continuous improvements in prediction reliability.

1.6 Objectives and scope of this thesis

1.6.1 Main objectives

This cumulative doctoral thesis explores the potential for enhancing various components of a combined simulation-optimization approach for the sustainable, long-term operation of fields equipped with multiple BHEs, used for energy supply through shallow geothermal systems.

The first objective of this research is to investigate the feasibility of extending the simulation-based optimization framework for load distribution among BHEs into dynamic routines. The extended framework aims to move beyond static optimal solutions for load distribution patterns, enabling dynamic control of individual BHE loads over time. By dynamic control, it is meant that the framework should be capable of self-tuning as new information becomes available or when the current thermal state of the subsurface deviates from predefined assumptions.

The second objective is to evaluate the framework in scenarios where uncertainties can be explained from a physics-based perspective, particularly in cases where heat transfer mechanisms are influenced by transient hydrogeological conditions. Since these conditions may not be easily predicted initially, dynamic revisions of the optimal load distribution patterns are necessary. To further enhance the reliability of the simulations and the resulting optimal load distributions, the integration of parameter estimation into the simulation-optimization process should be explored.

The third objective is to explore the potential of Bayesian data assimilation methods to enhance the applicability and predictive accuracy of analytical BHE modeling tools. This approach should allow the modeling framework to identify and statistically analyze deviations between temperature simulations and measurements, using these insights to adjust the model parameters accordingly.

1.6.2 Scope and limitations

To define the scope and limitations, the key features of the BHE systems and case study settings that will be examined in this dissertation are outlined as follows:

- The BHEs will be limited to closed-loop shallow systems, defined as those operating at depths of no more than a few hundred meters.
- The BHEs will be vertical and operate in parallel, enabling individual control of each BHE.
- Given the iterative nature of optimization routines, computational efficiency will be essential for the integrated predictive model. Therefore, the presented work will utilize computationally efficient line-source analytical models for temperature simulations.
- Temperature simulations will refer to temperature changes in the surrounding subsurface of the BHEs at specified observation points.

- The objective function of optimization procedures will aim to minimize thermal anomalies in the subsurface, without directly optimizing GSHP operations.
- Application cases will consider the effects of subsurface heterogeneity, groundwater flow, and fluctuations in expected energy demand. However, subsurface heterogeneities are limited to layered structures.
- Simulation, optimization, and data integration will be performed monthly, but the methodology will not be restricted to a specific time resolution.
- Although the procedures will be developed for various operation modes, all case studies will focus solely on heating applications.
- Numerical models will be used to design case study setups and will be implemented using COMSOL Multiphysics®. Additional implementations and visualizations will be created using MATLAB and Python programming languages.

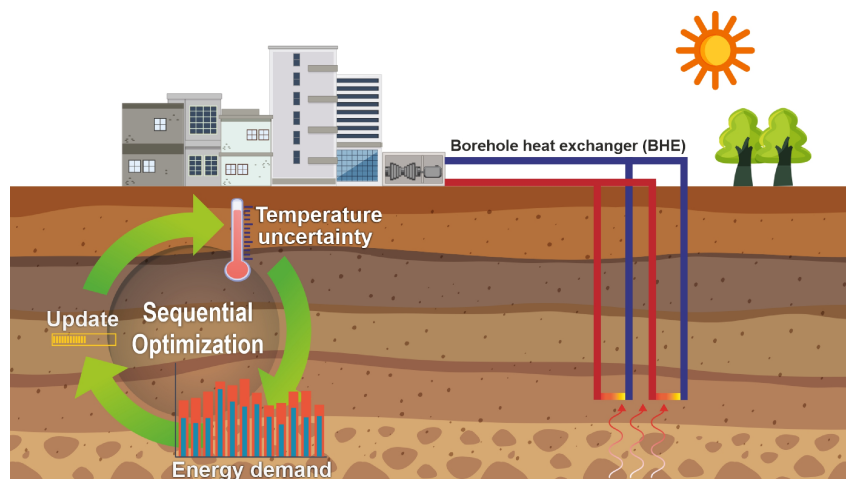
Chapter 2

Sequential optimization of BHE fields under uncertainty

This chapter has been published as:

Soltan Mohammadi, H., Ringel, L. M., de Paly, M., & Bayer, P. (2024).
Sequential long-term optimization of shallow geothermal systems under
descriptive uncertainty and dynamic variation of heating demand.
Geothermics (121), 103021, 2024.

<https://doi.org/10.1016/j.geothermics.2024.103021>



2 Sequential optimization of BHE fields under uncertainty

Abstract

Unmanaged heat extraction, as well as the adjacency of multiple BHEs in a field, can lead to undesirable thermal conditions in the ground. The failure to properly control induced thermal anomalies is perceived as a severe risk to closed-loop geothermal systems, as the detrimental effects on the ground can substantially deteriorate performance or nullify the compatibility of an operating system with regulatory mandates. This chapter presents a flexible framework for the combined simulation-optimization of BHE fields during the entire lifespan. The proposed method accounts for the uncertainties in subsurface characteristics and energy consumption in order to minimize the temperature change caused by the heat extraction during the operation. The descriptive uncertainty is introduced as a deviation of the monitored temperature from the simulated temperature change, whereas the variation of the energy demand appears as over- or under-consumption against the scheduled demand. The presented new sequential procedure, by updating the thermal conditions of the ground with temperature measurements, continuously executes the optimization during the operation period and enables the generation of revised load distributions. In this chapter, two fields with five and 26 BHEs are considered to demonstrate the performance of the proposed method. Sequential optimization outperforms single-step optimization by providing the basis for more strategic load-balancing patterns and yielding lower temperature anomalies of about 2.9 K and 8.9 K in each BHE configuration, respectively, over 15 operational years.

2.1 Introduction

Environmental concerns, climate change, and global energy crisis are all among the reasons that compel us to use renewable energy resources. In recent decades, shallow geothermal energy has emerged as one of the potential resources to achieve this goal, especially for heating and cooling purposes. Worldwide, geothermal resources provided approximately 108,000 MW of thermal energy in 2019 for 88 countries, representing a growth of about 52% compared to 2014 (Lund and Toth, 2021; Lund and Boyd, 2016). Shallow geothermal energy as an omnipresent resource can be accessed by means of drilling boreholes to a depth of a few tens of meters to a couple of hundred meters in the ground. The boreholes equipped with tubes are BHEs that circulate a heat carrier fluid connected with an aboveground heat pump to

supply a given heating (or cooling) demand (Gil et al., 2020). The energy supplied by a BHE for a given time can be termed as “load”.

Since the subsurface thermal processes are normally slow, unmanaged energy harvesting can yield undesired local cooling, and in the worst case trigger thermal shocks that the ground cannot fully dissipate. Imbalanced operation of multiple BHEs or disproportionate extraction or injection can cause environmental and technical issues that may jeopardize the efficiency and even the feasibility of operation. Exemplifying this issue, Chen et al. (2021) have assessed the under-performance of a field of 56 BHEs in Leicester, UK, by comparing numerical simulation with monitoring data. They found that the studied BHE field can be efficiently operated for a maximum of 20 years under the designed scenario due to heat accumulation in the central BHEs. In addition to a potential technical malfunction, long-term performance of BHE systems can result in subsurface thermal anomalies that violate local environmental regulations. In most countries with geothermal plants (Blum et al., 2021; Gil and Moreno, 2020; Haehnlein et al., 2010; Tsagarakis et al., 2020), there is a defined maximum threshold for the tolerable induced temperature anomalies in the ground, which is the basis for the design and operation of such systems.

To counteract the shortcomings in the performance of BHE fields and to mitigate the thermal anomalies, accurate subsurface characterization and simulation of the long-term system performance are needed. In order to properly design and operate BHE systems, it is crucial to have a thorough knowledge of the thermal properties of the ground, such as thermal conductivity and borehole resistivity (Erol and François, 2014; Heim et al., 2022; Hein et al., 2016). The most straightforward approach in practice for obtaining these parameters is to conduct in-situ measurements such as the TRT (Gehlin, 2002; Spitler and Gehlin, 2015). Given that TRTs are local measurements over a short period of time before the start of operation, they only examine the in-situ conditions in the vicinity of a borehole and they cannot resolve characteristic subsurface heterogeneities (Boban et al., 2020; Lee, 2011; Luo et al., 2014; Pasquier et al., 2019; Raymond and Lamarche, 2013; Wagner et al., 2012; Zhang et al., 2022). Aside from this, multiple further factors influence the performance of BHEs such as groundwater flow (Antelmi et al., 2023; Previati and Crosta, 2024; Signorelli et al., 2007; Zanchini et al., 2012), surface water bodies (Perego et al., 2022), ground-surface thermal coupling (Bidarmaghz et al., 2016; Nguyen et al., 2017), seasonal variations and consumer behavior (Yoshioka et al., 2022), and the type or the arrangement of BHEs (Zhang et al., 2021). This limited predictability of the system's performance over the operational lifespan motivates the use of optimization and control techniques. The concept of individual load optimization in a BHE field was introduced by Beck et al. (2010), and it was further developed to also consider groundwater (Hecht-Méndez et al., 2013). Beck et al. (2013) suggested a procedure for optimal BHE positioning and allocation of loads, and this was modified to detect the least effective BHEs and put them out of service (Bayer et al., 2014). Several alternative solutions have been presented to optimize irregular BHE spacing and minimize their numbers while fulfilling a given energy demand (Cimmino and Bernier, 2014b; Egidi et al., 2023; Noel and Cimmino, 2022; Spitler et al., 2022, 2020). Notwithstanding, these optimization concepts

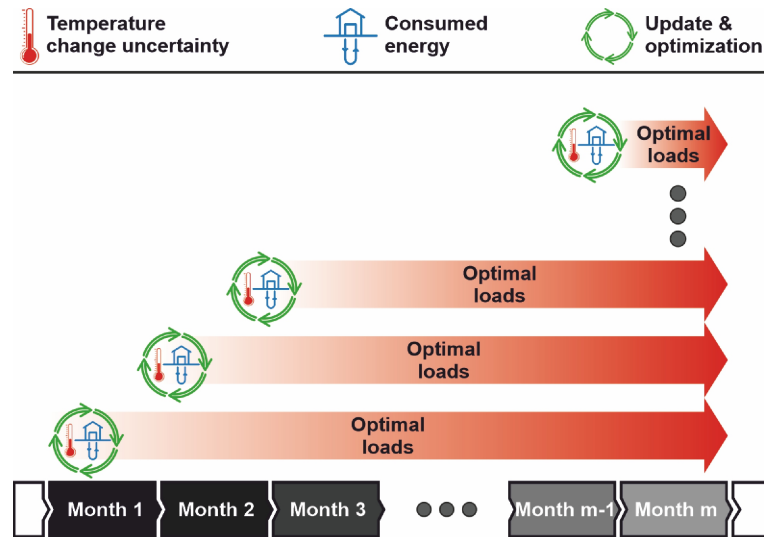


Figure 2.1: Conceptual diagram of the sequential optimization.

do not take into account the dynamics of the ground and possible uncertainties that may arise due to the interaction of multiple BHEs (Ma et al., 2020).

The general idea of optimal control techniques is to regularly monitor the ground during operation to provide an automated mechanism that compares the model-based simulations with the recorded data at specific time intervals (BniLam and Al-Khoury, 2020; Shoji et al., 2023). Some studies have presented several optimum operating scenarios, but the derived operational strategy is based on the comparison of a limited number of selected scenarios (Liu et al., 2015; Yavuzturk and Spitler, 2000; Zhou et al., 2016). Available control methods typically focus on applying dynamic programming, model predictive control, or artificial neural networks, while the adopted BHE and subsurface simulation models are often simplified (Atam et al., 2016; De Ridder et al., 2011; Gang et al., 2014). As pointed out by Ikeda et al. (2017), one of the main concerns with optimal control strategies is that the developed methodologies mostly fail to properly account for the thermal conditions and response of the ground.

The main motivation of this chapter is to enhance the flexibility of combined simulation-optimization for computing the heating load patterns in order to efficiently prolong the operational life and simultaneously comply with regulatory requirements and environmental concerns. Although this study only focuses on cases with heating applications, the proposed framework is also applicable to cooling purposes. Our approach is to simultaneously monitor the subsurface temperature evolution and actual energy demand at the particular time-steps to be able to update the subsurface thermal conditions for optimization of load balancing in an iterative framework. Hence, initial postulates and rough estimations are used to initialize the operation in an optimal way. A schematic illustration of our methodology is shown in Figure 2.1. In this chapter, we first present the governing equations for the simulation of the temporal temperature change caused by multiple BHEs in a field. Thereafter, the objective function and the relevant optimization constraints are defined. For demonstration of the new proposed procedure, two theoretical case studies are developed, and in the next section, the

maximum temperature changes in both fields are compared when single-step and sequential optimization are applied. The results section proceeds with a comparative study on the optimal load distributions, and the capability of the new sequential optimization procedure to deal with uncertainties in energy demand is evaluated.

2.2 Methodology

2.2.1 Simulation of a borehole heat exchanger field

The spatial and temporal temperature change induced by a single BHE can be approximated by a finite line-source (FLS) model (Beck et al., 2013; Stauffer et al., 2013; Zeng et al., 2002):

$$\Delta T(q, \Delta x, \Delta y, \Delta z, t) = \frac{q}{4\pi\lambda} \left(\int_0^L \frac{1}{r} \operatorname{erfc} \left(\frac{r}{\sqrt{4\alpha t}} \right) dz' - \int_{-L}^0 \frac{1}{r} \operatorname{erfc} \left(\frac{r}{\sqrt{4\alpha t}} \right) dz' \right) \quad (2.1)$$

This assumes conduction in a homogeneous and isotropic subsurface medium with properties that are independent of the temperature. In the equation, $\Delta T = T_\infty - T$ refers to the deviation from the ambient, unperturbed temperature distribution T_∞ . Since we are only concerned with the evaluation of temperature change in this chapter and FLS assumes a uniform and undisturbed temperature at $t = 0$ in the whole domain, the absolute value of T_∞ is not relevant for our study, and exclusively the temperature change is attributed to operation. L is the length of the borehole, λ is the thermal conductivity, α is the thermal diffusivity, and r represents the horizontal distance to the borehole axis Δx , Δy , and the vertical axis of a borehole $(z - z')$, such that $r = \sqrt{\Delta x^2 + \Delta y^2 + (z - z')^2}$. q is the heat flow rate per length of the borehole, which is a positive value in the case of heat extraction. If cooling is intended to be taken into account, this is realized by heat injection rather than extraction and is expressed by a negative sign.

The superposition principle can be applied to account for a set of boreholes $k = 1, \dots, N_{\text{BHE}}$ at locations (x_k, y_k) and a temporal variation of the load as a series of $l = 1, \dots, N_t$ load pulses $\mathbf{q} = \left(q_{1,1}, \dots, q_{N_{\text{BHE}},1}, \dots, q_{1,N_t}, \dots, q_{N_{\text{BHE}},N_t} \right)^T$ for each borehole (Abdelaziz et al., 2014; Bernier et al., 2004; Cimmino et al., 2013; Cimmino and Bernier, 2014a; Eskilson, 1987; Fasci et al., 2021; Lamarche, 2011; Lazzarotto, 2016; Lazzarotto and Björk, 2016; Marcotte et al., 2010; Marcotte and Pasquier, 2008; Michopoulos and Kyriakis, 2009). This leads to an estimation of the temperature change at any location relative to a borehole Δx_i , Δy_j at time t

$$\Delta \mathbf{T}(\mathbf{q}, \Delta x_i, \Delta y_j, t) = \sum_{l=1}^{N_t} \sum_{k=1}^{N_{\text{BHE}}} q_{k,l} \omega_{k,l}(\Delta x_i, \Delta y_j, t) \quad (2.2)$$

with the response coefficient:

$$\begin{aligned}
\omega_{k,l}(\Delta x_i, \Delta y_j, t) = & \frac{1}{4\pi\lambda} \left(\int_0^L \frac{1}{r} \operatorname{erfc} \left(\frac{r}{\sqrt{4\alpha(t-t_{l-1})}} \right) dz' \right. \\
& - \int_{-L}^0 \frac{1}{r} \operatorname{erfc} \left(\frac{r}{\sqrt{4\alpha(t-t_{l-1})}} \right) dz' \\
& - \int_0^L \frac{1}{r} \operatorname{erfc} \left(\frac{r}{\sqrt{4\alpha(t-t_l)} } \right) dz' \\
& \left. + \int_{-L}^0 \frac{1}{r} \operatorname{erfc} \left(\frac{r}{\sqrt{4\alpha(t-t_l)} } \right) dz' \right) \quad (2.3)
\end{aligned}$$

where t is the current time $t \geq t_l$ (Beck et al., 2013). Due to the assumption of temperature-independent parameters, the temperature distribution can be formulated as a linear problem

$$\Delta \mathbf{T}(\mathbf{q}, \Delta x_i, \Delta y_j, t) = \boldsymbol{\omega}(\Delta x_i, \Delta y_j, t) \mathbf{q} \quad (2.4)$$

with $\boldsymbol{\omega} = (\omega_{1,1}, \dots, \omega_{N_{\text{BHE}},1}, \dots, \omega_{1,N_t}, \dots, \omega_{N_{\text{BHE}},N_t})$. As initial condition, $\Delta \mathbf{T}(\mathbf{q}, \Delta x_i, \Delta y_j, t_0) = 0$ holds for $t_0 = 0$.

2.2.2 Optimization objective

The optimization procedure we use here is adopted from the method that was proposed by de Paly et al. (2012). The objective is to avoid local ground temperature decline in the field by minimizing the maximum temperature change induced by all BHE operations. The underlying rationale is that the ground heat exchange is optimal when ‘‘cold’’ BHEs are avoided, and thus also the performance of the heat pump is indirectly optimized. In the mathematical formulation this means identifying the position in the considered region $\Delta x_i, \Delta y_j \in S$ where the maximum temperature change occurs, and distributing the loads temporarily and spatially such that the weighted sum of the maximum temperature change of the entire operation period and the timestep-wise maximum temperature change is minimized:

$$\arg \min \left(w \cdot \max \left(\left(\Delta \mathbf{T}(\mathbf{q}, \Delta x_i, \Delta y_j, t_{N_t}) \right) + \sum_{l=1}^{N_t} \max(\Delta \mathbf{T}(\mathbf{q}, \Delta x_i, \Delta y_j, t_l)) \right) \right) \quad (2.5)$$

subject to

$$E_l = \sum_{k=1}^{N_{\text{BHE}}} q_{k,l}, \quad \Delta x_i, \Delta y_j \in S, \quad \forall l = 1, \dots, N_t \quad (2.6)$$

The first constraint ensures that the heat demand is met in each time-step and the latter restricts the max-norm to the investigated region. N_t specifies the number of time segments l and thus defines the time resolution, e.g., for computation of daily or monthly changing optimal individual BHE loads. The first term in the objective function is of greater importance to us since the primary concern is to minimize the temperature change for the entire time period and not for individual time-steps. To make this superiority explicit, a weighting factor w is

defined that grants a higher weight to the first term. w is fixed at 100 in this chapter. If the entire operation time is discretized by l segments, and an optimal transient loading pattern is derived based on the given initial conditions at t_0 before the operation of the BHE field only, then we define this procedure as “single-step optimization”.

2.2.3 Sequential optimization procedure

We investigate the potential to learn during BHE field operation. Most convenient is to re-run the optimization after a period of operation and take the prevailing ground thermal state as a new initial condition. In our application example, we study the case where the monthly extracted heat demand deviates from the predicted one. Furthermore, we assume that the line-source model is not exact due to simplifying assumptions on the ground thermal properties and processes. The resulting deviations between simulated and observed real thermal conditions in the ground are regularly inspected during the course of operation and the BHE loading strategy is optimized again.

For this purpose, the previously defined objective function (Equation (2.5)) is reformulated such that the optimization problem can be posed and solved as linear problems by applying auxiliary virtual variables τ_0 and τ_l :

$$\min \left(w \cdot \tau_0 + \sum_{l=1}^{N_t} \tau_l \right) \quad (2.7)$$

subject to the constraints:

$$\begin{aligned} \Delta \mathbf{T}(\mathbf{q}, \Delta x_i, \Delta y_j, t_{N_t}) - \tau_0 \mathbf{e} &< 0, \\ -\Delta \mathbf{T}(\mathbf{q}, \Delta x_i, \Delta y_j, t_{N_t}) - \tau_0 \mathbf{e} &< 0, \\ \Delta \mathbf{T}(\mathbf{q}, \Delta x_i, \Delta y_j, t_l) - \tau_l \mathbf{e} &< 0, \\ -\Delta \mathbf{T}(\mathbf{q}, \Delta x_i, \Delta y_j, t_l) - \tau_l \mathbf{e} &< 0, \end{aligned} \quad (2.8)$$

$$E_l = \sum_{k=1}^{N_{\text{BHE}}} q_{k,l}, \quad \Delta x_i, \Delta y_j \in S, \quad \forall l = 1, \dots, N_t.$$

\mathbf{e} denotes the vector of ones with N_{BHE} entries. The optimization is repeated iteratively for predefined time-steps t_m ($m = 1, \dots, N_{t_{\text{opt}}}$), which we call “sequential optimization”.

Based on the actual extracted energy and the measured ground temperatures at each time-step, the real-time subsurface temperature change, $\Delta \mathbf{T}_{\text{meas}}(\Delta x_i, \Delta y_j, t_{m-1})$, is determined, which differs from the model-based simulations, $\Delta \mathbf{T}(\mathbf{q}, \Delta x_i, \Delta y_j, t_{m-1})$. This real temperature change of the BHE field is considered as the most accurate starting point for the recalculation of the optimal load patterns of the upcoming months. The measured temperature is assumed to be a representative proxy for the current thermal response and conditions of the ground. The final outcome of the sequential optimization at each time-step is a new load allocation, \mathbf{q} , for the individual boreholes in the remaining time-steps.

This sequential optimization is realized as a loop for $m = 1, \dots, N_{t_{opt}}$:

$$\min \left(w \cdot \tau_0 + \sum_{l=m}^{N_t} \tau_l \right) \quad (2.9)$$

subject to the constraints:

$$\begin{aligned} \Delta \mathbf{T}(\mathbf{q}, \Delta x_i, \Delta y_j, t_{N_t}) - \Delta \mathbf{T}(\mathbf{q}, \Delta x_i, \Delta y_j, t_{m-1}) - \tau_0 \mathbf{e} &< -\Delta \mathbf{T}_{\text{meas}}(\mathbf{q}, \Delta x_i, \Delta y_j, t_{m-1}), \\ -\Delta \mathbf{T}(\mathbf{q}, \Delta x_i, \Delta y_j, t_{N_t}) + \Delta \mathbf{T}(\mathbf{q}, \Delta x_i, \Delta y_j, t_{m-1}) - \tau_0 \mathbf{e} &< \Delta \mathbf{T}_{\text{meas}}(\mathbf{q}, \Delta x_i, \Delta y_j, t_{m-1}), \\ \Delta \mathbf{T}(\mathbf{q}, \Delta x_i, \Delta y_j, t_l) - \Delta \mathbf{T}(\mathbf{q}, \Delta x_i, \Delta y_j, t_{m-1}) - \tau_l \mathbf{e} &< -\Delta \mathbf{T}_{\text{meas}}(\mathbf{q}, \Delta x_i, \Delta y_j, t_{m-1}), \\ -\Delta \mathbf{T}(\mathbf{q}, \Delta x_i, \Delta y_j, t_l) + \Delta \mathbf{T}(\mathbf{q}, \Delta x_i, \Delta y_j, t_{m-1}) - \tau_l \mathbf{e} &< \Delta \mathbf{T}_{\text{meas}}(\mathbf{q}, \Delta x_i, \Delta y_j, t_{m-1}), \\ E_l = \sum_{k=1}^{N_{bhe}} q_{k,l}, \quad \Delta x_i, \Delta y_j \in S, \quad \forall l = m, \dots, N_t. \end{aligned} \quad (2.10)$$

In this loop, the simulated temperature change from previous time-steps is iteratively replaced with the actual measured temperature. For $m = 1$, the results of the sequential and single-step optimization coincide. The flowchart of the proposed method is shown in Figure 2.2.

2.2.4 Parameter settings of case studies

Two hypothetical case studies with different configurations of the BHE field are defined. In case study I, five BHEs, and in case study II, 26 BHEs are considered for layouts as shown in a top view in Figure 2.3. The BHEs are located in a $35 \text{ m} \times 40 \text{ m}$ and $50 \text{ m} \times 60 \text{ m}$ area, respectively, where their positions are denoted by circles. The spacing between the BHEs is set to 5 m, which in practice may be sufficient to prevent strong thermal interference from adjacent boreholes (Gultekin et al., 2016; VDI, 2001), but commonly long-term operation yields superpositioning of the thermal effects of neighboring BHEs (Rivera et al., 2017). Only conductive heat transfer to the BHEs is simulated based on Equation (2.1), respecting a given time-dependent heat demand profile for an operating period of 15 years.

We account for inaccuracy in the models used to predict the ground temperatures of the two cases. It is assumed that the thermal response of the boreholes, which are represented by filled circles in Figure 2.3, are prone to deviations from the simulation. In both case studies, the temperature change is calculated once before the start of operation using Equation (2.1) for all time-steps and considered as a prior value. At each time-step, the simulated temperature change is compared to the measured temperature (Equation (2.10)). To construct a virtual reality that resembles the measured temperature, an uncertainty percentage is assumed at the location of each borehole. Figure 2.3 shows the assumed distribution of the uncertainty rates in both fields, and the structure of this variation can be attributed to local heterogeneity of the subsurface.

In addition to that, the BHEs can be subject to further sources of uncertainty such as the thermal impact of underground infrastructures like underground car parks (Noethen et al.,

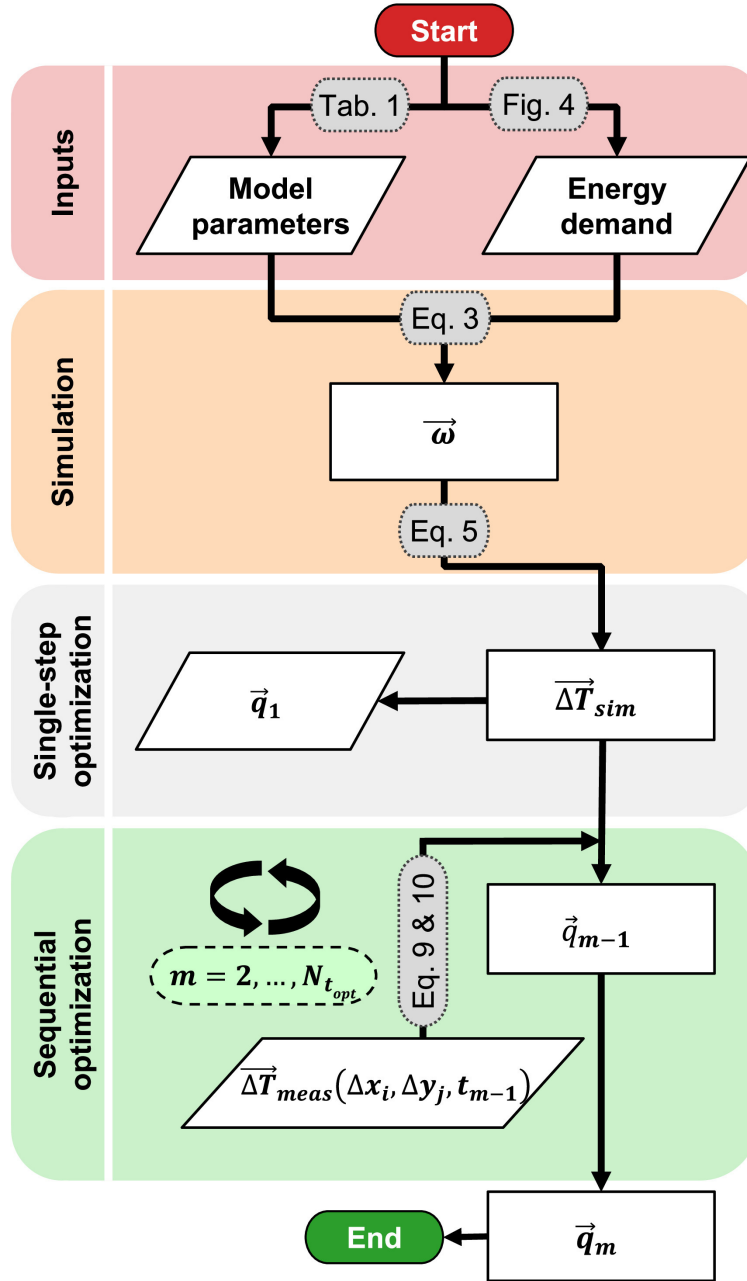


Figure 2.2: Flowchart of the sequential optimization method.

2023b), clogged wells (Song et al., 2020), or interference with other subsurface thermal systems such as other active BHE fields or aquifer thermal energy storage systems (Noethen et al., 2023a). The mentioned examples have in common that their effect on the temperature changes in the ground cannot be explicitly captured by the FLS model (Equation (2.1)). Instead, this is reflected by incorporating measured temperature changes in the sequential optimization (Equation (2.10)). In case studies I and II, the maximum uncertainty range is up to 5% and 7%, respectively. These values that represent the descriptive uncertainty rates are multiplied by the increase or decrease of temperature from the previous time-step, $\Delta \mathbf{T}_{DU}(\Delta x_i, \Delta y_j, t_m)$, and added to the simulated value, $\Delta \mathbf{T}_{sim}(\Delta x_i, \Delta y_j, t_m)$, in order to

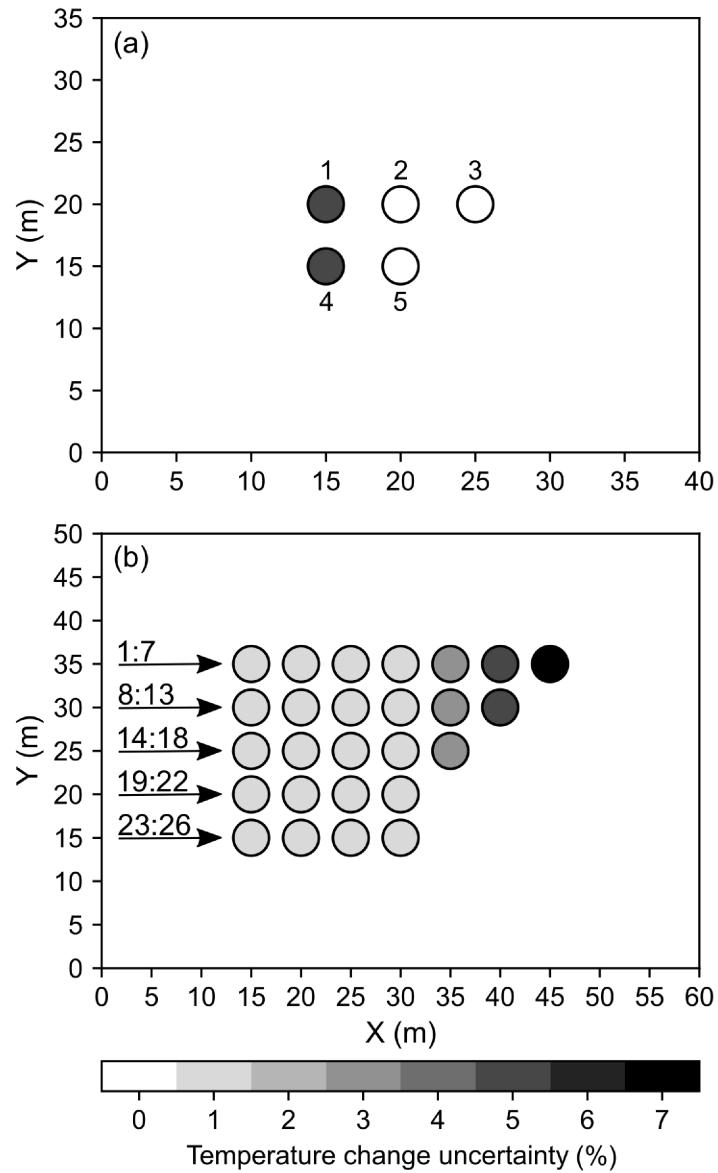


Figure 2.3: Geometric layout of numbered BHEs of (a) case study I and (b) case study II. The numbers on the arrows in (b) indicate the index of the BHEs, from left to right, in each row of the array. These numbers are used to refer to each individual BHE.

generate the true temperature change. The temperature change caused by the excess load, $\Delta \mathbf{T}_{\text{excess}}$, is the other source of temperature variation that has to be included in the measured values. We can summarize the components of the measured temperature change by:

$$\begin{aligned} \Delta \mathbf{T}_{\text{meas}}(\Delta x_i, \Delta y_j, t_m) &= \Delta \mathbf{T}_{\text{sim}}(\Delta x_i, \Delta y_j, t_m) \\ &+ \Delta \mathbf{T}_{\text{DU}}(\Delta x_i, \Delta y_j, t_m) \\ &+ \Delta \mathbf{T}_{\text{excess}}(\Delta x_i, \Delta y_j, t_m) \end{aligned} \quad (2.11)$$

Both hypothetical BHE fields are located at a site where the ground consists mainly of clay

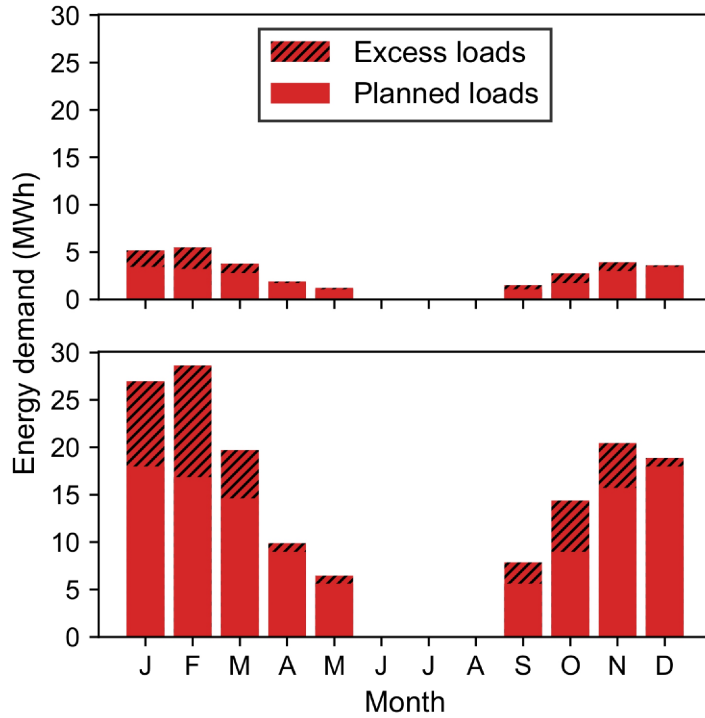


Figure 2.4: Original monthly heat demand profile and the corresponding excess load for the case with (a) 5 BHEs and (b) 26 BHEs.

and silt. The subsurface is considered homogeneous with negligible groundwater flow. The values for the thermal properties are taken from the guidelines of the Association of German Engineers (VDI, 2001), and the parameter specifications are listed in Table 2.1. Under the assumption that each individual borehole is 100 m long, the heat extraction rate per length is 24 Wm^{-1} , and the annual operating time is 1,800 h (de Paly et al., 2012; VDI, 2001). The total annual energy demands are 21.6 and 112.32 MWh for case studies I and II, respectively. This total energy demand is non-uniformly distributed over 12 months of the year, based on the assumption that the site is located in a country with Central European climate conditions and there is no heating demand during the summer months (June, July, and August). Even though the heating demand of consumers such as for space heating can be predicted, the true demand often varies significantly depending in particular on consumer behavior and climate variability. In order to account for this, our study considers a discrepancy between planned and actual energy demand in each month, the so-called excess load as shown in Figure 2.4. The optimal workloads in this chapter are always calculated based on the predefined heating

Table 2.1: Parameter specifications for case studies.

Parameter	Value	Unit
Length of borehole, L	100	m
Thermal conductivity, λ	1.7	$\text{W m}^{-1} \text{K}^{-1}$
Thermal diffusivity, α	7×10^{-7}	$\text{m}^2 \text{s}^{-1}$

demand. At the end of each month, the current optimal load pattern is then scaled relatively to fulfill the surplus, or shortfall load. Subsequently, the temperature change resulting from this over- or underload is calculated and applied as new knowledge in the next iteration of optimization. Sequential optimization gradually considers the deviation in the extracted load. Evidently, this cannot alter the past months, but it may be beneficial to modify the optimal patterns in the remainder of the operational lifetime. Here, as default it is assumed that the planned energy demand is always underestimated in comparison to the real demand.

Given the arrangement of the fields and the 180-month operation, this linear programming optimization problem for case study I and II covers 1,261 and 5,041 decision variables, composed of 900 loads, q , along with 361 virtual variables, and 4,680 loads, q , along with 361 virtual variables, respectively. Aside from this, the formulations include 4,861 and 23,761 constraints associated with the five and 26 BHEs, respectively.

In the next section, the optimal load allocation patterns proposed by both optimization methods are assessed. The criterion for evaluating the efficiency of the optimization techniques is the maximum of imposed thermal anomaly in the ground at the end of the operating time by applying the proposed patterns. For both case studies, the distribution of subsurface temperature changes at 50 m depth are calculated. The mid-depth temperature is chosen in line with previous work (Bayer et al., 2014) and according to the suggestions by Zeng et al. (2002) to consider this temperature as a representative value for applications. However, any site-specific conditions or e.g. layered heterogeneity of ground properties may be accounted for by alternative models (Erol and François, 2018). To compare the performance of single-step and sequential optimization, we need to scale the proposed scenarios of single-step optimization, which is only possible at the end of the operational time in order to have equal amounts of extracted load. This means, the optimized BHE loads of the single-step optimization are increased or decreased relatively to match the realized heat demand. This is based on the assumption that the initially optimized relative load pattern is implemented, but depending on the true heat demand the overall load may need to be adjusted.

The circle colors in Figure 2.3 indicate the assumed percentagewise deviation of the monthly temperature change compared to the simulated values for the given month due to the subsurface descriptive heterogeneity. So, the darker the color of BHEs, the higher the uncertainty.

2.3 Results and discussion

2.3.1 Maximum temperature change profiles

In this section, the maximum temperature changes during the operating time are presented for cases where single-step and sequential optimization procedures are applied. As demonstrated for both configurations in Figure 2.5, the resulting subsurface temperature changes from sequential optimization are significantly lower. The trend shows that in the first months of operation, there is no noticeable difference between the two optimization methods, but in the long run, the sequential outperforms the single-step method. There is an obvious benefit from

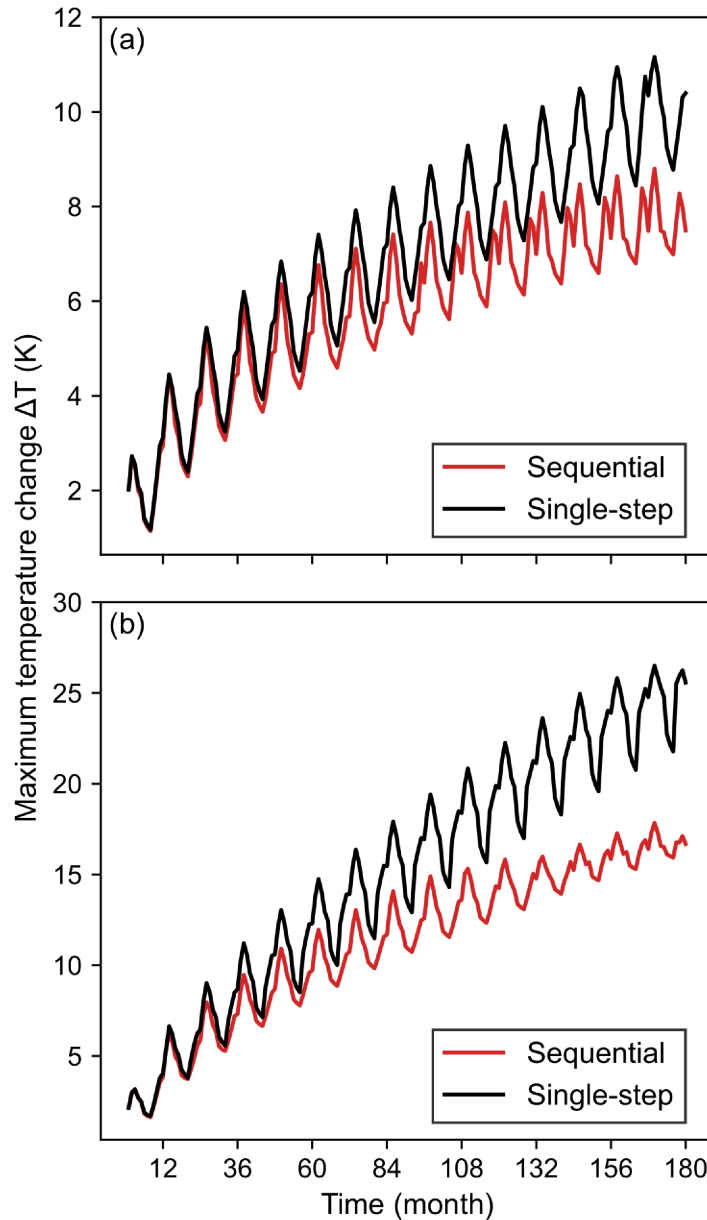


Figure 2.5: Maximum of temperature change at 50 m depth over 15 operational years by using single-step and sequential optimization for (a) case study I and (b) case study II.

the adaptive strategy underlying the sequential framework, where the subsurface temperature changes in the field are repeatedly measured during operation, and they are compared with the expected values at the end of each month. At each time-step, the implemented deviation between simulated and measured data implies that we were not able to optimize the system perfectly in the last month, but we can react. Thus, there is an opportunity to avert cumulative deviations in the upcoming months. By measuring the thermal state of the ground each month, new initial thermal conditions can be used to revise the prediction of the model. This leads to a new starting point for the optimizer and to potentially different optimal load distributions for the remaining months. Figure 2.5 reveals that the optimal patterns from the sequential

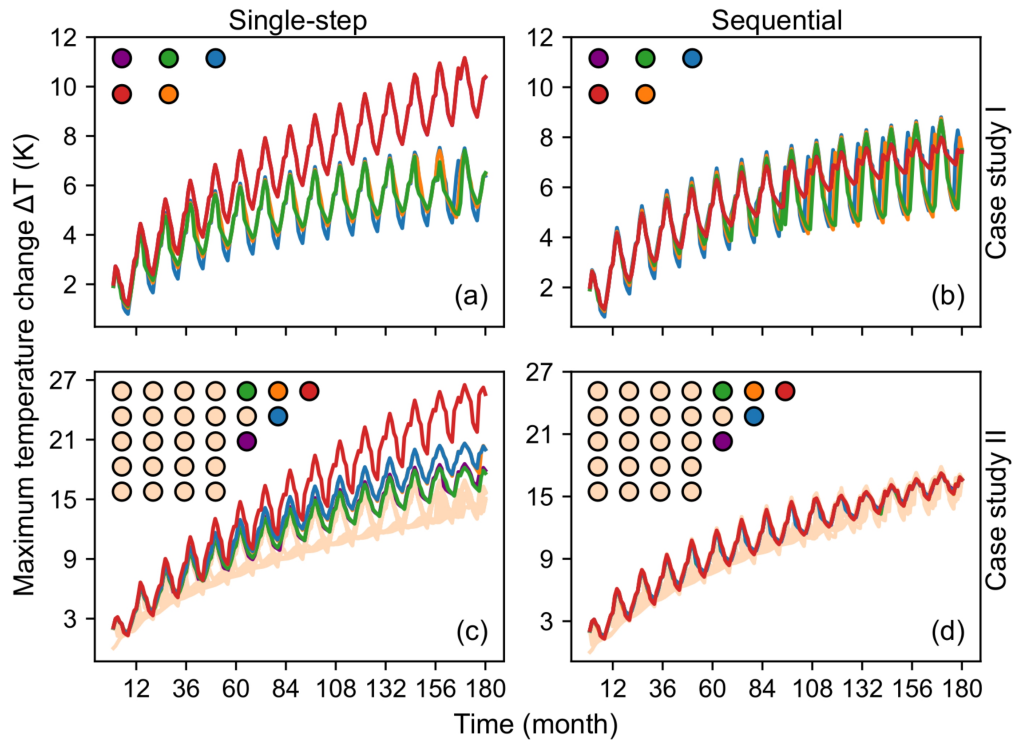


Figure 2.6: Temperature change evolution of each single borehole at 50 m depth in the (a, b) five BHEs and (c, d) 26 BHE field using (a, c) single-step optimization and (b, d) sequential optimization. The pictogram at the top left of each plot shows the relative position of the BHEs in the field based on Figure 2.3

variant result in lower temperature anomalies of about 2.9 K and 8.9 K in case studies I and II, respectively, over 15 years of operation. This means that the proposed approach leads to 27% lower temperature changes in the case of five BHEs and 34% lower temperature changes in the case of 26 BHEs compared to the single-step optimization at the end of the 15 years of operation. In Figure 2.5, only the maximum temperature change of the BHE fields over time is shown. Note that this is the criterion of the objective function (Equation (2.5)). However, for a more detailed insight into which BHE induces the maximum temperature change, Figure 2.6 presents the temperature change evolution of each BHE individually for case studies I and II. Obviously, in case study I the underestimation of the thermal effect of BHEs #1 and #4 (in accordance with Figure 2.3a) is critical for the solution obtained by single-step optimization. Together with the uncertainties in the heating demand, the single-step solution does not react to deviations and there is an increasing local cooling at these boreholes in Figure 2.6a. Figure 2.6b demonstrates that the general characteristics and seasonal dynamics of the temperature variations for all BHEs are in a similar range in the sequential framework. In contrast, the optimizer responds properly and mitigates the local cooling effects at #1 and #4. This is compensated by higher loads for the other BHEs. Interestingly, the critical BHEs in the sequential optimization result (Figure 2.6b) are other BHEs, the central BHEs BHEs #2, #3, and #5. This indicates that these BHEs have strongest interference with neighboring ones.

In a similar manner, the maximum temperature change in each borehole for case study II is calculated. For a better visual comparison in this dense case, only the imposed temperature change by critical BHEs are shown in different colors and the remaining BHEs with similar temperature change trend are not distinguished. Figure 2.6c shows that neglect of subsurface heterogeneity at the position of BHE #7 and not considering the actual extracted energy again is unfavorable. A maximum temperature change in around seven years by single-step optimization is of the same order of magnitude as the maximum temperature change caused by sequential optimization in 15 years (Figure 2.6d). Figure 2.6 confirms that sequential optimization tends to result in a more uniform temperature change across the entire field, thereby compensating for the uncertainties in the prediction of the induced temperature changes and heating demand. In the case of five BHEs for the single-step optimization, the BHEs experience a temperature change in the range of about 6.2 K to 10.5 K, while in the sequential optimization, the temperature change for all BHEs is approximately 7.5 K at the end of 15 years. In the case of 26 BHEs, single-step optimization leads to temperature changes between 15.6 K to 25.5 K, whereas the sequential optimization patterns restrict the temperature change for all BHEs to a tight range of about 17 K after 15 years.

2.3.2 Optimal load patterns

In this part, we present the distribution patterns of the optimal loads over the operating period resulting from the single-step as well as the sequential optimization for both case studies. The optimal load patterns of four time-steps are shown exemplarily in Figure 2.7 as a visual comparison of the load assignments by two methods. The single-step and sequential optimization propose an identical initial load distribution for both case studies, but over time they diverge from each other. In order to compare the different patterns, the values of the allocated loads on each individual borehole are divided by their length (100 m, Table 2.1) to derive a specific heat extraction rate, q . To simplify visual inspection, the intensity of the color and the size of the circles at the positions of the BHEs indicate the scale of load allocation to each particular BHE.

In an operating field with a similar configuration as case study I, if the thermal properties of the ground were fully known and there were no uncertainties, BHE #2 would be more likely to yield a more pronounced temperature anomaly in the subsurface than the others while this BHE is surrounded by the other BHEs that are actively operating. In the automatic optimal design of this field with the objective of minimizing the temperature change in the ground, the algorithm tends to reduce the assigned load on BHE #2 and distribute the excess load fairly evenly among the other BHEs. Figure 2.7a shows that the single-step algorithm adopts a similar strategy in case study I. In contrast, the sequential algorithm recognizes that previous model predictions do not match the truth. Therefore, the algorithm learns and automatically modifies the previously proposed scenarios for upcoming months (Figure 2.7b). It prevents local cooling by reducing the load of the BHEs where strong thermal anomalies have been created. It reduces the heat extraction of the poorly performing BHEs #1 and #4, and rather accentuates the role of other BHEs. This demonstrates that an underestimated temperature

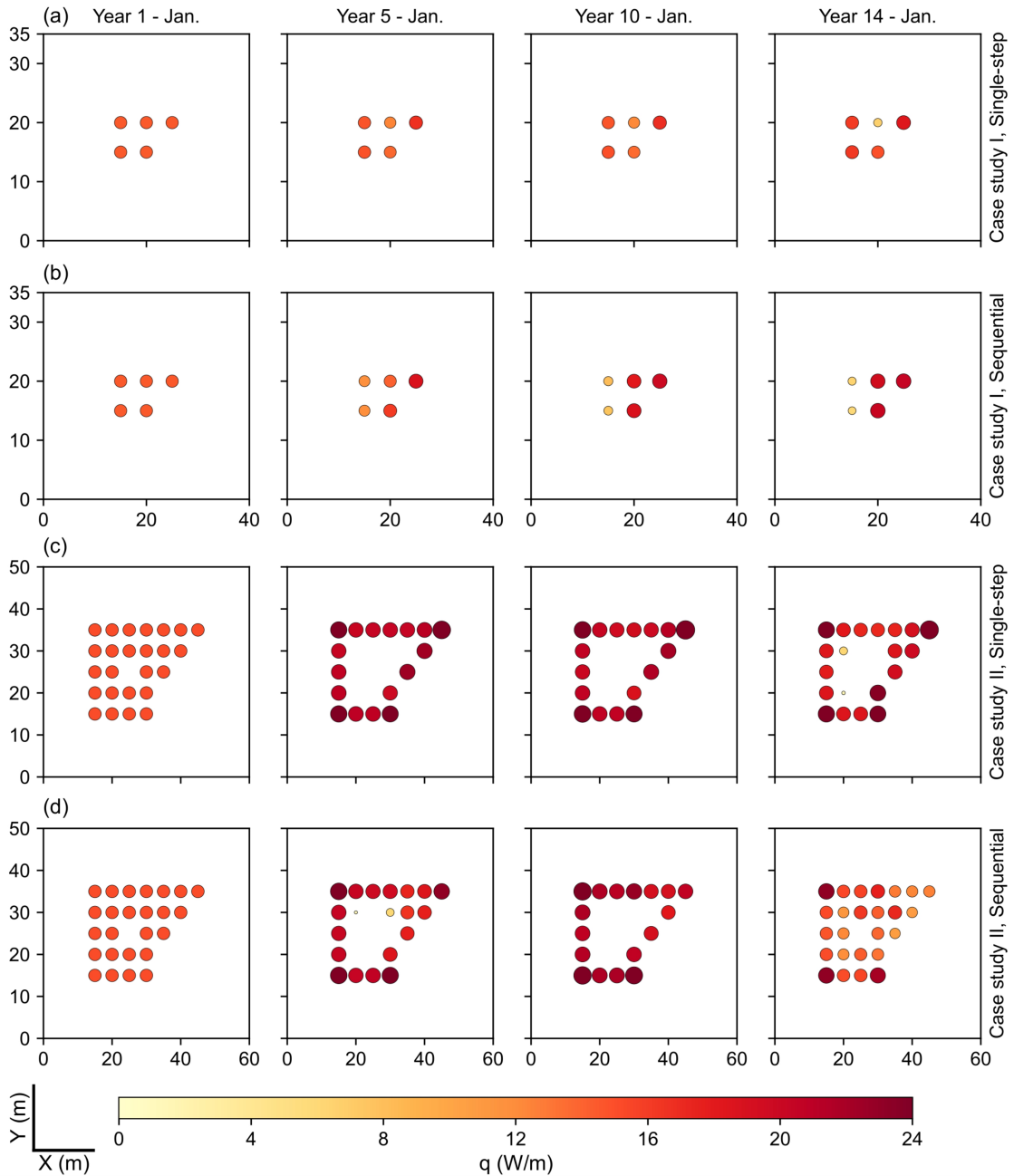


Figure 2.7: The resulting optimal load patterns at some selected operating intervals that are obtained for case study I by using (row a) single-step optimization, (row b) sequential optimization and for case study II by using (row c) single-step optimization and (row d) sequential optimization. The darker the color and the larger the BHEs, the higher the heat extraction rate.

change of 5% compared to the prediction by the analytical model each month already causes bad performance during long-term operation. Figure 2.7c shows that the single-step algorithm attempts to minimize the temperature change following the reasonable strategy of assigning the loads to the fringe of the field rather than to the inner part. As soon as the system is confronted with unexpected thermal behavior in these outer boreholes, this strategy no longer

works. For example, BHE #7, which is located on the edge of the field, is susceptible to a higher level of uncertainty. Similar to case study I, the single-step optimization will not be informed of the gradual thermal evolution of the ground and thus causes a relatively strong local cooling here. This is avoided by the sequential procedure (Figure 2.7d).

As the heat in the case examples of this chapter is transferred through conduction, the strongest thermal anomalies occur in the vicinity of the BHEs. Therefore, the uniformity of the thermal field is inversely proportional to the maximum temperature change. This is exemplified in the study by de Paly et al. (2012). Since the sequential optimization outperforms the single-step variant, it can be conceptually proven that the temperature field is much more uniform with sequential optimization.

2.3.3 Sensitivity analysis on the variability of heating demand

In the previous sections, the optimization procedure is applied assuming that the uncertainty in the heat demand is only due to an underestimation of the heat demand profile. Thus, as shown in Figure 2.4, this means that we were dealing only with excess heating loads. To further evaluate the general applicability of the proposed approach, the performance of sequential optimization under various uncertainty patterns of heat demand is tested. For this purpose, a stochastic study case is defined where the heat demand in each month can be overestimated, underestimated, or experience no uncertainty. We consider the configuration of the BHEs in case study I to conduct this analysis. In order to investigate the sensitivity of the proposed optimization method to varying loads, 10,000 samples are drawn from a normal distribution, $\sim N(0, 1)$. Each random sample provides a unique and new energy demand profile for the entire year that spans a differing range of uncertainty levels for each month. The optimizations, both the single-step and the sequential variants, are performed under the assumption that each random sample is a new heat demand that needs to be met. Error bars in Figure 2.8 show that the range of uncertainty in heat demand can vary from -50 % to +100 % of the initially planned profile (red bars). While all other scenario settings remain unchanged, each of these random samples is treated as an independent and unique energy demand profile for the optimization. Then, the maximum temperature change of each optimized sample is calculated over 15 operational years. A 95 % confidence interval in addition to the mean of all induced temperature changes by both optimization methods is shown in Figure 2.9.

Figure 2.9 shows even with this mixed combination of uncertainties in heat demand, the sequential method outperforms the single-step optimization by imposing on average a smaller maximum temperature change of about 2.7 K in the subsurface. This analysis guarantees that the proposed method is not tied to any particular mode or range of heating demand uncertainty. In addition, it can be stated that the seasonality of the temperature change dynamic can be captured by the proposed method in different ranges of the heat demand variations.

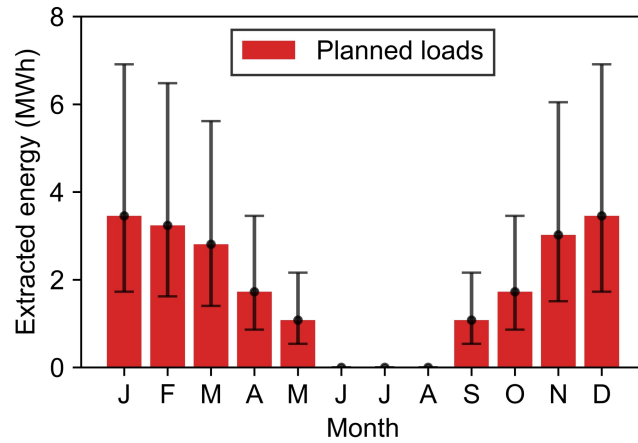


Figure 2.8: Original heat demand profile with the corresponding uncertainty range.

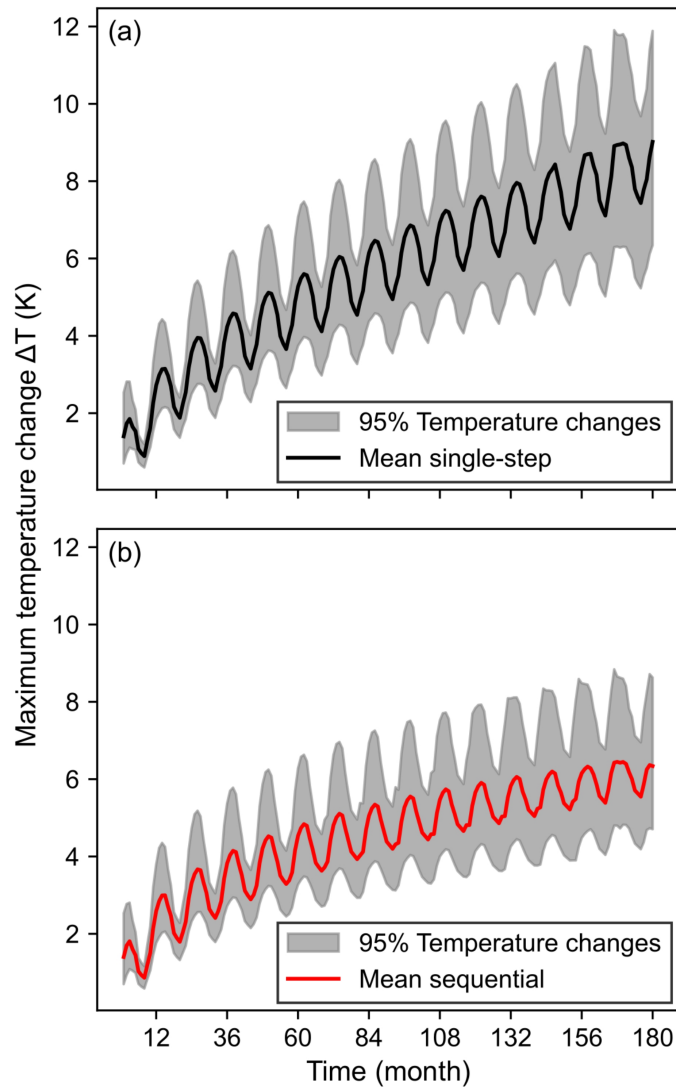


Figure 2.9: Maximum temperature change at 50 m depth considering 10,000 distinct series of uncertainty in heating demand profile by using (a) single-step optimization (b) sequential optimization for case study I.

2.4 Conclusions and outlook

Our presented work builds upon existing concepts of individual load optimization of BHEs operated together in a field. The novelty is that observations during operation are utilized to restart load optimization. This sequential concept revises the operational mode to avoid local cooling in a field. This straightforward procedure is implemented to account for deficiencies in describing ground thermal processes. We introduced the compound effect of any influencing factors that cause inaccuracy in the performance prediction in the form of a BHE-specific temperature change uncertainty level. In addition to ground-related uncertainties, the implication of energy demand variability on the evolution of thermal conditions is considered.

The results of two case studies reveal that the flexibility of sequential optimization in acquiring new information and possibility of load pattern modifications is beneficial. The allocated load patterns proposed by sequential optimization lead to lower temperature anomalies of 2.9 K and 8.9 K for fields with five and 26 BHEs, respectively, over 15 years of operation, compared to single-step optimization. The flexibility of our approach is in favor of extending the sustainable life of the system and alleviating negative environmental impacts by postponing the occurrence of the permissible maximum temperature change. In detail, the role of underestimation and overestimation of heating demand on the deterioration of optimized patterns is investigated. The advantage of the sequential optimization is demonstrated by the case studies with underestimated demand, and generally for fluctuations in heating demand in the range of -50 % and up to +100 % of the planned loads in a stochastic framework. As a next step, it is also recommended to further develop the current methodology to a procedure that not only updates the thermal conditions as a modified initial point for re-optimization, but also revises model settings in order to reduce the prediction uncertainty during the course of operation. Furthermore, it is suggested that in addition to optimizing the heat load distribution, the efficiency of the GSHP could also be included in the objective function to achieve a more inclusive optimization framework for the entire system.

Chapter 3

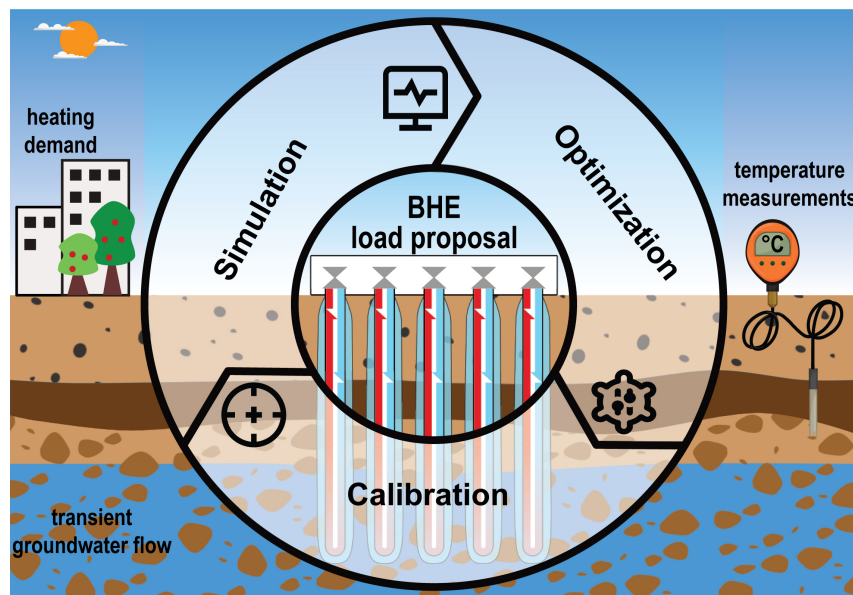
Adaptive management of BHE fields considering transient groundwater flow

This chapter has been published as:

Soltan Mohammadi, H., Ringel, L. M., Bott, C., & Bayer, P. (2024).
Adaptive management of borehole heat exchanger fields under transient
groundwater flow conditions.

Renewable Energy (234), 121060, 2024.

<https://doi.org/10.1016/j.renene.2024.121060>



3 Adaptive management of BHE fields considering transient groundwater flow

Abstract

Uncontrolled heat extraction by multiple interacting BHEs in high-density energy-use districts can lead to undesirable thermal conditions in the subsurface which can affect both system performance and regulatory compliance. The difficulty in controlling heat extraction arises in particular from predictive uncertainties, such as when forecasting trends in energy demand or groundwater flow. In this chapter, a combined simulation-calibration-optimization framework is introduced to consider BHE fields with the presence of a transient groundwater flow regime. In the first part, a semi-analytical modeling technique is proposed based on temporal superpositioning of variable flow conditions. Two synthetic case studies verify its accuracy under different groundwater fluctuation patterns. The mean absolute error of the proposed model in comparison to numerical calculation does not exceed 0.18 K over ten years of operation. In the second part, the model is augmented by a parameter estimation algorithm that is employed for continuous model updating. The benefit of resolving transient flow conditions is demonstrated by using this approach for monthly optimization of individual BHE heat extraction. The result of dynamic optimization compared to a synthetic case without calibration shows a 10 % lower imposed temperature change in the subsurface.

3.1 Introduction

In recent decades, shallow geothermal systems have arisen as a promising solution for meeting energy needs in the heating and cooling of buildings (Benz et al., 2022). Interest in these systems is driven by the pursuit of an energy transition and the impetus to reduce carbon emissions. Due to the relatively constant temperatures of the ground, sustainable heating and cooling is achieved by extracting and injecting heat through a heat carrier fluid within BHEs coupled with GSHP (Stauffer et al., 2013). Even though BHEs are the cornerstone of shallow geothermal systems, their optimal performance depends on various factors, including the often overlooked dynamic hydrogeological conditions of the subsurface. Beyond considering engineering and mechanical aspects, a detailed insight into the thermal properties of the subsurface is crucial for the reliable design of these systems. To this end, TRTs are the standard procedure to thermally characterize the subsurface that is the target for installation of single or multiple BHE fields. Here, a controlled thermal load is imposed and the subse-

quent temperature response of the subsurface is measured (Gehlin, 2002; Spitler and Gehlin, 2015). The main limitation of TRTs is their short-term nature and they are mainly carried out during the design phase. While TRTs provide valuable initial characteristics of a field including GWF effects, they cannot capture the long-term transient behavior of the subsurface thermal regime. This is due to dynamic factors and uncertainties such as seasonal variations (Yoshioka et al., 2022), long-term climatic changes (Noethen et al., 2023a), heterogeneity (Heim et al., 2022; Lee, 2011; Robert et al., 2022; Wagner et al., 2012; Zhang et al., 2022), and transient hydrogeological conditions of the subsurface (Luo et al., 2018), which can profoundly affect the performance of operating BHE fields in practice (Albers et al., 2024; Zhang et al., 2023a).

The role of hydrogeological conditions in a field with operating BHEs has been examined in various studies as they affect the governing heat transfer mechanism in the subsurface (Banks, 2015; Zhao et al., 2022). For example, Ma et al. (2021), in a system of BHEs coupled with pumping-injection well, investigated the role of groundwater-forced seepage on the thermal performance of BHEs. The impact of tidal-induced GWF on the heat exchange rate of a BHE was evaluated by Moreira et al. (2022). He et al. (2024), by creating a numerical model in combination with a physical sandbox experiment, studied various BHE configurations to optimize the operation in the presence of GWF. Deng et al. (2024) investigated the consideration of thermal imbalance in BHEs during operating periods in areas with strong seasonal groundwater fluctuations. The underlying rationale was that the accumulated heat can be balanced by the use of groundwater heat in the other seasons, thus achieving a year-round thermal balance. In a laboratory seepage box supported by a numerical model, Li et al. (2020) attempted to determine the role of GWF on the heat exchange of a BHE in a layered geological setting with saturated and unsaturated zones.

Most studies focused on investigating the role of GWF in the performance of BHEs. This emphasis stems from the constraints imposed by economic considerations and legislation, as significant changes in subsurface thermal conditions of groundwater bodies are often restricted (Blum et al., 2021; VDI, 2001). As the thermal processes in the subsurface are generally gradual and slow, uncontrolled energy extraction can lead to irreversible and potentially critical thermal anomalies. Short-term thermal imbalances directly affect the performance of heat pumps, while rectifying these anomalies in the long term poses a significant hurdle and can lead to environmental and technical complications that may call into question the feasibility of continued operation. As a remedy, various optimization methods have been developed to systemically distribute the heating/cooling demand among individual BHEs in a field. Beck et al. (2010, 2013) pioneered mathematical optimization of BHE fields, aiming to minimize temperature anomalies by tuning individual loads, thus addressing both ecological and economic concerns. Bayer et al. (2014) followed the same optimization concept and suggested identifying inefficient BHEs and decommissioning them to enhance the overall performance of the field. In further work, Hecht-Méndez et al. (2013) integrated GWF into the combined simulation-optimization framework. Aside from these earlier works, multiple efforts were undertaken to mathematically fine-tune the spacing, placement, length, and number of BHEs in fields with fixed energy demand Cimmino and Bernier (2014b); Egidi et al. (2023); Noel

and Cimmino (2022); Spittler et al. (2022, 2020). However, these optimization procedures primarily target minimizing capital costs and achieving economic efficiency by optimizing the design parameters and not the operational parameters. These procedures rely entirely on deterministic models in a commonly static manner. Static means that the modeling tool does not take into account naturally variable or uncertain future thermal states of the ground and optimal solutions are fully based on the initial prediction. However, the thermal evolution in the subsurface for several decades, given the wide array of complexities in the ground, and the ramifications of initial uncertainties, can hardly be predicted.

To increase the applicability of optimization algorithms for real world cases, it is advantageous to use dynamic optimal control strategies. The underlying idea of most optimal control strategies is centered on model simulation and retrieving feedback from the real system in a given time horizon (Heim et al., 2024a; Javadi et al., 2019). In these algorithms, by monitoring measurements and using the deviation between the measurements and the simulations, the model input parameters are adjusted and consequently, new optimized parameters are provided (Kümpel et al., 2022; Stoffel et al., 2022, 2023). Although advanced control algorithms have been employed for geothermal systems (Atam et al., 2016; De Ridder et al., 2011; Gang et al., 2014), the applied predictive models are highly simplified and typically cannot accurately reproduce the thermal dynamics of the subsurface (Ikeda et al., 2017). For instance, Soltan Mohammadi et al. (2023, 2024a) extended the optimization of load balancing in a BHE field in a sequential fashion to account for subsurface and energy demand uncertainties. However, advective heat transfer was not considered, the model parameters were not calibrated, and the uncertainty in the subsurface thermal response was not addressed from a physics-based perspective.

To make this approach more robust, the novel strategy in this work is to revisit the optimization process systematically at a certain frequency, and to update the proposals for the next months' load patterns by calibrating the model parameter based on the measured thermal history of the field. However, the frequency of model calibration can differ from the temporal resolution of the optimal load proposals. In this chapter, the learning potential of iterative simulation-optimization for management of a BHE field with transient hydrogeological conditions during the operation is investigated. The general proposed approach is to reperform the optimization after a certain period of operation, here on a monthly basis, and to take the measured thermal state of the ground as the new initial condition for the simulation of the upcoming months. By sequentially minimizing the maximum temperature variations arising from the operation of the BHEs, it is intended to impede local decline of the underground temperatures. The key idea is to mitigate extreme cooling by switching the allocated energy demand from the most critical BHEs to the ones that are theoretically less prone to local cool-downs based on the simulated results of a predictive model.

For testing and demonstration, we investigate scenarios in which the subsurface thermal conditions change due to the natural dynamics of GWF. For this, in Section 3.2.1 the moving finite line source (MFLS) is formulated to include transient GWF conditions. All details about the integration of this model in a sequential optimization-calibration process are described in

Section 3.2.2. The configuration of the BHEs, the model parameters, and the groundwater fluctuation patterns in different scenarios are presented in Section 3.2.3. In Sections 3.3.1 and 3.3.2, numerical models are developed and employed to verify the accuracy of the proposed formulation of the analytical model for a single BHE and a BHE field, respectively. The results of optimized load patterns for the BHE field and the calibration are presented in Section 3.3.3. Section 3.4 concludes the current work with an outlook on future studies.

3.2 Methodology

3.2.1 Simulation of a borehole heat exchanger field

The spatial and temporal evolution of the temperature distribution in the subsurface due to the operation of a BHE system in an aquifer can be estimated by a semi-analytical solution, the so-called MFLS model (Molina-Giraldo et al., 2011; Zeng et al., 2002):

$$\begin{aligned} \Delta T(q, x, y, z, t) = & \frac{q}{2\pi\lambda} \exp\left(\frac{\nu_T x}{2\alpha}\right) \left(\int_0^L \frac{1}{4r} \left(\exp\left(\frac{-\nu_T r}{2\alpha}\right) \operatorname{erfc}\left(\frac{r - \nu_T t}{2\sqrt{\alpha t}}\right) \right. \right. \\ & + \left. \exp\left(\frac{\nu_T r}{2\alpha}\right) \operatorname{erfc}\left(\frac{r + \nu_T t}{2\sqrt{\alpha t}}\right) \right) dz' \\ & - \int_{-L}^0 \frac{1}{4r} \left(\exp\left(\frac{-\nu_T r}{2\alpha}\right) \operatorname{erfc}\left(\frac{r - \nu_T t}{2\sqrt{\alpha t}}\right) \right. \\ & \left. \left. + \exp\left(\frac{\nu_T r}{2\alpha}\right) \operatorname{erfc}\left(\frac{r + \nu_T t}{2\sqrt{\alpha t}}\right) \right) dz' \right). \end{aligned} \quad (3.1)$$

This assumes that heat is distributed through both conduction and advection via GWF in a homogeneous subsurface with an isotropic thermal conductivity. The properties of the porous media do not depend on the temperature. Further assumptions are that the subsurface is initially at thermal equilibrium conditions, that the surface temperature is constant, and that the heat is extracted at a constant rate over the BHE length.

In Equation (3.1), $\Delta T = T_\infty - T$ refers to the temperature change with respect to the undisturbed temperature T_∞ . L denotes the borehole length, λ is the thermal conductivity, α is the thermal diffusivity, and r signifies the horizontal distance to the BHE axis ($\Delta x, \Delta y$) and the vertical axis of a borehole ($z - z'$), calculated as $r = \sqrt{\Delta x^2 + \Delta y^2 + (z - z')^2}$. It is important to emphasize that the MFLS solution provides temperature at specific distances and depths, denoted by r and z , respectively, and should not be regarded as a fully resolved 3D solution. q stands for the heat injection/extraction per length of the BHE, with a positive value indicating heat extraction. u is the specific discharge, v_a is the seepage velocity, and ν_T is the effective heat transport velocity determined by the following equations:

$$vhc_s = c_s \rho_s \quad (3.2)$$

$$vhc_w = c_w \rho_w \quad (3.3)$$

$$vhc_m = (1 - n) \times vhc_s + n \times vhc_w \quad (3.4)$$

$$v_a = u/n \quad (3.5)$$

$$\nu_T = v_a \times n \times vhc_w/vhc_m \quad (3.6)$$

The superposition principle can be applied to account for a set of boreholes $k = 1, \dots, N_{\text{BHE}}$ at locations (x_k, y_k) , a temporal variation of the load as a series of $l = 1, \dots, N_t$ load pulses $\mathbf{q} = (q_{1,1}, \dots, q_{N_{\text{BHE}},1}, \dots, q_{1,N_t}, \dots, q_{N_{\text{BHE}},N_t})^T$ for each borehole and each time-step, and a velocity $\nu_{T,l}$ that changes in each time-step l (Beck et al., 2010; Hecht-Méndez et al., 2013). This results in determining the temperature variation at any given location relative to a borehole, denoted as x_i, y_j , and at a specific time t :

$$\Delta \mathbf{T}(\mathbf{q}, x_i, y_j, z, t) = \sum_{l=1}^{N_t} \sum_{k=1}^{N_{\text{BHE}}} q_{k,l} \omega_{k,l}(x_i, y_j, z, t), \quad (3.7)$$

with the response coefficient $\omega_{k,l}(x_i, y_j, z, t, \nu_{T,l})$ defined as:

$$\begin{aligned} \omega_{k,l}(x_i, y_j, z, t, \nu_{T,l}) &= \frac{1}{2\pi\lambda} \exp\left(\frac{\nu_{T,l-1}x}{2\alpha}\right) \\ &\left(\int_0^L \frac{1}{4r} \left(\exp\left(\frac{-\nu_{T,l-1}r}{2\alpha}\right) \operatorname{erfc}\left(\frac{r - \nu_{T,l-1}\Delta t_{l-1}}{2\sqrt{\alpha\Delta t_{l-1}}}\right) \right. \right. \\ &\quad \left. \left. + \exp\left(\frac{\nu_{T,l-1}r}{2\alpha}\right) \operatorname{erfc}\left(\frac{r + \nu_{T,l-1}\Delta t_{l-1}}{2\sqrt{\alpha\Delta t_{l-1}}}\right) \right) dz' \right. \\ &- \int_{-L}^0 \frac{1}{4r} \left(\exp\left(\frac{-\nu_{T,l-1}r}{2\alpha}\right) \operatorname{erfc}\left(\frac{r - \nu_{T,l-1}\Delta t_{l-1}}{2\sqrt{\alpha\Delta t_{l-1}}}\right) \right. \\ &\quad \left. \left. + \exp\left(\frac{\nu_{T,l-1}r}{2\alpha}\right) \operatorname{erfc}\left(\frac{r + \nu_{T,l-1}\Delta t_{l-1}}{2\sqrt{\alpha\Delta t_{l-1}}}\right) \right) dz' \right. \\ &- \int_0^L \frac{1}{4r} \left(\exp\left(\frac{-\nu_{T,l}r}{2\alpha}\right) \operatorname{erfc}\left(\frac{r - \nu_{T,l}\Delta t_l}{2\sqrt{\alpha\Delta t_l}}\right) \right. \\ &\quad \left. \left. + \exp\left(\frac{\nu_{T,l}r}{2\alpha}\right) \operatorname{erfc}\left(\frac{r + \nu_{T,l}\Delta t_l}{2\sqrt{\alpha\Delta t_l}}\right) \right) dz' \right. \\ &+ \int_{-L}^0 \frac{1}{4r} \left(\exp\left(\frac{-\nu_{T,l}r}{2\alpha}\right) \operatorname{erfc}\left(\frac{r - \nu_{T,l}\Delta t_l}{2\sqrt{\alpha\Delta t_l}}\right) \right. \\ &\quad \left. \left. + \exp\left(\frac{\nu_{T,l}r}{2\alpha}\right) \operatorname{erfc}\left(\frac{r + \nu_{T,l}\Delta t_l}{2\sqrt{\alpha\Delta t_l}}\right) \right) dz' \right). \quad (3.8) \end{aligned}$$

In Equations (3.7) and (3.8), the time-steps are calculated as $\Delta t_{l-1} = t - t_{l-1}$ and $\Delta t_l = t - t_l$, where t is the current time, $t \geq t_l$ (Bayer et al., 2014; Beck et al., 2010, 2013; de Paly et al., 2012; Erol and François, 2018; Erol et al., 2015). Due to the assumption of temperature-independent parameters, the temperature distribution can be formulated as a linear problem according to:

$$\Delta \mathbf{T}(\mathbf{q}, x_i, y_j, t, \nu_{T,l}) = \boldsymbol{\omega}(x_i, y_j, t, \nu_{T,l}) \mathbf{q} \quad (3.9)$$

with $\omega = (\omega_{1,1}, \dots, \omega_{N_{\text{BHE}},1}, \dots, \omega_{1,N_t}, \dots, \omega_{N_{\text{BHE}},N_t})$. As an initial condition, $\Delta \mathbf{T}(\mathbf{q}, x_i, y_j, t_0) = 0$ holds for $t_0 = 0$.

Due to the simplifying assumptions of MFLS, the absolute temperatures simulated by this model may not fully represent the exact thermal conditions in the subsurface (Fossa, 2011). However, it can approximate the relative thermal states around BHEs accurately (Pasquier and Lamarche, 2022; Zhao et al., 2022). Since the proposed optimization approach does not depend on absolute temperature simulations, MFLS is used as a fast proxy to estimate the effects of groundwater flow in a field with multiple active BHEs. This allows for assessing the contribution of each BHE in providing the heating/cooling demands in an iterative optimization framework.

3.2.2 Optimization-calibration procedure

The underlying optimization strategy is derived from the approach originally developed by de Paly et al. (2012). Mathematically, the proposed approach involves determining the position of the BHE within a field domain $x_i, y_j \in S$ at which the highest temperature change occurs. Based on this, it reallocates the loads temporally and spatially to the other available BHEs in order to minimize the weighted sum of the maximum temperature changes over the operating time and the individual time-steps:

$$\arg \min \left(w \cdot \max(\Delta \mathbf{T}(\mathbf{q}, x_i, y_j, t_{N_t})) + \sum_{l=1}^{N_t} \max(\Delta \mathbf{T}(\mathbf{q}, x_i, y_j, t_l)) \right), \quad (3.10)$$

subject to the constraints

$$E_l = \sum_{k=1}^{N_{\text{BHE}}} q_{k,l}, \quad \forall x_i, y_j \in S, \quad l = 1, \dots, N_t \quad (3.11)$$

Within the optimization framework, this constraint serves as an essential criterion, ensuring the consistent fulfillment of energy demands across all time-steps. In Equation (3.10), priority is given to the primary term to minimize temperature variance across the entire temporal spectrum by applying a weighting factor of $w = 100$. The original concept of tuning BHE loads is to divide the operating time into l discrete intervals and derive an optimal transient heat load distribution based solely on the initial conditions at time t_0 (before the BHE field is operated), which hereafter is referred to as “single-step optimization”. This approach can only propose optimal patterns at the design stage based on the initial thermal conditions of a field.

To enable a computationally efficient solution, the previously defined objective function (Equation (3.10)) is revised to facilitate posing and solving the optimization problem as a linear one. This is accomplished by introducing virtual auxiliary variables τ_0 and τ_l :

$$\min \left(w \cdot \tau_0 + \sum_{l=1}^{N_t} \tau_l \right) \quad (3.12)$$

subject to the constraints

$$\begin{aligned}
& \Delta \mathbf{T}(\mathbf{q}, x_i, y_j, t_{N_t}) - \tau_0 \mathbf{e} < 0, \\
& -\Delta \mathbf{T}(\mathbf{q}, x_i, y_j, t_{N_t}) - \tau_0 \mathbf{e} < 0, \\
& \Delta \mathbf{T}(\mathbf{q}, x_i, y_j, t_l) - \tau_l \mathbf{e} < 0, \\
& -\Delta \mathbf{T}(\mathbf{q}, x_i, y_j, t_l) - \tau_l \mathbf{e} < 0, \\
& E_l = \sum_{k=1}^{N_{\text{BHE}}} q_{k,l}, \quad x_i, y_j \in S,
\end{aligned} \tag{3.13}$$

for all $l = 1, \dots, N_t$. \mathbf{e} denotes the vector of ones with N_{BHE} entries.

In the adaptive strategy, monthly deviations between the simulated and measured temperatures form the basis for a new optimization and the allocation of the new load patterns for the following months. The adaptive optimization process is conducted iteratively over predefined time intervals t_m ($m = 1, \dots, N_{t_{\text{opt}}}$). $\Delta \mathbf{T}_{\text{meas}}(x_i, y_j, t_{m-1})$ is considered as the real-time monitored data in the field, and $\Delta \mathbf{T}(\mathbf{q}, x_i, y_j, t_{m-1})$ is the output of simulations based on the proposed MFLS model. Taking into account the monthly measured temperature as an indicator of the actual thermal conditions of the subsurface, a revised optimal load pattern, \mathbf{q} , is computed for the individual BHEs at each time-step. This approach is implemented as an iterative loop for $m = 1, \dots, N_{t_{\text{opt}}}$:

$$\min \left(\tau_0 + \sum_{l=m}^{N_t} w_l \tau_l \right), \tag{3.14}$$

subject to the constraints:

$$\begin{aligned}
& \Delta \mathbf{T}(\mathbf{q}, x_i, y_j, t_{N_t}) - \Delta \mathbf{T}(\mathbf{q}, x_i, y_j, t_{m-1}) - \tau_0 \mathbf{e} < -\Delta \mathbf{T}_{\text{meas}}(x_i, y_j, t_{m-1}), \\
& -\Delta \mathbf{T}(\mathbf{q}, x_i, y_j, t_{N_t}) + \Delta \mathbf{T}(\mathbf{q}, x_i, y_j, t_{m-1}) - \tau_0 \mathbf{e} < \Delta \mathbf{T}_{\text{meas}}(x_i, y_j, t_{m-1}), \\
& \Delta \mathbf{T}(\mathbf{q}, x_i, y_j, t_l) - \Delta \mathbf{T}(\mathbf{q}, x_i, y_j, t_{m-1}) - w_l \tau_l \mathbf{e} < -\Delta \mathbf{T}_{\text{meas}}(x_i, y_j, t_{m-1}), \\
& -\Delta \mathbf{T}(\mathbf{q}, x_i, y_j, t_l) + \Delta \mathbf{T}(\mathbf{q}, x_i, y_j, t_{m-1}) - w_l \tau_l \mathbf{e} < \Delta \mathbf{T}_{\text{meas}}(x_i, y_j, t_{m-1}), \\
& E_l = \sum_{k=1}^{N_{\text{BHE}}} q_{k,l}, \\
& x_i, y_j \in S,
\end{aligned} \tag{3.15}$$

for all $l = m, \dots, N_t$. In this iterative process, the simulated temperatures are replaced by the measured temperatures, when they become available.

As a further modification, the first term of the objective function is divided into two separate time windows: a short-term horizon (upcoming 12 months) with higher significance ($w_l = 100$) and a long-term horizon (remaining time until the end of the operational lifetime) with lower significance ($w_l = 1$). Since the proposed optimization is an iterative process, at some point all time-steps will be considered as short time horizons with higher impact. The rationale for this is that due to different and mostly unpredictable uncertainties in long-time horizons, e.g., a few decades, it is better to consider the next year as the short-time horizon, which merits a

higher weight since its predictability is better.

In addition, the assumed model parameters will be updated simultaneously based on the measured data from all previous time-steps. This enables the algorithm not only to initiate the optimization from a correct thermal state but also to learn about the evolution of time-varying parameters that could be the cause of the deviations between the measurements and the simulations, thereby avoiding accumulation of errors. This proposed simulation-optimization-calibration procedure is referred to hereafter as “sequential optimization”.

To consider the effects of GWF on optimal BHE load patterns and system performance, this chapter assumes that the only model parameter that varies is the GWF velocity. Therefore, in the example cases, unknown GWF evolution during the course of BHE field operation is the only cause of uncertainty in the subsurface temperatures. To calibrate the GWF velocity, the problem is mathematically formulated as nonlinear least squares minimization. The discrepancy between the measured and simulated temperature is considered as an argument for the objective function. The Trust-Region-Reflective algorithm, implemented in MATLAB as an optimization technique, is employed to solve this problem. In this method, the optimization variables are iteratively adjusted within a trust region, i.e., a local region around the current solution. This algorithm effectively balances local and global information to navigate efficiently through the optimization domain, making it robust for dealing with nonlinear constraints and boundary conditions on the optimization variables. By adaptively updating the size of the confidence region and the model parameter, the algorithm converges to a local minimum of the objective function and provides a solution to the parameter estimation problem (Byrd et al., 2000).

In the proposed adaptive framework, the temporal resolution of calibration and optimization does not necessarily have to be identical. However, in this chapter, it is assumed that at the end of each month, the optimal load patterns are modified and proposed for the remaining months. Since it is presumed that monitoring takes place at the end of each month as well, the model is also calibrated on a monthly basis. Therefore, in this chapter, both the iteration of the optimization and the calibration have a length of one month. To start the optimization, the initial estimate of GWF velocity is assumed to be correct for the first month based on the site characterization measurements before the field is commissioned. From the second month onwards, once no more true information is available to revise the model parameters, model calibration makes sense. In calibration calculations, the previous month's GWF velocity is used as the initial guess. This serves as the best rough estimate. By minimizing the calibration function, a new GWF is determined and used as the input for the simulation and optimal proposals of the next months. The flowchart of the proposed method is shown in Figure 3.1.

3.2.3 Model setup

In this chapter, two scenarios of BHEs are considered; one is a single BHE, and the other is an array of ten BHEs with a spacing of 10 m. As depicted in Figure 3.2a and c, the BHEs are located in an area with a length of 200 m in each direction to reduce the influence of the model domain and boundary conditions on the results. Apart from conductive heat transfer,

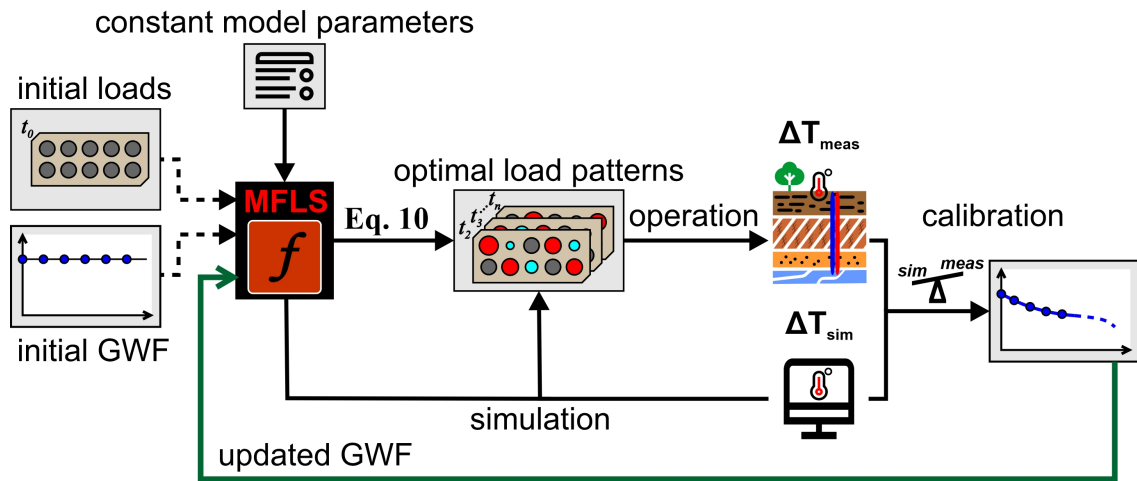


Figure 3.1: Conceptual flowchart of the proposed adaptive optimization of individual loads for BHEs in a field.

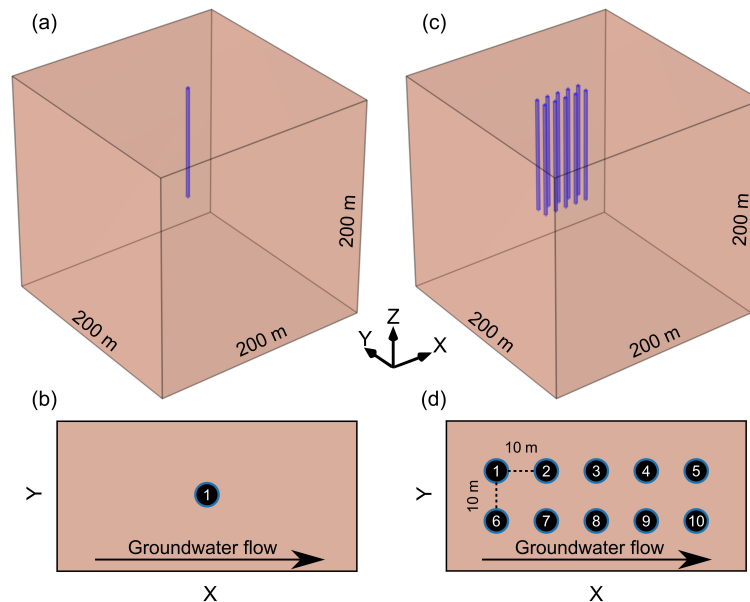


Figure 3.2: Spatial 3D layout of a field with (a) one BHE and (c) multiple BHEs. Subplots (b) and (d) depict groundwater flow direction and the top view of the field with one BHE and multiple BHEs, respectively.

advective heat transport due to GWF also contributes to the evolution of the thermal regime of the subsurface. Therefore, it is required to consider a distance of 10 m between the BHEs in order not to violate any of the underlying thermal equilibrium assumptions of the MFLS model and to avert extreme thermal influences of neighboring BHEs (Cimmino, 2015; Hecht-Méndez et al., 2013). Figure 3.2b and d illustrate the GWF direction as well as the top view of the lattice arrangement of the BHEs. Here, BHE numbers are also introduced, which will be used in the following to refer to each particular BHE. All required materials and physical properties of the subsurface and the BHEs used for the MFLS and numerical models are given in Table 3.1. For each BHE configuration, a monthly heating demand profile for the considered

Table 3.1: Parameter specifications for case studies.

Parameter	Value	Unit
Length of borehole, L	100	m
Thermal conductivity, λ	2.42	$\text{W m}^{-1} \text{K}^{-1}$
Thermal diffusivity, α	4.32×10^{-7}	$\text{m}^2 \text{s}^{-1}$
Specific heat capacity of solid, c_s	1920	$\text{J kg}^{-1} \text{K}^{-1}$
Specific heat capacity of water, c_w	4192	$\text{J kg}^{-1} \text{K}^{-1}$
Volumetric heat capacity, vhc	4819200	$\text{J m}^{-3} \text{K}^{-1}$
Solid density, ρ_s	2650	kg m^{-3}
Fluid density (at 15 °C), ρ_w	1000	kg m^{-3}
Porosity, n	0.26	-

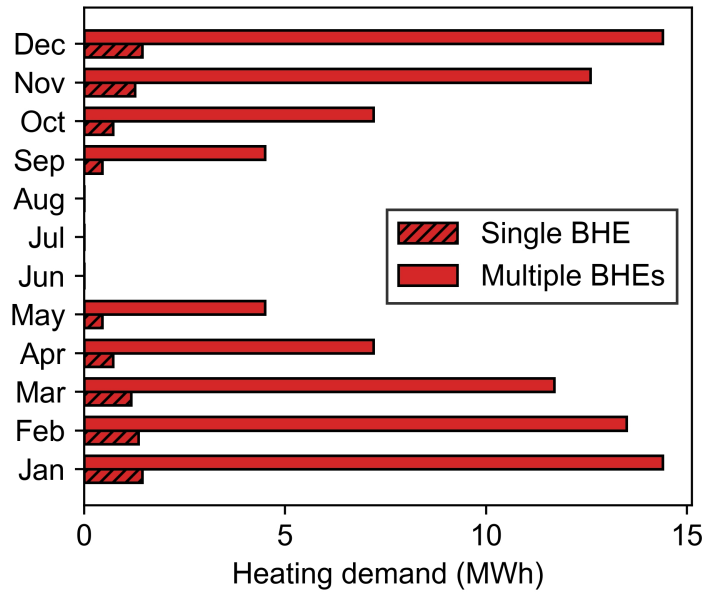


Figure 3.3: Monthly heat demand profile for both BHE fields.

BHE fields is presented in Figure 3.3. This pattern is repeated for ten years of operation. The presented energy demand is estimated for a BHE field with an annual operational duration of 1800 h. We assume a specific heat extraction rate of 50 Wm^{-1} is assumed, with a monthly distribution for a field located in a site with Central European weather conditions, only with heating application, and no energy demand in summer months. In the considered scenario with multiple BHEs, the operation takes place in parallel and each BHE is individually controllable. To evaluate the impact of GWF, six different theoretical transient GWF fluctuation patterns with monthly resolution are considered. Different evolution patterns, including linear, non-linear, and periodic with increasing, decreasing, or noisy trends, are introduced to validate the proposed rearrangement of the MFLS model (Equation (3.8)). This includes transient GWF. All GWF patterns vary from $1 \times 10^{-8} \text{ ms}^{-1}$ to $1 \times 10^{-7} \text{ ms}^{-1}$, and they are presented in Figure 3.4. In order to characterize the relative dominance of advection to diffusion in the

transport of heat in the field, the Péclet number is defined as:

$$\text{Pé} = \frac{v_a \rho_w c_w H}{\lambda} \quad (3.16)$$

where the spacing of the BHEs is considered as the characteristic length (H). The Péclet number varies in the range of 0.58 to 5.78, which represents groundwater flow velocities from low to high. These Péclet numbers indicate a broad range of heat transfer mechanisms, from scenarios where conduction dominates over advection ($\text{Pé} < 1$) to those where advection is the dominant heat transfer mechanism ($\text{Pé} > 1$). To evaluate transient heat transfer in the field, the Fourier number is calculated as:

$$\text{Fo} = \frac{\alpha t}{H^2} \quad (3.17)$$

The Fourier number for a characteristic time of ten years results in a value of 1.36.

3.3 Results and discussion

3.3.1 Single borehole heat exchanger

This section investigates the accuracy of heat transfer simulations using the proposed rearrangement of MFLS (Equations (3.7), (3.8), and (3.9)). To validate the results obtained from this semi-analytical solution, a numerical model is employed. The numerical model is implemented using the COMSOL Multiphysics® software. Temperature changes are simulated over ten years, recording the temperature change with a monthly resolution, based on the monthly energy demand profile presented in Figure 3.3. Temperature changes are recorded at four measurement locations (north, east, west, and south) around the BHE with a distance of 0.5 m from the BHE, at a depth of 50 m. The top surface of the numerical model has a fixed temperature boundary condition, and all other model boundaries are thermally insulated. A fixed temperature is applied throughout the domain as the initial undisturbed ground temperature for the model. The numerical model is carefully examined to ensure that the domain is sufficiently large, preventing any undesired effects from the boundaries due to thermal isolation. The BHEs are implemented as line heat sources with constant heat extraction rates along their lengths. To ensure the robustness of the approach, the temperature variations under the six different GWF scenarios of Figure 3.4 are considered. Figure 3.5 illustrates the resulting temperature evolution corresponding to each GWF pattern (A–F) over time. The color-coded circles in the figures indicate the error between the results obtained from the semi-analytical and numerical models. Further, the mean absolute error (MAE) of temperature change is reported for each hydrogeological scenario. The accuracy of the proposed formulation for a single BHE case among all six GWF patterns is substantiated by an acceptable error level and the replicated temperature trend, which mimics the trend of the numerical results. Across all scenarios, the MAE is between 0.07 and 0.11 K. Comparing patterns A–D indicates that decreasing GWF velocities lead to a slightly lower error level than the increasing patterns,

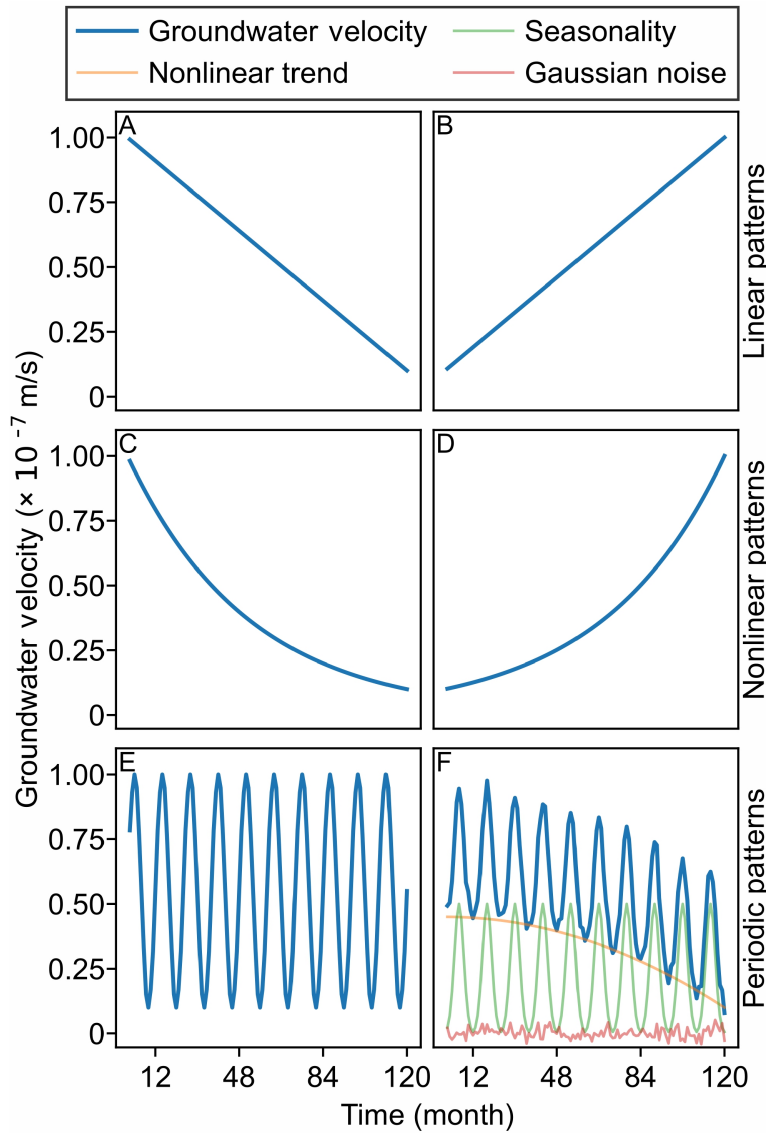


Figure 3.4: Fluctuation in groundwater velocity over the ten years of operation with (A) linearly decreasing, (B) linearly increasing, (C) non-linearly decreasing, (D) non-linearly increasing, (E) periodic, and (F) periodically decreasing pattern. Pattern (F) is the overlay of a nonlinear decreasing trend, a periodic pattern, and a random noise.

which can be attributed to slower heat propagation with decreasing thermal gradients. This is consistent with the initial thermal equilibrium assumptions made during the development of the semi-analytical model. Simultaneously, more fluctuating patterns (case E and F) still show a good agreement between the semi-analytical and numerical models. The magnitude of the error for this case is in the range of the measurement error of standard monitoring devices and therefore considered acceptable in practice.

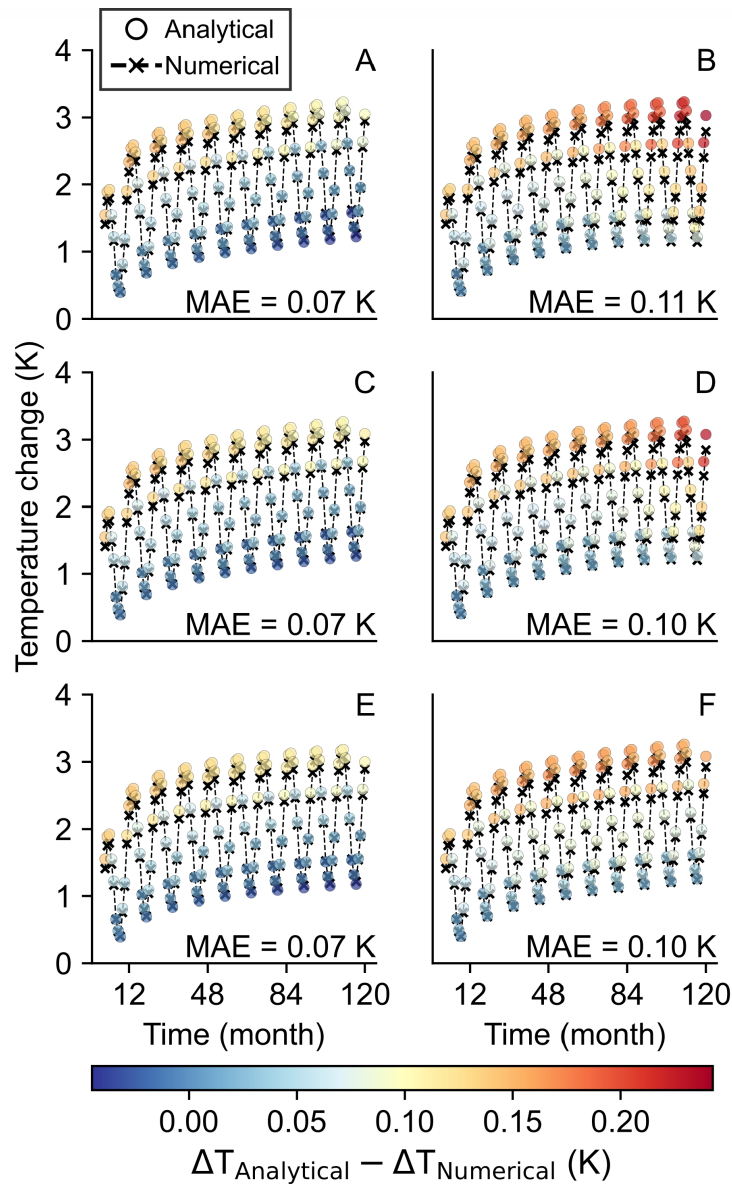


Figure 3.5: Single BHE temperature obtained at a depth of 50 m for the groundwater flow patterns A–F (see Figure 3.4).

3.3.2 Multiple borehole heat exchangers

In the previous section, the applicability and accuracy of the rearranged MFLS model are validated against a numerical model for a single BHE. However, since the optimization of BHE fields is the ultimate goal of this study, the applicability of the proposed semi-analytical formulation in an operational field with multiple BHEs needs to be verified. For this purpose, a field with ten BHEs in operation with the layout as shown in Figure 3.2 is considered. To investigate the effects of transient GWF, patterns C and F are selected for this case study (Figure 3.4). Pattern C is chosen because its nonlinear decreasing trend of GWF highlights the importance of optimization-calibration. Without model parameter estimation, the high GWF velocity at the beginning is considered for the entire operational period. Therefore, local

cooling is expected to be naturally mitigated by the high-velocity heat transport, reducing the need for optimization. However, if the hydrogeological regime changes such that the GWF decreases, the incorrect proposed load patterns can cause local thermal anomalies, if this information is not incorporated into the model. Furthermore, Pattern F is also chosen since it exhibits random fluctuations in addition to the decreasing tendency, which further complicates the simulation.

A similar numerical model is employed to serve as a reference and the accuracy of the temperature changes simulated with the MFLS model is compared with it. The boundary conditions of the numerical model are the same as those in the case of the single BHE. The temperatures are compared at a depth of 50 m and at four points evenly distributed around all individual BHEs at a distance of 0.5 m. As this is a symmetrical case, Figure 3.6 only shows the temperature development of BHE #1, #3, and #5 for both the numerical and the semi-analytical model over ten years of operation. Similarly, the color within the circles corresponds to the discrepancy between the two models. It should be noted that the maximum MAE is slightly higher for the case with multiple BHEs compared to a single BHE. Figure 3.5 shows the MAE for the whole system under six different GWF patterns, while Figure 3.6 indicates the MAE at the position of three BHEs and only for GWF patterns C and F. Therefore, the MAE values in these figures should be carefully compared. To better assess the error in each case study, the range of error for the case with one BHE is reported as 0.29 K, whereas for multiple BHES, this is 0.56 K. Despite the higher level of error, the results of the semi-analytical model for the field with multiple BHEs are still encouraging, as the absolute temperature change is also higher compared to the case with a single BHE. In addition to comparing the absolute values of the models, the evolution trend of the temperature change is also entirely consistent, which is an essential factor for optimization. The results confirm that the proposed restructured MFLS formulation can be adopted as a sound proxy for integration into a combined simulation-optimization-calibration framework for this BHEs configuration and the GWF patterns.

3.3.3 Optimal load balancing

In this section, the results of the proposed optimal load pattern for the case with ten BHEs assuming GWF pattern C are presented. The superiority of the proposed adaptive method compared to the single-step optimization approach for three selected time-steps is shown in Figure 3.7. The size of the circles depicts the relative load distribution among the BHEs in the field and the red circles show the position of the BHEs that cause the maximum temperature change. The advantage of the proposed method lies not only in the lower maximum temperature change, but also in the repositioning of the critical BHEs, which affects the location of the highest temperature change. Figure 3.7 shows a modest improvement manifested in a 10% reduction in the imposed temperature change, but it should be emphasized that both scenarios are subject to optimization, and this slight improvement highlights the role of model parameter estimation through the adaptive optimization strategy. It is also important to recognize that this discrepancy increases with longer operating time. The lack of calibra-

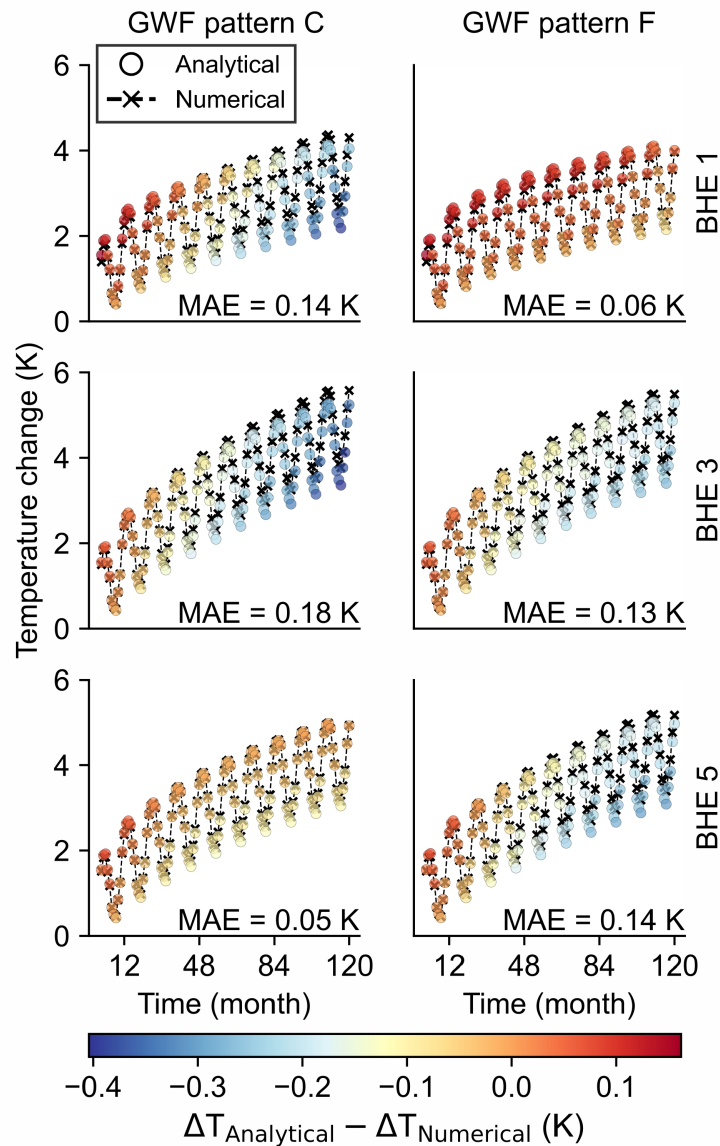


Figure 3.6: Temperature change profile (analytical vs. numerical) for BHEs #1, #3, and #5 of the considered BHE field for groundwater flow velocity pattern C and F (see Figure 3.4) over 10 years of operation.

tion functionality in the initial case by the single-step optimization, which assumes a steady and constant GWF over the operating time, leads to a misinterpretation of the critical BHEs. Essentially, the results highlight that the use of a data assimilation strategy favors a more even load distribution within the BHE field and mitigates the impact of GWF magnitude on the upstream BHEs. The calibrated GWF values compared to the real trend are shown in Figure 3.8. One interesting aspect is that, for calibration, the highest deviations occur in the summer months. This is evident as stagnation is attributed to the absence of any heating demand in the field. Thus, no new insights into the thermal conditions of the ground can be gained, which delays the learning process of the calibration, as no better values than in the previous months can be determined.

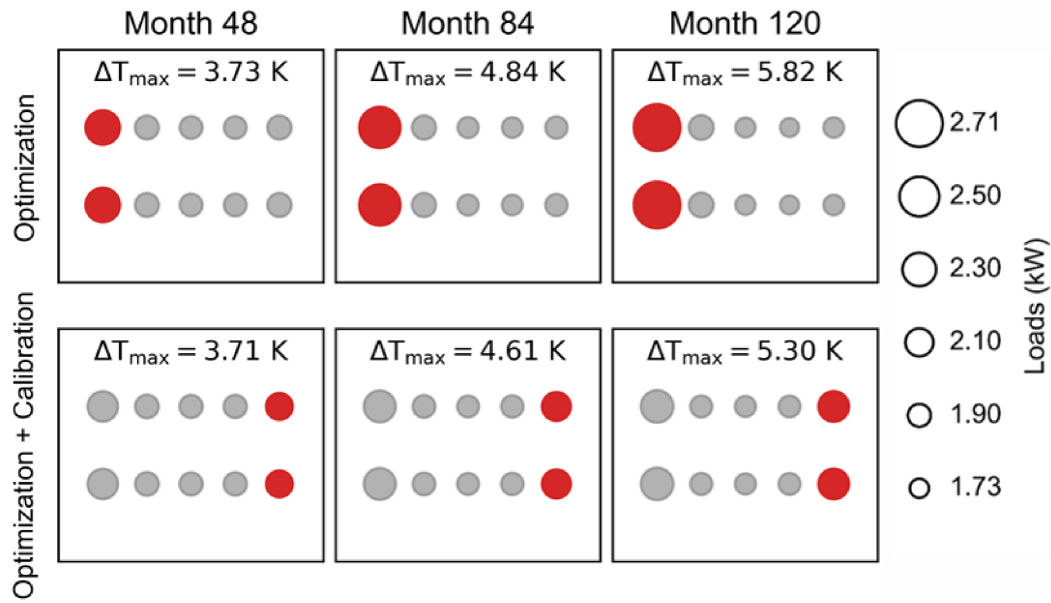


Figure 3.7: Optimal load patterns at three time-steps for the BHE field using the single-step optimization (top row) and the adaptive technique (bottom row). The size of the circles indicates the assigned load on each BHE and the red circle shows the BHE with the highest temperature change. The empty circles in the legend represent the relationship between heat extraction and the size of the circles.

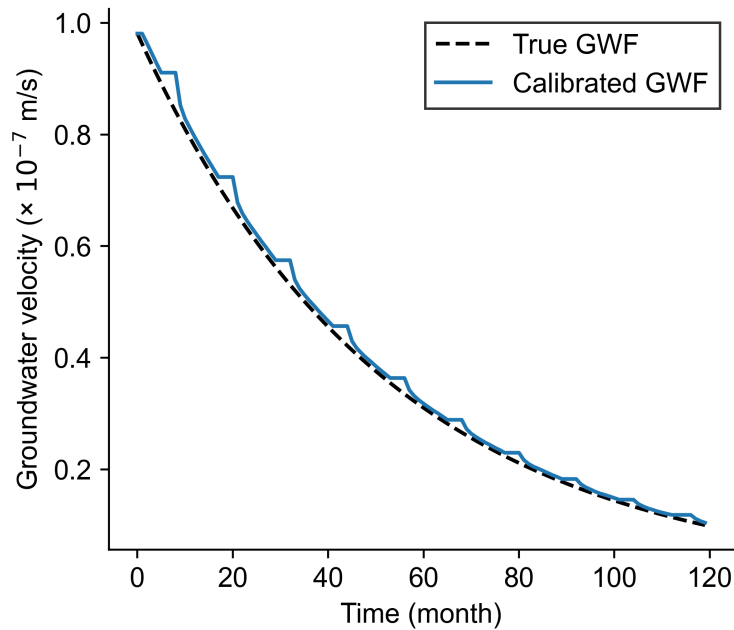


Figure 3.8: Comparison of the monthly calibrated groundwater flow velocity values obtained by adaptive optimization (blue line) with the true pattern (dashed line).

The thermal plume from the top view at a depth of 50 m is presented in Figure 3.9. To avoid errors in reporting the absolute values of temperature change in this section, the optimal load balancing is executed using the proposed approach by the semi-analytical model due

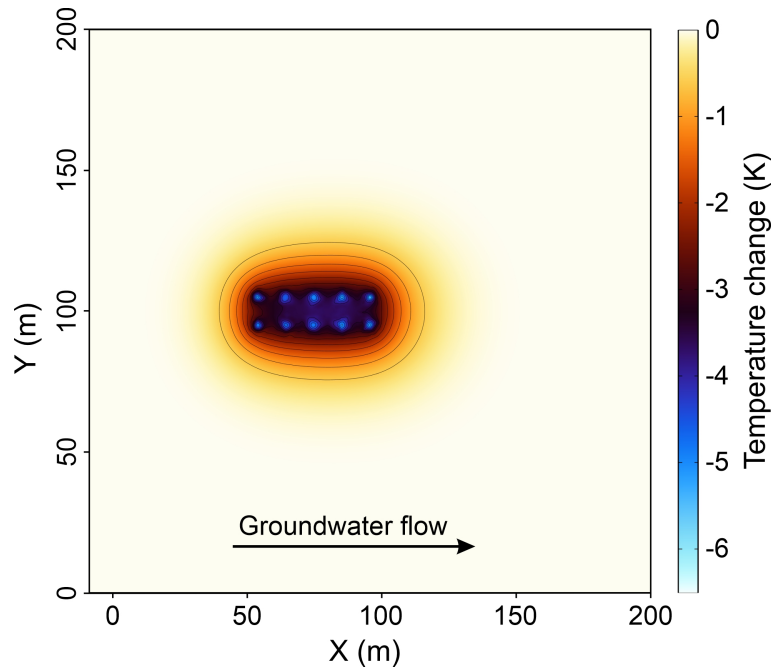


Figure 3.9: Distribution of the resulting heat plume at a depth of 50 m after 10 years of operation in the case with simulation-optimization-calibration.

to its computational efficiency and flexibility enabling the combined optimization-calibration algorithm. The absolute temperature values are based on the implementation of resulting load patterns in a numerical model.

3.4 Conclusions and outlook

This chapter focuses on tuning the heating load of individual systems within a field operating with multiple BHEs. The proposed workflow involves a four-step recursive process: simulation, measurement, calibration, and optimization. What sets this work apart from previous studies is twofold: firstly, the functionality of the widely used MFLS analytical modeling tool through the rearrangement of its formulation is enhanced. This enhancement allows us to account for transient GWF, thereby accommodating more realistic and complex subsurface conditions. It should be recalled that although the numerical model is more reliable, due to the iterative characteristic of the proposed methodology, the integration of the numerical model in the iterative simulation-optimization procedure is not computationally comparable. Secondly, the optimization process is more informative as it includes a parameter estimation in each time-step. To validate the proposed formulation, numerical modeling of two case studies with varying GWF velocity patterns as a benchmark study is conducted. Then, the modified MFLS model is employed as the predictive tool for optimization. By solving a least square problem based on monthly measurements and simulations, the GWF velocity for the subsequent month is calibrated and updated optimal load patterns for the upcoming months are proposed. The result of the optimization for the case study with multiple BHEs indicates that the potential

of the new workflow is to provide more insightful optimal load patterns that can be continuously modified. Through this modification, the imposed undesired thermal anomalies in the subsurface will be minimized. The main target of this workflow is to improve the sustainability and durability of closed-loop geothermal systems by addressing environmental concerns as well as making them economically viable. For future studies, it is proposed to integrate more robust simulation tools that can handle additional subsurface complexities, such as heterogeneity. Additionally, developing efficient proxy models to represent the subsurface complexity in a computationally feasible manner is recommended. Furthermore, using intelligent learning techniques for parameter estimation can have the potential to further enhance the efficiency of the calibration process.

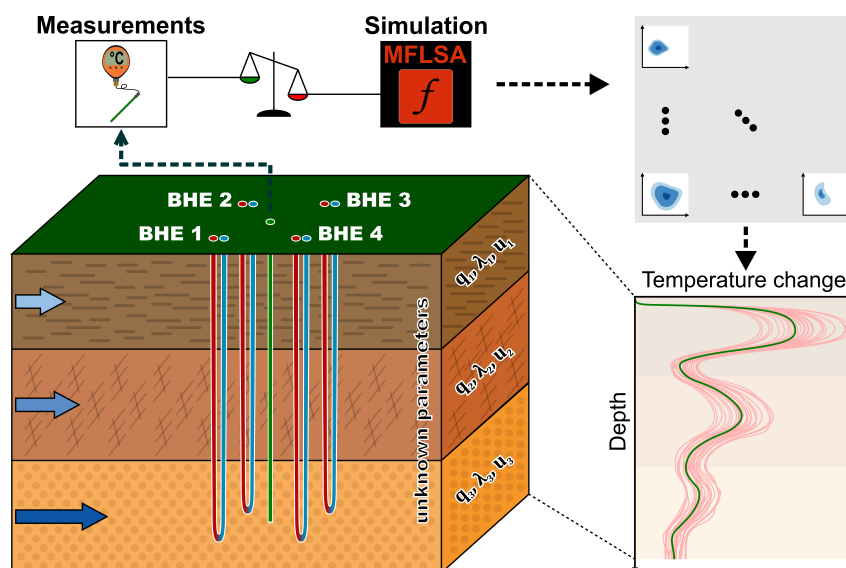
Chapter 4

Bayesian inference for stochastic modeling of BHE fields

This chapter has been published as:

Soltan Mohammadi, H., Ringel, L. M., Bott, C., Erol, S., & Bayer, P. (2025) Bayesian uncertainty quantification in temperature simulation of borehole heat exchanger fields for geothermal energy supply. *Applied Thermal Engineering* (265), 125210, 2025.

<https://doi.org/10.1016/j.applthermaleng.2024.125210>



4 Bayesian inference for stochastic modeling of BHE fields

Abstract

Accurate temperature prediction is crucial for optimizing the performance of BHE fields. This chapter introduces an efficient Bayesian approach for improving the forecast of temperature changes in the ground caused by the operation of BHEs. The framework addresses the complexities of multi-layer subsurface structures and groundwater flow. By utilizing an affine invariant ensemble sampler, the framework estimates the distribution of key parameters, including heat extraction rate, thermal conductivity, and Darcy velocity. Validation of the proposed methodology is conducted through a synthetic case involving four active and one inactive BHE over five years, using monthly temperature changes around BHEs from a detailed numerical model as a reference. The moving finite line source model with anisotropy (MFLSA) is employed as the forward model for efficient temperature approximations. Applying the proposed methodology at a monthly resolution for less than three years reduces uncertainty in long-term predictions by over 90%. Additionally, it enhances the applicability of the employed analytical forward model in real field conditions. Thus, this advancement offers a robust tool for stochastic prediction of thermal behavior and decision-making in BHE systems, particularly in scenarios with complex subsurface conditions and limited prior knowledge.

4.1 Introduction

As part of the ongoing transition to more sustainable and renewable energy sources, shallow geothermal systems present an attractive solution for heating and cooling buildings (Benz et al., 2022). These systems use the relatively stable temperatures found at depths ranging from a few tens to hundreds of meters in the subsurface. At the core of these systems are BHEs, which typically consist of high density polyethylene (HDPE) pipes arranged in U-pipe, coaxial, or double U-pipe configurations (Gil et al., 2020). A heat transfer fluid circulates through these pipes, absorbing heat from the ground in the cold season to supply buildings with heat, and returning excess heat from buildings to the subsurface in the warm season (Stauffer et al., 2013). Although BHEs are established technologies, their efficiency and ability to meet energy demands heavily rely on precise planning. This is because BHE systems are influenced by variable factors such as seasonal variations and time dependent, coupled physical processes in the subsurface. Therefore, simulating these systems for a reliable prediction of

underground thermal behavior is crucial. Accurate predictions can help avoid issues like thermal imbalance, where excessive heat extraction or injection deteriorates the system's efficiency over time. Additionally, models can assist in assessing the environmental impact and ensure that a BHE system operates sustainably throughout its intended lifespan. For example, Chen et al. (2021) examined the underperformance of a 56-BHE field implemented in Leicester, UK. They concluded that thermal anomalies in the center of the field prevent the system from operating efficiently for more than two decades.

Aside from technical issues, the thermally imbalanced operation of a BHE field can violate regulations. Haehnlein et al. (2010) and Tsagarakis et al. (2020) surveyed the legal frameworks for shallow geothermal applications in different countries. Existing frameworks and guidelines are diverse, and they delineate acceptable application windows constrained by factors such as temperature thresholds (Bayer et al., 2019; Rivera et al., 2017). Blum et al. (2021) warned that unplanned, continuous thermal exploitation of the shallow subsurface can lead to heat or cold being deemed as a pollutant. Reliable long-term predictions are therefore needed to assess compliance with precautionary regulations while ensuring safe and cost-efficient operation.

A wide variety of modeling tools has been developed to predict the thermal state, both inside and outside of BHEs. These tools range from analytical and semi-analytical to fully numerical methods. (Semi-) analytical solutions, such as those based on the so-called *g*-functions, offer simplified, closed-form formulations that allow for a quick approximation of the subsurface thermal response (Li and Lai, 2015). While these models efficiently reflect overall system thermal performance, they have their limitations when applied to complex subsurface structures with heterogeneous material properties or coupled heat transport processes. Although efforts have been made to extend the applicability of (semi-)analytical models to account for multi-layer subsurface (Guo et al., 2023), advective heat transport e.g., due to groundwater flow (Molina-Giraldo et al., 2011), land use effects and surface ground conditions (Guo et al., 2024; Rivera et al., 2015), and heterogeneous-discontinuous thermal loads (Coen et al., 2021), the majority of existing analytical models still have conceptual simplifications. Alternatively, numerical models enable detailed simulations by solving complex heat transfer equations under more realistic boundary conditions (Al-Khoury, 2011; Biglarian et al., 2017; Brettschneider and Perković, 2024; Dube Kerme and Fung, 2020; Florides et al., 2013; Huang et al., 2024; Jahangir et al., 2018; Yu et al., 2020). Numerical methods are beneficial for the design phase and initial planning, but it remains a challenge to choose a flexible and computationally efficient predictive model for real-time optimization and control of BHE fields (Heim et al., 2024a; Soltan Mohammadi et al., 2024a).

To simulate BHEs' performance analytically or numerically, ground properties must be characterized as a prerequisite. For this purpose, TRTs are usually performed at the beginning of the operation to determine the thermal properties of the subsurface, such as thermal conductivity, heat capacity, and thermal resistivity (Gehlin, 2002; Spitler and Gehlin, 2015). However, these early-phase experiments often provide only a snapshot of subsurface conditions and cannot fully capture the complex, dynamic nature of subsurface heat transfer over time. Factors such as seasonal temperature fluctuations, transient groundwater movement, and long-term

thermal interactions between BHEs within a field can significantly alter the thermal conditions in the subsurface, which initial TRT results are not able to resolve. Ideally, regular monitoring and continuous updating of subsurface models of BHE fields would be needed to account for uncertainties in model parameters or model simplifications (Heim et al., 2022).

When inferring subsurface thermal parameters or g-functions from TRTs, parameter identification typically involves defining a mathematical minimization problem or realizing the statistical distributions of parameters to assess the associated uncertainty. Among model calibration strategies, for example, (Dion et al., 2022, 2024b,a), suggest a deconvolution-based framework. This approach directly infers the transfer function from TRT data, eliminating the need for a predefined thermal model. It uses a multi-objective optimization to reconstruct the derivatives of the temperature, allowing for a data-driven construction of g-functions. Aside from this, different types of optimization techniques, such as particle swarm optimization with pattern search (Puttige et al., 2020), or trust region (Soltan Mohammadi et al., 2024b) have been explored to calibrate model parameters and improve model predictability. However, these procedures are commonly not applied in the long term, or they do not fully account for the complex conditions of the underground.

While classic model calibration techniques are computationally efficient, capturing the full complexity of subsurface conditions is challenging. This is particularly true when dealing with advective heat transport in heterogeneous ground or when numerous model parameters need to be characterized. Then, ill-posedness of the formulated calibration problem is likely to yield non-unique solutions, as well as insensitive and correlated parameters. Alternatively, probabilistic methods such as Kalman filters can be employed to enhance the accuracy of simulations by dynamically adjusting model parameters based on monitoring data (Cupeiro Figueroa et al., 2021; Shoji et al., 2023). While Kalman filter methods are efficient and capable of real-time updates, they rely on Gaussian assumptions. These can lead to inaccuracies when exploring correlated and non-Gaussian parameter spaces. Moreover, Kalman filters can encounter difficulties in dealing with highly nonlinear systems or when there is significant model misspecification, resulting in suboptimal performance in complex subsurface environments.

Bayesian inference, as another probabilistic approach, represents a promising alternative, especially through methods like Markov Chain Monte Carlo (MCMC). Unlike classic calibration methods, Bayesian inference does not merely seek to identify optimal parameter values or assume a specific distribution for the model parameters. Instead, it samples from the posterior distribution to explore a wide range of probable parameter sets.

In several studies, Bayesian frameworks have been employed to estimate subsurface thermal conductivity and borehole thermal resistance, along with the associated uncertainties (Choi et al., 2018a, 2022). Their findings highlighted the importance of test duration in enhancing the accuracy of the estimates. In other attempts, Bayesian methods have also been used to distinguish between errors arising from the TRT experiments and those stemming from the model structure itself to explicitly quantify the model bias (Choi et al., 2018b; Menberg et al., 2019). To further improve computational efficiency in Bayesian inference, Pasquier and Marcotte (2020) developed a new closed form likelihood formulation combined with neural

networks which also addresses temporal correlations in TRTs for inference of five parameters.

As recently demonstrated by Shin et al. (2024) through a global sensitivity analysis, the contribution of parameters in uncertainty assessment changes temporally during BHE operation, underscoring the need for dynamic uncertainty assessments in BHE systems. However, the majority of previous studies on the long-term thermal evolution of BHE fields have concentrated on developing sophisticated modeling tools rather than utilizing data assimilation techniques. With advancements in measurement technologies, such as distributed temperature sensing (DTS), there is an opportunity to better harness high-resolution subsurface data. This can be used to enhance model predictability and reduce input parameter uncertainty over the long term, particularly in cases involving complex subsurface structures and coupled processes (Gebhardt et al., 2024; Zhang et al., 2023a).

To address this scientific gap, this chapter introduces a new Bayesian inference-based framework that learns during operation and models the thermal evolution of BHE fields in a stochastic manner. In particular, this chapter focuses on conditions with stratified subsurface heterogeneity in the presence of groundwater over five years of operation. This framework integrates temperature measurements taken from the synthetic BHE field at defined time intervals to infer the statistical distributions of key model parameters, such as heat extraction rates, Darcy velocity, and thermal conductivity for each layer.

By characterizing these statistical distributions, a robust measure is achieved for assessing uncertainties in the model's predictions based on the most likely input parameter sets. The incorporation of temperature measurements reflects the true thermal state, which refines the predictive model, reduces uncertainties, and improves predictive accuracy. The continuous updating process is a core strength of the Bayesian approach, allowing dynamic adaptation of model parameters in response to new information.

The presented framework employs the MFLSA as the forward model (Erol and François, 2014). This model is particularly well-suited for BHE systems due to its computational efficiency, enabling the rapid evaluation of different parameter proposals during the Bayesian inference process. The MFLSA simulates the thermal state at the monitoring location in an operating field, considering the layered structure of the subsurface and the influence of groundwater flow. This accounts for variability and uncertainty in boundary conditions, changes in operational settings, and other unforeseen fluctuations in the system. A conceptual illustration of the proposed framework is presented in Figure 4.1.

The proposed methodology introduces several important advancements in modeling and analysis of the thermal behavior in closed-loop geothermal systems. Its primary contribution is an extension of probabilistic modeling to simulate temperature changes in the subsurface surrounding a BHE field over multiple years of operation. Additionally, the Bayesian framework is designed to effectively manage the highly correlated, high-dimensional parameter space associated with conductive-advective heat transport in a multi-layered subsurface, focusing on operational thermal simulation rather than using the inversion procedures for site characterization. Furthermore, the presented work broadens the applicability of analytical FLS models by relaxing the assumption of a constant heat extraction rate across the layers, thus enhancing

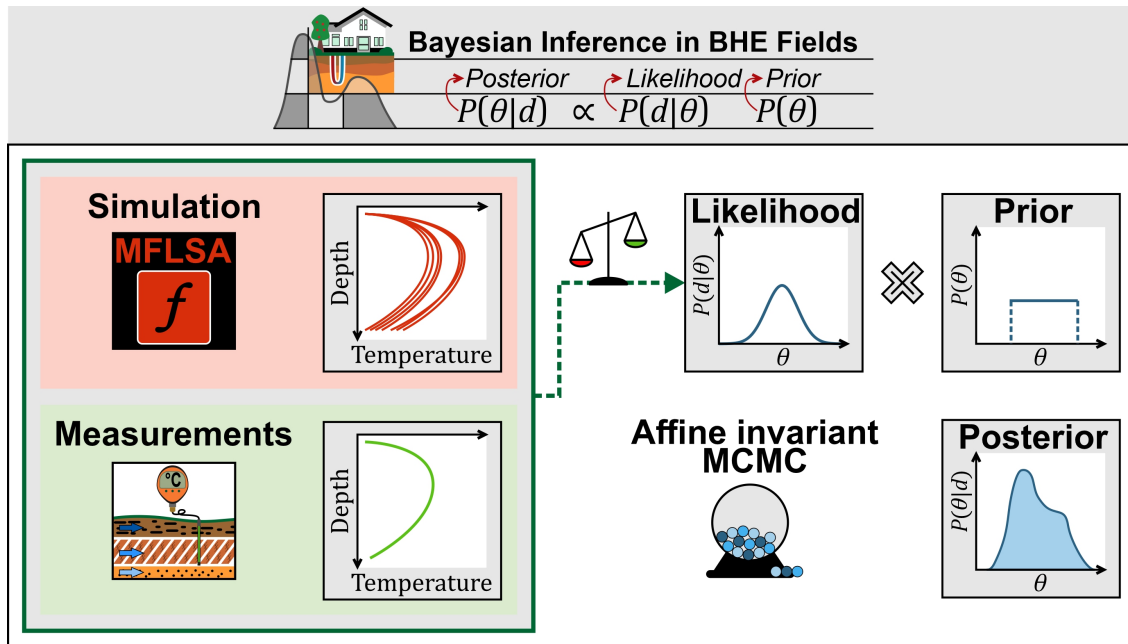


Figure 4.1: Conceptual framework of the proposed Bayesian method for stochastic predictions of temperature changes in the BHE field based on temperature measurements and using the MFLSA as the forward model.

the realism of thermal predictions in heterogeneous geological settings.

Building on these advancements, the primary objective of this chapter is to employ statistical inference to enhance the understanding of thermal state evolution within BHE fields, utilizing high-resolution operational data over time. A secondary objective is to explore the capability of Bayesian inversion to dynamically update model parameters, enabling the model to adaptively reflect observed thermal states rather than developing a new modeling tool with additional constraints.

The structure of this chapter is as follows: Section 4.2 provides an overview of the methodology, including the derivation of the forward model, the details of the Bayesian inference approach, the development of a synthetic case study, and the inversion implementation. The results of this chapter are presented and discussed in Section 4.3, followed by conclusions in Section 4.4.

4.2 Methodology

4.2.1 Forward modeling

To assess and reduce uncertainties in predicting temperature changes in a BHE field through a Bayesian framework, a forward model needs to be set up. This model should reproduce the true temperature distribution, enabling the comparison with observed data and iterative refinement of predictions. In this chapter, a line source model for BHEs is employed that considers advection and dispersion mechanisms in a multilayer porous medium. In particular,

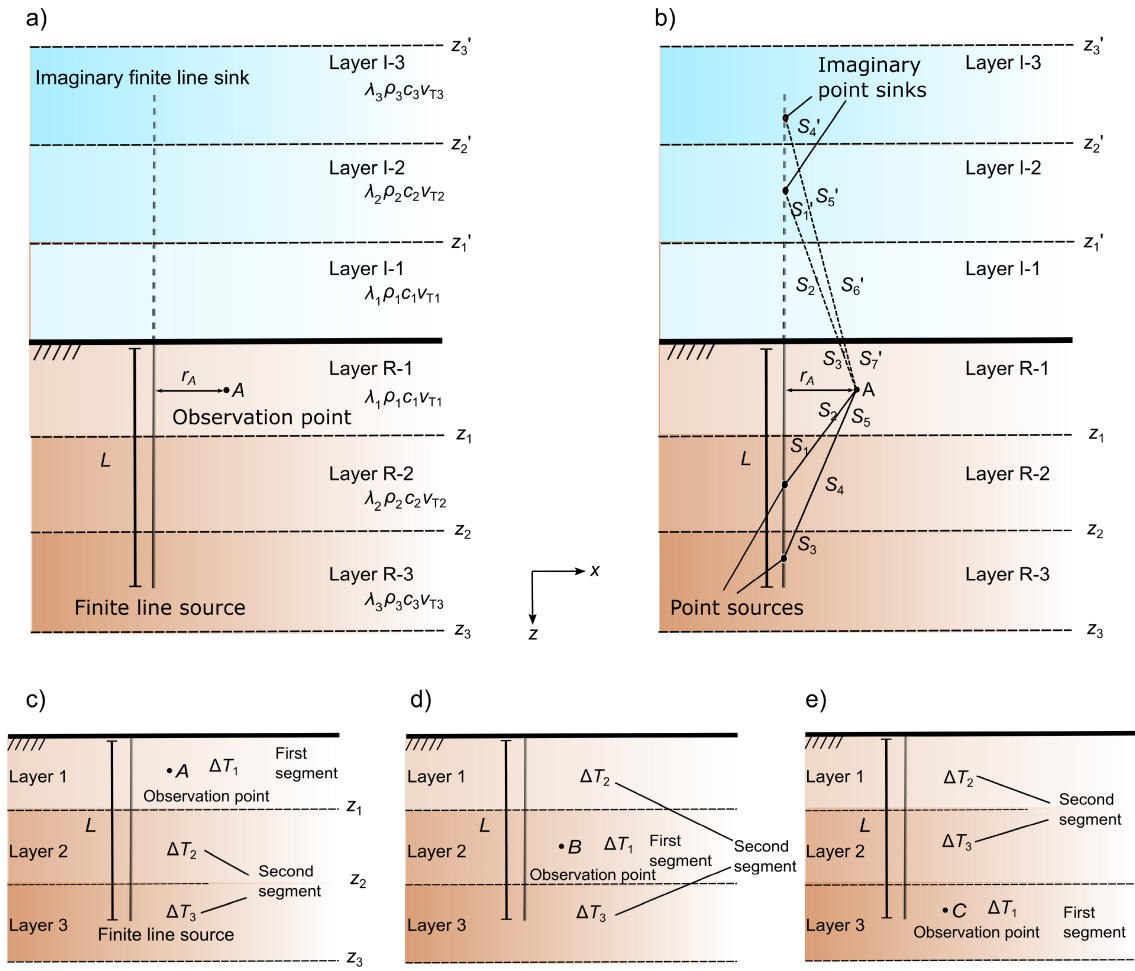


Figure 4.2: The illustration of the composite model approach for a single BHE with a finite length of L and its imaginary part passing through multi-layers.

anisotropy is added to the MFLS model. Furthermore, a composite computational approach is applied, and layers are subdivided into segments to calculate the temperature difference at a point of interest located in one of the layers. Groundwater flow is separately considered in the layers. The composite method segregates the layers and their thermal properties and adds the calculated temperature differences from each layer. For instance, if the observation point is situated in the first layer, this layer is designated as the first segment, while the other layers are assigned to the second segment (Figure 4.2). The temperature difference is computed as follows:

$$\Delta T_1(x, y, z, t) = \frac{q}{2\pi\lambda_{y1}} \exp\left(\frac{xv_{T1}}{2\alpha_{x1}}\right) \left[\int_0^{z_1} f(x, y, z, t) dz' - \int_{-z_1}^0 f(x, y, z, t) dz' \right] \quad (4.1)$$

where q is the heat exchange rate. The subscript 1 denotes the first layer and the function $f(x, y, z, t)$ is given by:

$$f(x, y, z, t) = \frac{1}{4r_A} \left[\exp\left(-\frac{v_{T1}r_A}{2\alpha_{x1}}\right) \operatorname{erfc}\left(\frac{r_A - v_{T1}t}{2\sqrt{\alpha_{x1}t}}\right) + \exp\left(\frac{v_{T1}r_A}{2\alpha_{x1}}\right) \operatorname{erfc}\left(\frac{r_A + v_{T1}t}{2\sqrt{\alpha_{x1}t}}\right) \right] \quad (4.2)$$

in which v_T is the thermal transport velocity that is calculated as:

$$v_{T1} = \frac{\text{Pé} \alpha_{x1}}{H} = u_x \frac{\rho_w c_w}{\rho_m c_m} \quad (4.3)$$

where α_{x1} is the thermal diffusivity in the first segment, $\frac{\lambda_x}{\rho_m c_m}$, H is the characteristic length, and Pé is the Péclet number:

$$\text{Pé} = \frac{u_x \rho_w c_w H}{\lambda_x} \quad (4.4)$$

Here, u_x is Darcy's velocity in the x-direction. $\rho_m c_m$ is the volumetric heat capacity of the medium, which can be calculated concerning the porosity n as the weighted arithmetic mean of the solids $\rho_s c_s$ and the volumetric heat capacity of water $\rho_w c_w$:

$$\rho_m c_m = (1 - n)\rho_s c_s + n\rho_w c_w \quad (4.5)$$

The components of effective longitudinal and transverse thermal conductivities are defined in the directions of x , y , and z as follows:

$$\lambda_x = \lambda_m + \alpha_l \rho_w c_w u_x \quad (4.6)$$

$$\lambda_y = \lambda_z = \lambda_m + \alpha_t \rho_w c_w u_x \quad (4.7)$$

where λ_m is the bulk thermal conductivity of the porous medium in the absence of groundwater flow, α_l and α_t are the longitudinal and transverse dispersivities, respectively. The thermal dispersion is a linear function of groundwater flow and relates to the anisotropy of the velocity field.

If groundwater does not exist in a layer, the heat transport velocity v_{T1} becomes zero, and the thermal diffusivity and conductivity values take on isotropic values. The integration limits $[0z_1]$ correspond to the depth coordinates of the BHE in the considered first segment layer with its imaginary part. Two additional layers (i.e., layers 2 and 3) are paired by the second segment. The subsequent layer (layer 2) is calculated as:

$$\Delta T_2(x, y, z, t) = \frac{q}{2\pi} \left[\int_{z_1}^{z_2} f_{R2}(x, y, z, t) dz' - \int_{-z_2}^{-z_1} f_{I2}(x, y, z, t) dz' \right] \quad (4.8)$$

$$f_{R2}(x, y, z, t) = \frac{1}{4\lambda_c R_2 r_A} \exp\left(\frac{xv_{T2}}{2\alpha_c R_2}\right) \left[\exp\left(-\frac{v_{T2}r_A}{2\alpha_c R_2}\right) \operatorname{erfc}\left(\frac{r_A - v_{T2}t}{2\sqrt{\alpha_c R_2 t}}\right) + \exp\left(\frac{v_{T2}r_A}{2\alpha_c R_2}\right) \operatorname{erfc}\left(\frac{r_A + v_{T2}t}{2\sqrt{\alpha_c R_2 t}}\right) \right] \quad (4.9)$$

The real and the imaginary parts of this mathematical solution are based on the method of images, which is a particular use of Green's functions. When the distribution has a geometric center, such as the point-line source, and the boundary is a flat surface, as shown in Figure 4.2, the method of images enables the distribution to be reflected in a straightforward mirror-like manner to fulfill several boundary conditions. For instance, consider the heat distribution as a function of z and a single boundary at z_b . In this case, the real domain is $z \geq z_b$, while the imaginary domain is $z < z_b$. The subscript c represents the composite and R is the real part of the geometry.

$$f_{I2}(x, y, z, t) = \frac{1}{4\lambda_c I2 r_A} \exp\left(\frac{xv_{T2}}{2\alpha_c I2}\right) \left[\exp\left(-\frac{v_{T2} r_A}{2\alpha_c I2}\right) \operatorname{erfc}\left(\frac{r_A - v_{T2} t}{2\sqrt{\alpha_c I2 t}}\right) + \exp\left(\frac{v_{T2} r_A}{2\alpha_c I2}\right) \operatorname{erfc}\left(\frac{r_A + v_{T2} t}{2\sqrt{\alpha_c I2 t}}\right) \right] \quad (4.10)$$

where I denotes the imaginary part. The computation of layer 3 in the second segment is:

$$\Delta T_3(x, y, z, t) = \frac{q}{2\pi} \left[\int_{z_2}^L f_{R3}(x, y, z, t) dz' - \int_{-L}^{-z_2} f_{I3}(x, y, z, t) dz' \right] \quad (4.11)$$

where the real part of this function is:

$$f_{R3}(x, y, z, t) = \frac{1}{4\lambda_c R3 r_A} \exp\left(\frac{xv_{T3}}{2\alpha_c R3}\right) \left[\exp\left(-\frac{v_{T3} r_A}{2\alpha_c R3}\right) \operatorname{erfc}\left(\frac{r_A - v_{T3} t}{2\sqrt{\alpha_c R3 t}}\right) + \exp\left(\frac{v_{T3} r_A}{2\alpha_c R3}\right) \operatorname{erfc}\left(\frac{r_A + v_{T3} t}{2\sqrt{\alpha_c R3 t}}\right) \right] \quad (4.12)$$

and its imaginary part is:

$$f_{I3}(x, y, z, t) = \frac{1}{4\lambda_c I3 r_A} \exp\left(\frac{xv_{T3}}{2\alpha_c I3}\right) \left[\exp\left(-\frac{v_{T3} r_A}{2\alpha_c I3}\right) \operatorname{erfc}\left(\frac{r_A - v_{T3} t}{2\sqrt{\alpha_c I3 t}}\right) + \exp\left(\frac{v_{T3} r_A}{2\alpha_c I3}\right) \operatorname{erfc}\left(\frac{r_A + v_{T3} t}{2\sqrt{\alpha_c I3 t}}\right) \right] \quad (4.13)$$

The detailed derivation of the model, the composite calculation equations of the thermal properties of layers, and the verification of the analytical solution for different hydraulic and thermal properties by comparison with a numerical solution can be found in (Erol and François, 2018). Finally, the temperature difference at the observation point A located in layer 1 is summed up as:

$$\Delta T_A(x, y, z, t) = \Delta T_1 + \Delta T_2 + \Delta T_3 \quad (4.14)$$

If the observation point is moved to layer 2, then layer 1 and layer 3 can be regarded as being in the second segment computation, by which layer 2 becomes the first segment (Figure 4.2d). The same methodology can be used to assess the observation point placed in layer 3 by shifting the segments between layers (Figure 4.2e).

The long-term temperature responses of this model over depth and time are validated for the same (hydro)geological scenario investigated in this chapter using data from (Erol and François, 2018). Details are given in the Appendix.

4.2.2 Inverse modeling

A framework is proposed that leverages Bayes' rule to invert the unknown input model parameters of the MFLSA using monthly temperature changes observed in a BHE field. Specifically, the aim is to quantify the posterior probability distributions of the model parameters $p(\theta|d_{\text{meas}})$ by using the measured temperature change data, as expressed by the following relation:

$$p(\theta|d_{\text{meas}}) \propto p(d_{\text{meas}}|\theta)p(\theta) \quad (4.15)$$

Here, θ represents the unknown thermal and hydraulic properties of the subsurface, which are treated as random variables characterized by a probability density function $p(\theta|d_{\text{meas}})$. The likelihood quantifies how well the forward model, which simulates temperature changes, agrees with the observed data. The likelihood is assumed to follow a Gaussian distribution, making the log-likelihood function proportional to the sum of squared errors between the simulated and observed temperature changes across all measurement points:

$$\log p(d_{\text{meas}}|\theta_{(1,\dots,n)}) \propto -\frac{1}{2\sigma^2 N_{d_{\text{meas}}}} \sum_{i=1}^{N_{d_{\text{meas}}}} (d_{\text{meas},i} - F(\theta_{(1,\dots,n)})_i)^2 \quad (4.16)$$

where $F(\theta_{(1,\dots,n)})$ represents the simulated temperature changes computed by the forward model, given a set of n input parameters $\theta_{(1,\dots,n)}$. The prior probability distribution function $p(\theta)$ can encapsulate any prior knowledge, assumptions, or conceptual understanding of the model parameters. The prior can be informative, based on previous studies or expert knowledge, or non-informative, such as a uniform distribution, when limited or no prior information is available.

A commonly used method for exploring the target distribution, i.e., the posterior distribution, within the parameter space is MCMC sampling (Gilks et al., 1995). MCMC generates samples that converge towards the target distribution and thus provide a numerical approximation to the posterior value. Numerous strategies have been developed in the literature to efficiently sample (Brooks et al., 2011). However, MCMC algorithms can face challenges when the posterior distribution contains sharp correlations in the parameter space and/or when dealing with a highly parameterized space. In these settings, convergence is often intractable, therefore requiring extensive tuning to improve the performance.

To tackle this issue, Goodman and Weare (Goodman and Weare, 2010) introduced the affine invariant ensemble sampler (AIES), an efficient algorithm that performs well under these conditions. AIES initializes an ensemble of L Markov Chains, known as "walkers", denoted as $\vec{\theta} = \{\theta_1, \dots, \theta_L\}$, to collectively explore the parameter space. The walkers are set up at distinct starting positions within the parameter space. Subsequently, each walker in the ensemble proposes new candidate parameter values (positions) by perturbing its current value (position) through a "stretch move" mechanism that is invariant to affine transformations of the parameter space. This means that the sampling algorithm's performance is consistent regardless of scaling, rotation, or translation of the target distribution. The proposal for each

walker ($\tilde{\theta}_i$) is generated based on a random linear combination of the current positions of the walker (θ_i), another randomly chosen complementary walker (θ_j), and an affine invariant stretch move (ζ), ensuring that the exploration of the parameter space is robust to different scales and correlations by using:

$$\tilde{\theta}_i = \theta_j + \zeta \cdot (\theta_i - \theta_j) \quad (4.17)$$

where the “stretch move” is randomly drawn from the following distribution:

$$g(z) \propto \begin{cases} \frac{1}{\sqrt{\zeta}} & \text{if } \zeta \in \left[\frac{1}{a}, a\right], \\ 0 & \text{otherwise.} \end{cases} \quad (4.18)$$

The acceptance of the proposed position is determined by comparing the log probabilities of the proposed and current values. The Metropolis-Hastings acceptance criterion is used as:

$$\log \left(\frac{p(d_{\text{meas}} | \tilde{\theta}_i)}{p(d_{\text{meas}} | \theta_i)} \right) > \log(s) \quad (4.19)$$

where p denotes the posterior probability density, and $s \sim U(0, 1)$. The schematic workflow of the sampling procedure is shown in Figure 4.3.

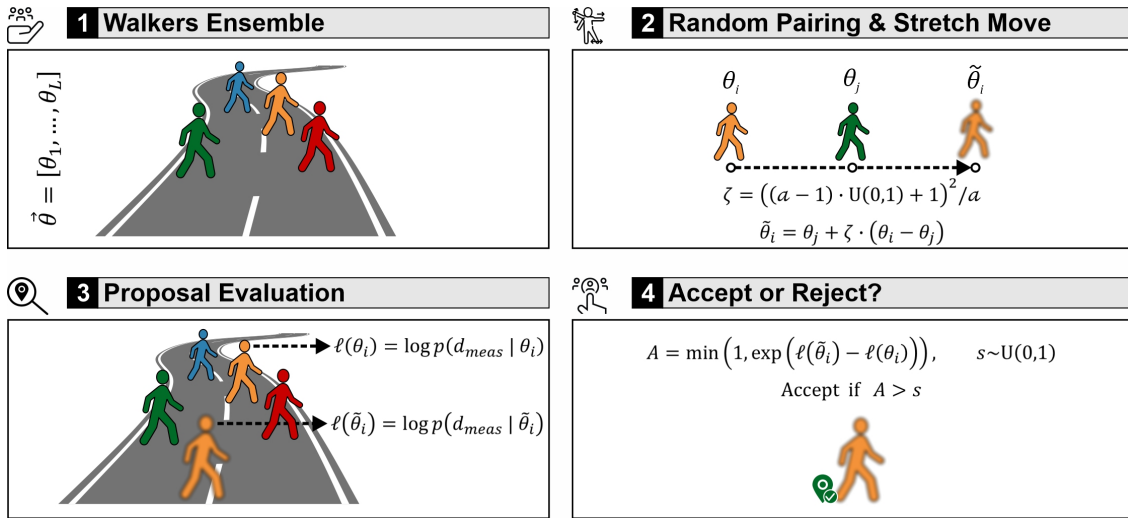


Figure 4.3: Schematic illustration of the affine invariant ensemble MCMC sampler strategy for proposing new model samples.

4.2.3 Model setup for the demonstration case

This chapter explores a synthetic BHE field to demonstrate the uncertainty quantification. The setup comprises four active BHEs and one inactive BHE, as illustrated in Figure 4.4. The active BHEs operate only in heating mode to meet thermal demands, while the inactive BHE functions as a DTS monitoring site, collecting data on subsurface temperature changes caused by the heating operation of the active BHEs, following a similar configuration as in (Gebhardt

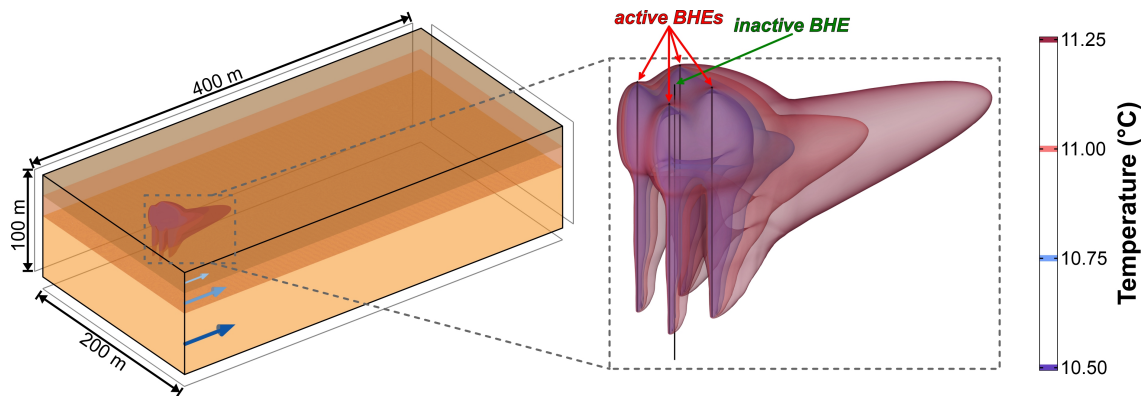


Figure 4.4: Three-dimensional view of the numerical model with three layers and groundwater flow in COMSOL (left) and the configuration of BHEs in the field showing the thermal plume after five years of operation (right).

et al., 2024). Throughout this chapter, temperature prediction using Bayesian inference focuses on the temperature evolution in the subsurface at the location of the inactive BHE over five years, resulting from the operation of the four active BHEs. Temperatures are measured monthly with a spatial resolution of 1 m, up to a depth of 60 m. As this chapter focuses primarily on the investigation of temperature dynamics in the field, temperature changes are considered rather than absolute values. The subsurface of the field is characterized by its heterogeneity, consisting of three distinct layers, each with unique thermal properties. Each layer is assumed to be 20 m thick, and each BHE reaches a depth of 50 m.

The arrangement of the BHEs in the field is carefully designed to mitigate potential extreme thermal impacts on the surrounding environment. Therefore, the BHEs are spaced 10 m apart, adhering to recommendations from (Hecht-Méndez et al., 2013). This spacing is particularly important in managing the thermal plume distribution, which is influenced by conductive heat transfer and advective mechanisms driven by groundwater flow.

Additionally, the variability in groundwater flow velocities among the different layers is considered, as it significantly affects the thermal conditions in the subsurface. As a result, the thermal state of each layer is closely tied to the prevailing hydrogeological conditions, with variations in groundwater velocity across the layers influencing the distribution and intensity of the generated thermal plume around the BHEs.

To achieve realistic thermal dynamics within this BHE field, temperatures and heat extraction rates in the layers are simulated using a numerical model developed in COMSOL Multiphysics® software. This numerical model represents the BHEs as double U-pipes, utilizing the Pipe Flow Module to simulate heat and fluid transfer within the pipes. The inactive BHE, which does not extract or inject heat, is solely dedicated to monitoring temperature variations through strategically placed sensors.

For the simulation, the inlet temperature and flow rates of the heat carrier fluid need to be specified. Each BHE is assigned a constant flow rate of 0.25 ms^{-1} , with an inlet fluid temperature set to $4 \text{ }^\circ\text{C}$. The surface and the entire model domain are maintained at an undisturbed temperature of $12 \text{ }^\circ\text{C}$, with all remaining model boundaries thermally insulated.

Table 4.1: Reference model parameters for different layer.

Parameter	Layer 1	Layer 2	Layer 3
λ_m (W m ⁻¹ K ⁻¹)	1.5	2	2.5
u (ms ⁻¹)	1×10^{-7}	1×10^{-6}	3×10^{-6}
ρ_m (kg m ⁻³)	1600	2000	2000
c_m (J kg ⁻¹ K ⁻¹)	1200	1300	1500
n	0.26	0.26	0.26

The simulation domain encompasses an area of 400 m \times 200 m \times 100 m, divided into three subdomains to represent the geological layers. The numerical model is sufficiently sized to avoid unwanted effects from the model boundaries. A fine mesh with 1,073,656 elements ensures adequate resolution and accuracy.

The Heat Transfer in the Porous Media Module is employed to account for advective heat transfer, incorporating the material properties detailed in Table 4.1 and taken from (Erol and François, 2018). By assuming a constant effective porosity, the groundwater flow velocity is proportional to the presented Darcy flow rate. The horizontal component of groundwater velocity in each layer is considered in the simulation. The study spans a simulation period of five years, with monthly monitoring of temperature changes along the observation points (inactive BHE) and the averaged heat extraction rates (active BHEs) from each geological layer for each month. This simulation period allows for a thorough analysis of the long-term thermal performance and the interaction between the BHEs and the surrounding subsurface.

Figure 4.5 shows the simulated temperature changes along the depth profile over the entire time. These values are derived from the numerical model and serve as a reference for temperature changes in the inversion process.

The average heat extraction rate from all BHEs in each layer over the entire duration is presented in Figure 4.6. These values, obtained from the numerical model, will be used exclusively to assess the efficiency of the inversion process of heat extraction rates. As illustrated in Figure 4.6, the heat exchange rate in the BHE field is primarily influenced by the subsurface properties and hydrogeological conditions of the first two geological layers, as the BHEs are 50 m deep. In layer 1 (0–20 m), heat transfer is dominated by conduction due to the very low groundwater velocity and moderate thermal conductivity. As a result, the thermal anomaly forms around the BHEs and gradually spreads outward over time. This slower heat dissipation means the heat exchange and thermal evolution will take longer to reach steady-state conditions in this layer.

In layer 2 (20–40 m), heat exchange is more efficient because of higher thermal conductivity and a moderate groundwater flow rate, which facilitates both conduction and convection. The increased groundwater flow carries heat away more effectively, allowing the system to reach steady-state conditions faster in this layer compared to layer 1.

Layer 3 (40–60 m), beyond the full reach of the BHEs, has minimal impact on heat transfer, although heat diffuses into it over time. Layer 3 has the highest groundwater velocity and thermal conductivity and it does not fully interact with the BHEs, limiting its effect on heat

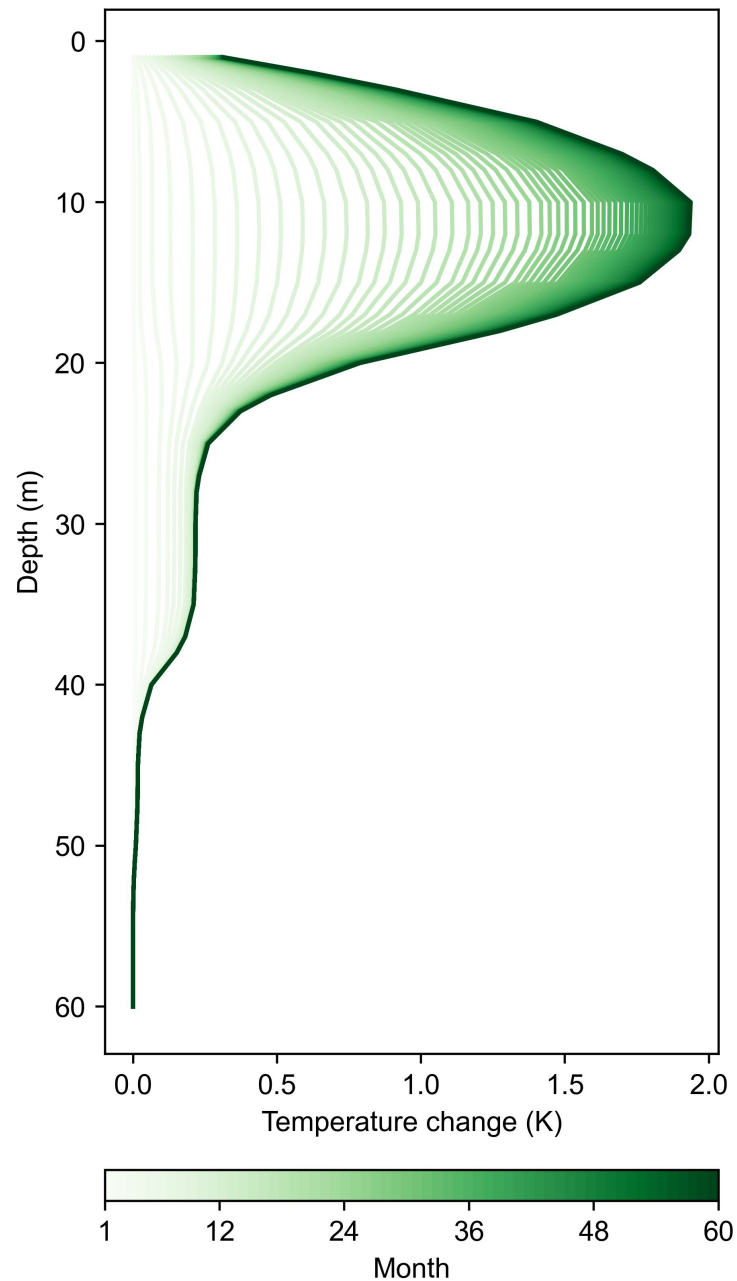


Figure 4.5: Reference monthly temperature changes along the depth, simulated by the numerical model.

exchange. As a result, steady-state conditions in this layer are reached faster than in the others, which has a minor influence on the overall heat exchange performance.

In the following sections, the synthetic operational scenario simulated by the numerical model will be used to showcase the application of the proposed Bayesian procedure. It is important to note that the numerical model and its results are not part of the proposed Bayesian framework; they are solely used to demonstrate how the procedure works. In practice, the COMSOL model results should be replaced with field data measurements. The effectiveness

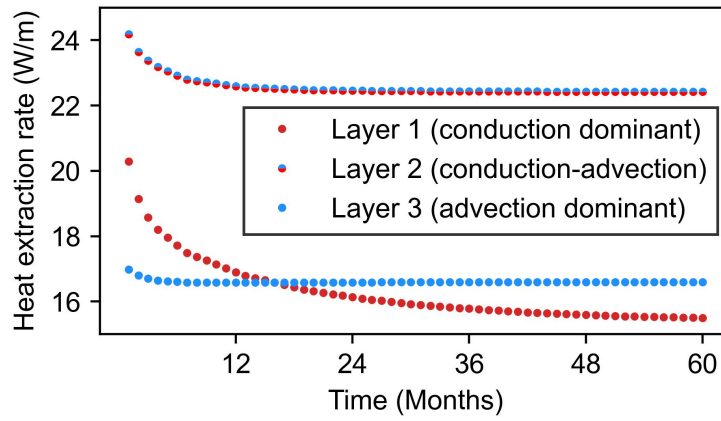


Figure 4.6: Reference average heat extraction rate of BHEs in different layers, simulated by the numerical model.

of the Bayesian inversion procedure in modeling and predicting the subsurface temperature changes depends on the suitability of the forward model in accurately describing the underlying physical processes.

To model temperature changes around the BHEs in a multi-layered subsurface with groundwater flow, the well-established, computationally efficient MFLSA is employed, as discussed in Section 4.2.1. This analytical model captures the key physics involved, ensuring the reliability of the Bayesian inversion results. Although the numerical setup developed in this section serves only as a synthetic case for measured temperatures in the field to demonstrate the proposed approach and does not require validation, it is useful to ensure that associated uncertainties in the inversion procedure are not caused by unexplained variability in temperature changes due to the modeling tools. To address this, the numerical setup is validated against the MFLSA using reference model parameter values at selected time-steps, as shown in Figure 4.7. The MFLSA analytically simulates temperature changes at these time-steps, assuming that temperature changes from earlier time-steps are measured and known. The results indicate that the MFLSA predictions closely align with the numerical model, confirming two key points: first, the forward model can accurately represent the numerical setup in this case, and second, the uncertainties of interest, which will be discussed in later sections, are not due to the inherent reliability of either the numerical or analytical model.

4.2.4 Implementation of the inversion procedure

This section details the specific setting of the inversion problem for the introduced BHE field. The goal of the inversion process is to determine the distribution of three unknown parameters — heat extraction rate (q), thermal conductivity (λ), and Darcy velocity (u) — across three layers, resulting in an inverse problem with nine parameters over 60 time-steps.

For each unknown parameter, a uniform prior distribution within a specified range $[\alpha, \beta]$ is

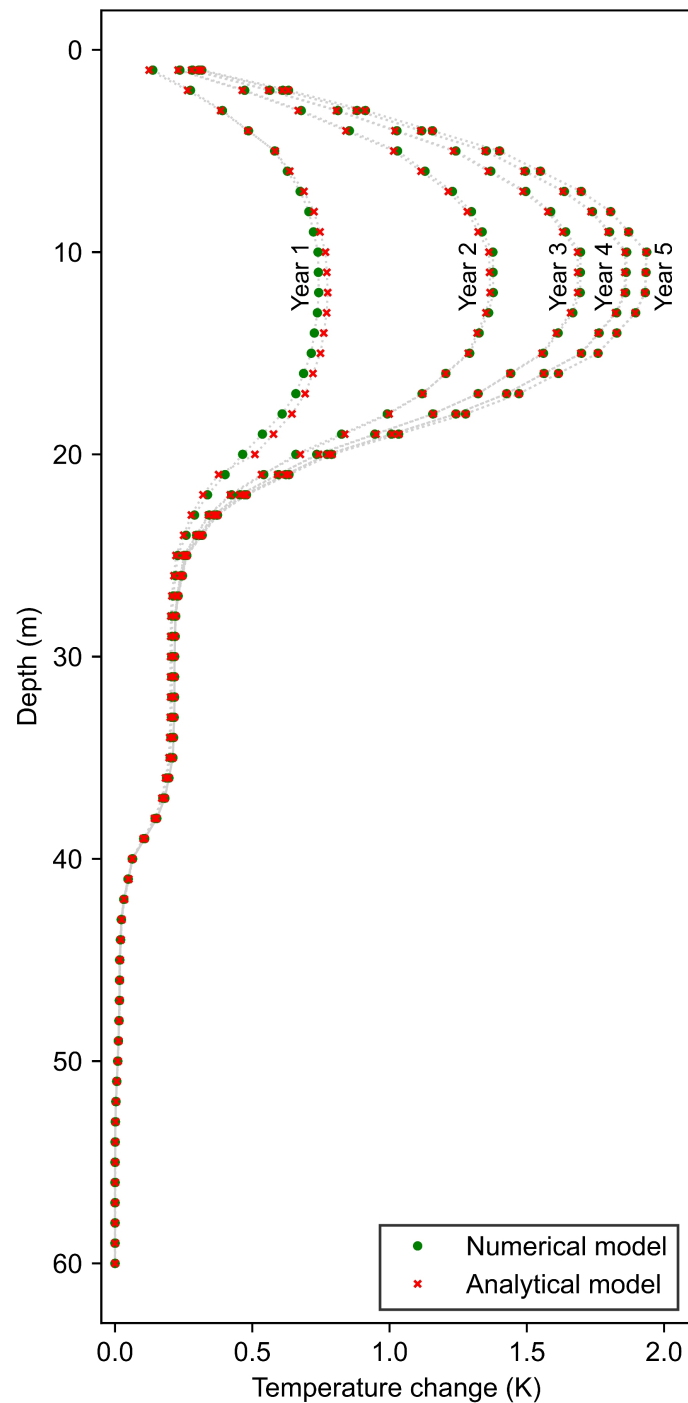


Figure 4.7: Validation of the numerical results against the forward model at five time-steps, using reference input values and assuming known temperature changes from earlier time-steps.

assumed, reflecting the absence of strong prior information:

$$p(\theta) = \begin{cases} \frac{1}{\beta-\alpha}, & \text{if } \alpha \leq \theta \leq \beta, \\ 0, & \text{otherwise.} \end{cases} \quad (4.20)$$

The choice of this prior ensures that all values within the range $[\alpha, \beta]$ are equally likely before considering the observed data, thereby allowing the data to primarily drive the inversion process.

Specifically, the range for parameters is as follows: heat extraction rate ranges from 5 to 40 Wm^{-1} , thermal conductivity ranges from 0.5 to 4 $\text{Wm}^{-1}\text{K}^{-1}$, and Darcy velocity can vary from $6 \times 10^{-8} \text{ms}^{-1}$ to $6 \times 10^{-6} \text{ms}^{-1}$.

The variance of the likelihood function in each time-step is derived from the error between simulated and observed temperature changes in the previous time-step.

For the implementation of AIES, similar to the “walk move” formulation in Christen and Fox (2010), this density function is simulated using a transformed uniform distribution. However, unlike the “walk move”, which is not affine invariant, the “stretch move” applied by the AIES formulation ensures affine invariance (Grinsted, 2018):

$$\zeta = ((a - 1) \cdot U(0, 1) + 1)^2 / a \quad (4.21)$$

Here, a is the step size and is set to 2 in our study, and U is a uniform distribution between 0 and 1.

In this chapter, the MATLAB implementation by Grinsted (2018) is used. In each time-step, 50,000 iterations and 180 walkers are employed to generate 5,040 samples for each unknown parameter.

The temperature changes shown in Figure 4.5 are assumed to be the actual measurements, with MFLSA being used in the forward solver for predicting temperature changes. At the end of each time-step, the median of all samples for each parameter is considered as the inferred model parameter for the simulation of the upcoming months. Additionally, simulated temperature change values of the current month are replaced by measured data as they become available. The process involves superimposing the current measured temperatures onto the predictions for future time-steps.

4.3 Results and discussion

4.3.1 Statistical analysis of MCMC sampling

In this section, the performance of MCMC sampling with the affine invariant ensemble sampler (AIES) algorithm is evaluated. The purpose of this analysis is to determine whether the sampling process effectively explores the target distribution and has reached convergence—a state where the sampled values stabilize around the target distribution.

To assess convergence and sampling efficiency, trace plots are used, which display the progression of the parameter estimation. Trace plots help to reveal whether the “walkers” (or model samples) are thoroughly exploring the range of possible parameter values or, conversely, are becoming confined to certain areas. Effective sampling should ideally result in a trace plot where the walkers exhibit a random, well-distributed pattern, covering the parameter space without showing a clear trend. In this chapter, trace plots are examined at five selected

time-steps for nine unknown model parameters, including heat extraction rate (q), thermal conductivity (λ), and Darcy velocity (u) across three different layers. For clarity, only every tenth sample is shown in Figure 4.8. The mean of all samples is also analyzed, and an overall trend is identified using linear regression to capture any underlying patterns. The trace plots reveal an erratic pattern, indicating that the walkers are "well-mixed", i.e., they move freely across the parameter space without becoming confined to specific regions. This pattern suggests effective exploration of the target distribution (Brooks et al., 2011).

Most parameters in the trace plots exhibit stable, consistent patterns over time, with no discernible trends, suggesting that the samples have reached convergence, meaning they center around the target distribution. However, two exceptions occur: in the sixth month, thermal conductivity in the first layer displays a slight decreasing trend, while groundwater velocity in the third layer shows an increasing trend. These trends do not persist in later time-steps, further supporting the finding that the walkers have reached the target distribution. Over time, the parameter values fluctuate around a consistent mean, indicating that the samples are in a stationary state with stabilized sampling behavior. It is also observed that the amplitude (range) of fluctuations, in the trace plots increases slightly over time, i.e., in the earlier time-steps, the samples exhibit a tighter range of values for the model parameters. This is because, in the early months, larger temperature changes better constrain the parameter estimation, narrowing the search radius within the plausible exploration space. In summary, this analysis shows that the sampling has achieved stationarity, consistently exploring the parameter space without exploration bias, in a well-mixed manner. In the next step, to assess whether the generation of each sample is independent of other samples, autocorrelation plots are employed (Figure 4.9). Autocorrelation measures the similarity between the samples as a function of "lag", i.e. the number of iterations between samples. Constant high autocorrelation indicates that samples are too similar, suggesting poor mixing of the sampling methodology. Effective MCMC sampling should display decreasing autocorrelation with increasing lag, showing that samples become more independent as the gap between them grows (Roy, 2020).

In Figure 4.9, autocorrelation is calculated for the samples of each model parameter at various time-steps, with a thinning factor of 100 and a maximum lag of 50. For most parameters, autocorrelation decreases as the lag increases, indicating that realized samples are relatively independent and that the walkers mix well. However, an exception is found in the Darcy velocity of the first layer (u_1), where repetitive spikes in autocorrelation appear at later time-steps, indicating higher correlations between nearby samples. This pattern suggests that u_1 may have converged to its target distribution earlier, resulting in less variability in subsequent samples. This could indicate that the early temperature data strongly constrains this parameter, generating samples that consistently reflect the already determined target value. This implies a so-called high information content of the temperature data during early time-steps for the first layer.

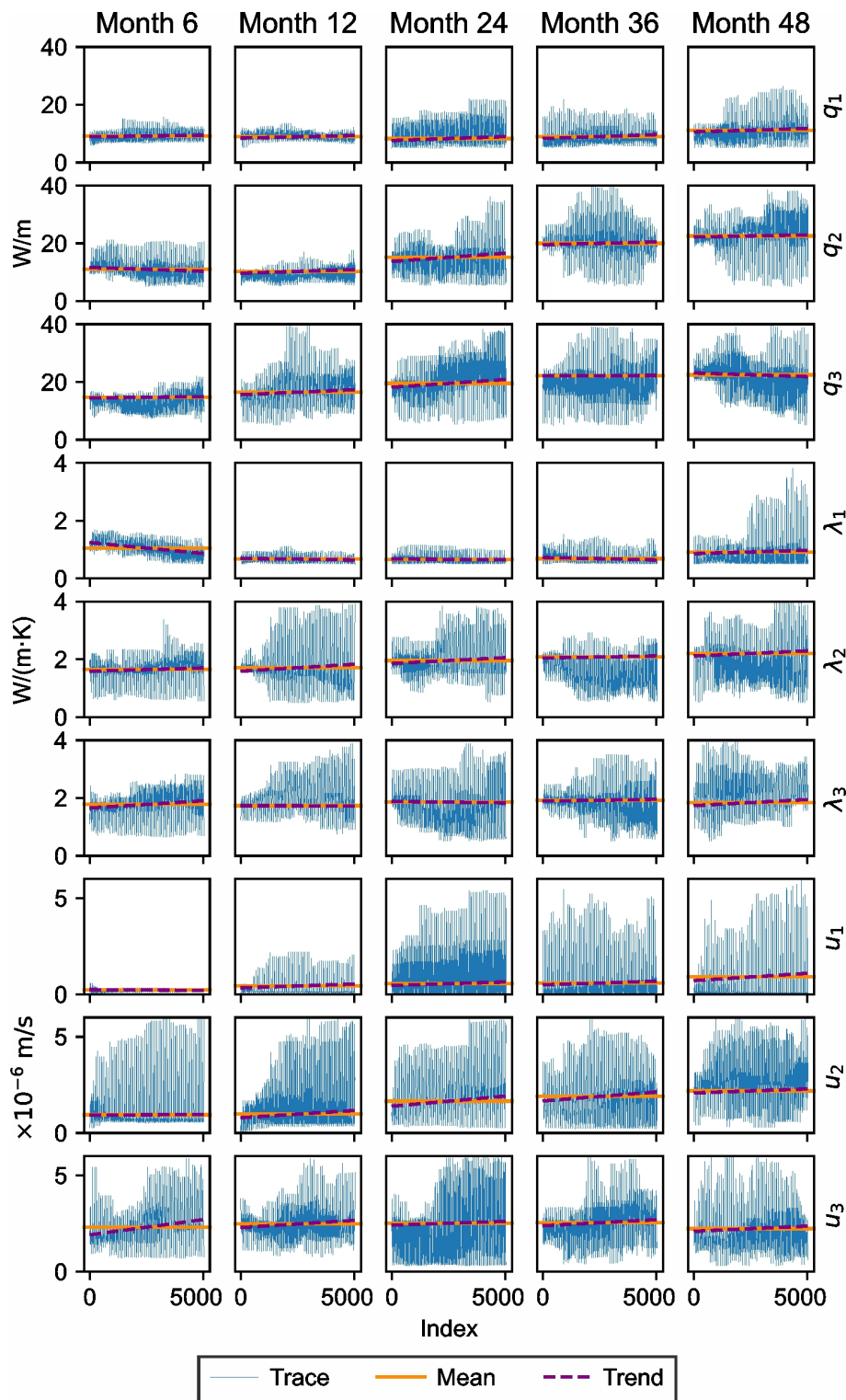


Figure 4.8: Trace plots of model samples for nine parameters (heat extraction rate (q), thermal conductivity (λ), and Darcy velocity (u) for three layers) at five different time-steps.

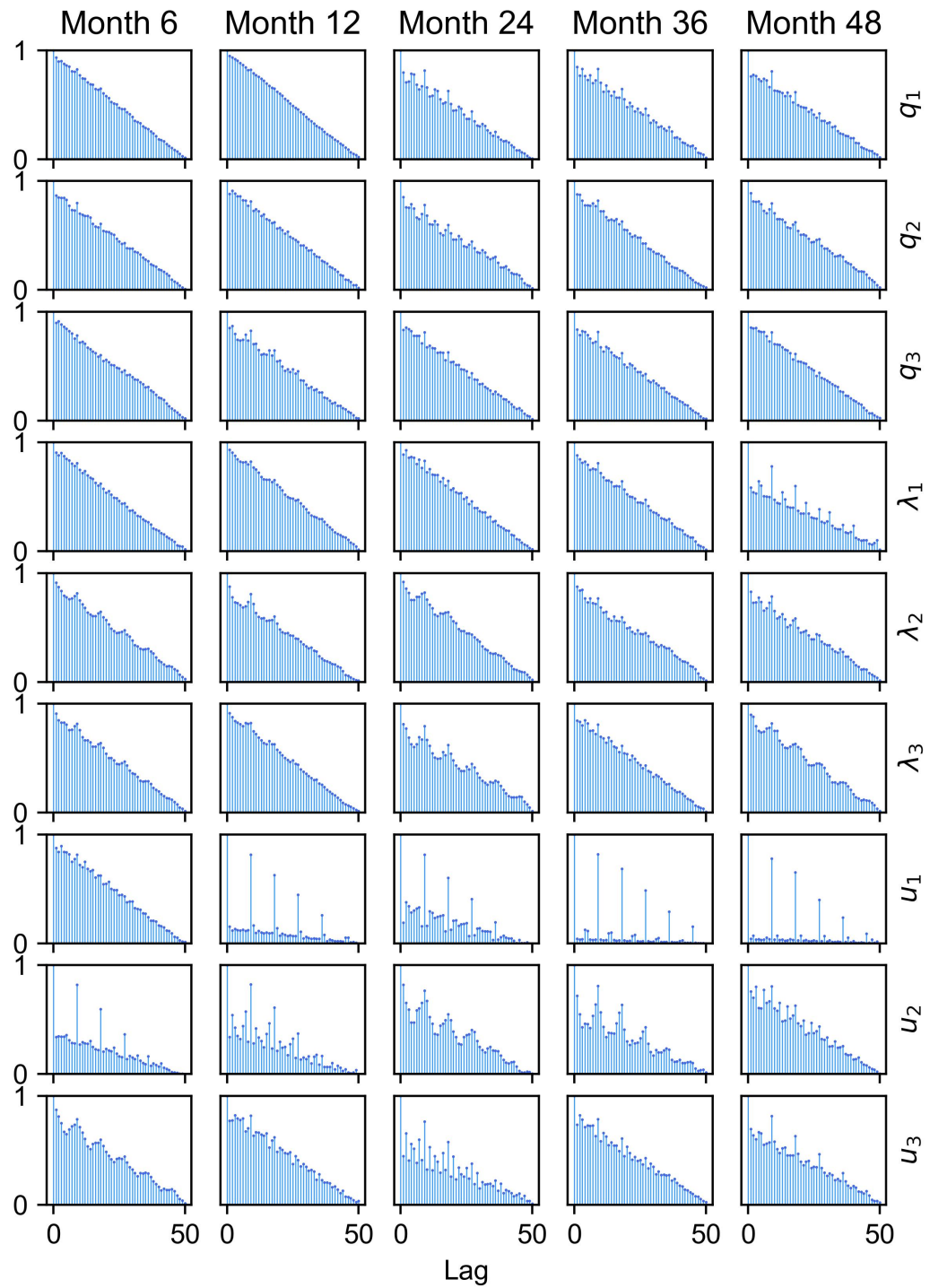


Figure 4.9: Autocorrelation of the nine model parameters (heat extraction rate (q), thermal conductivity (λ), and Darcy velocity (u) for three layers) at five different time-steps, up to a lag of 50.

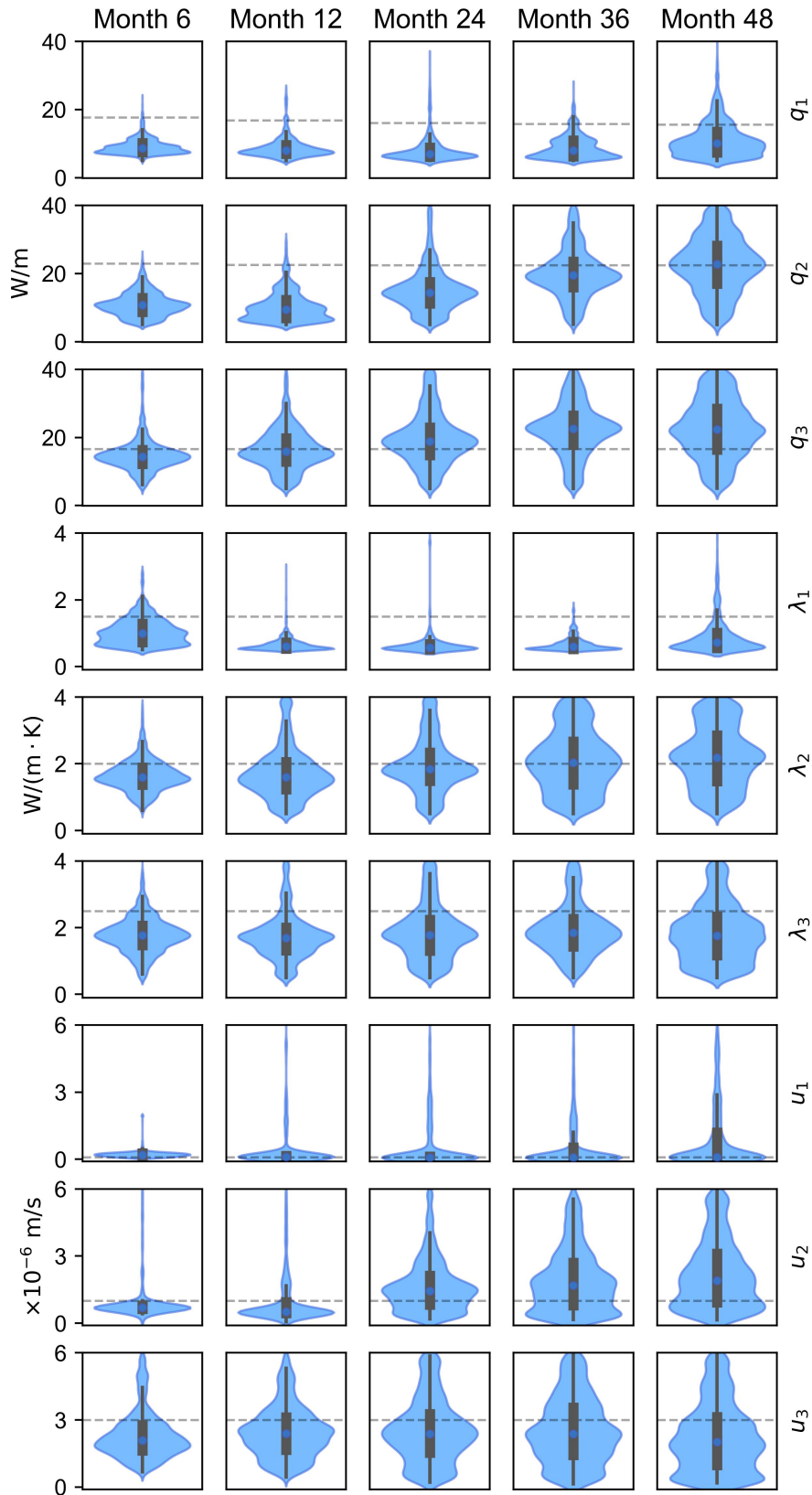


Figure 4.10: Violin plots of the nine model parameters (heat extraction rate (q), thermal conductivity (λ), and Darcy velocity (u) for three layers) at five different time-steps. The dashed line represents the reference value for each parameter.

4.3.2 Evaluation of the posterior samples

To gain a deeper understanding of the results from the MCMC sampling, violin plots are used to visualize the distributional characteristics of the generated model parameter samples (Figure 4.10). These plots are particularly useful in this context, as they reveal the density and variability of the generated model samples. Figure 4.10 illustrates this information for all parameters, using the same selected time-steps shown in the previous figures, providing a more comprehensive view of how the uncertainty in the model samples evolves. As shown in Figure 4.10, the parameters in the first layer are more tightly distributed when compared to those in the other layers.

This narrower distribution in the first layer corresponds to earlier findings, which suggested that the thermal state in this layer, influenced by lower advection, leads to more significant temperature changes. These changes indicate high parameter sensitivity, which in turn helps to constrain the parameter space more strictly.

In the first layer, the samples for both thermal conductivity (λ_1) and Darcy velocity (u_1) are clustered around a single mode for most time-steps, indicating high certainty in the parameter estimates. This is particularly evident for Darcy velocity (u_1), where the statistical distribution is especially tight. This aligns with the autocorrelation analysis from Figure 4.9, which showed that after a few months, the inference of groundwater flow rate in the first layer has stabilized. Therefore, further Bayesian investigations for this parameter would not be necessary and could be treated as a minimization problem instead. However, the strong correlations between parameters and interactions across layers still necessitate the use of the Bayesian framework to understand the relationships in the parameter space.

In contrast, the distributions of Darcy velocity samples in the second (u_2) and third (u_3) layers show greater variability. This can be attributed to the heat transfer dynamics in these layers, where slower thermal changes in later time-steps lead to less pronounced temperature shifts. As a result, a wider range of groundwater flow values can explain the observed temperatures, leading to greater uncertainty in the parameters for these layers. The consistent findings that the parameters in the first layer exhibit the strongest correlations indicate that they are the most influential factors in determining temperature changes in the field. To further explore the relationships between pairs of model parameters, an analysis of the correlation between the heat extraction rate (q_1), thermal conductivity (λ_1), and Darcy velocity (u_1) in the first layer in the sixth month is performed. This analysis is illustrated in Figure 4.11, where the lower left triangle of the figure displays contour plots, while the upper right triangle features hexbin plots. Each hexagon represents a minimum of 15 samples at that position in the parameter space, with darker colors indicating higher frequencies of samples. The diagonal subplots show histograms of sample distributions, along with the estimated kernel density distributions.

The histogram of correlations reveals a multimodal distribution for heat extraction rate and thermal conductivity, while a unimodal distribution is observed for groundwater flow.

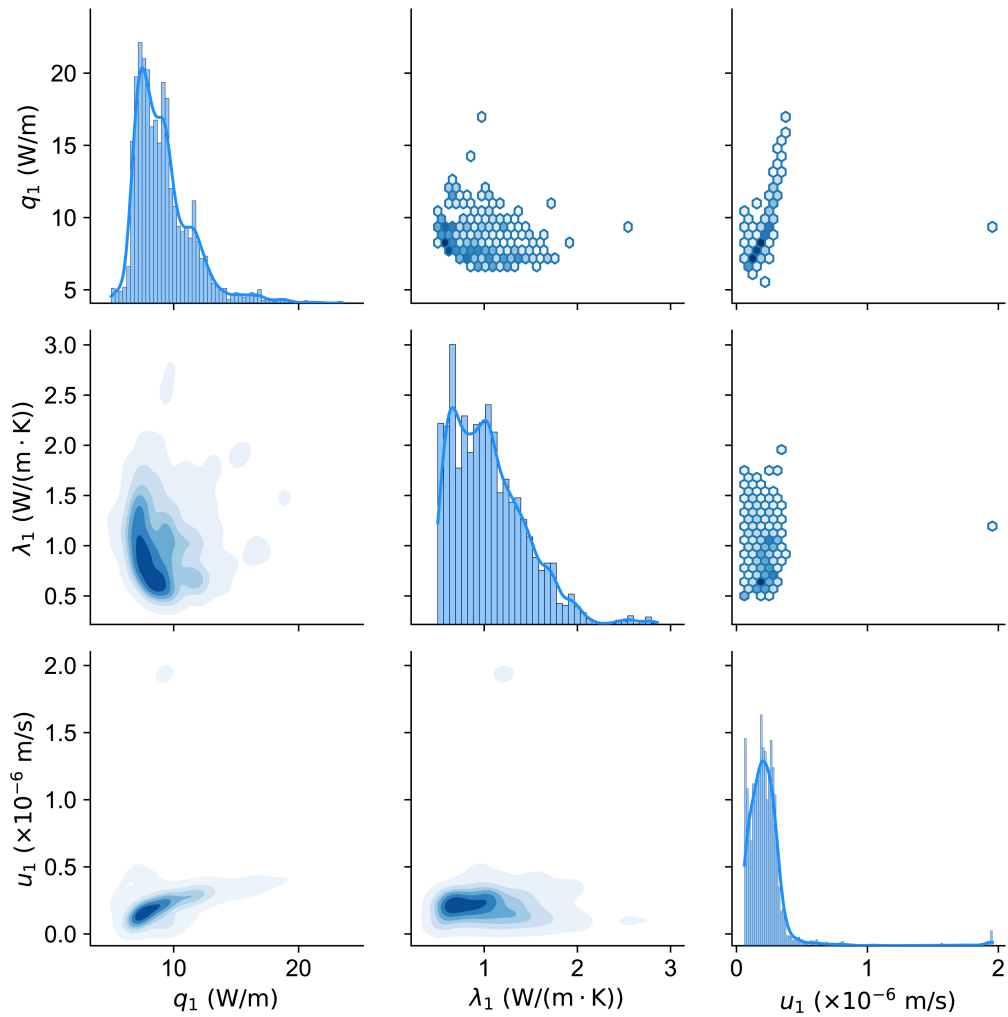


Figure 4.11: Pair plots of heat extraction rate (q_1), thermal conductivity (λ_1), and Darcy velocity (u_1) within the first layer at month 6.

Although all parameters are correlated at this time-step, the strongest correlation is between Darcy velocity and the heat extraction rate. For a more comprehensive analysis, the pair plots of all nine parameters at five different time-steps are presented in the Appendix. Notably, correlations are observed not only within individual layers but also between different layers over time. This observation aligns with the governing heat transfer in the domain. Initially, a significant temperature difference between the inlet fluid in the pipe and the surrounding environment can be assumed, leading to a higher expected heat exchange rate in the first layer at early times. Due to the higher temperature differences in the first layer, the fluid inside the pipe extracts a relatively large amount of energy from the ground. As a result, the heated fluid entering the second and third layers has a higher temperature, causing a decrease in the heat extraction rate in the first layer over time. However, higher advection in the second and third layers mitigates the cooling effect, maintaining a relatively constant heat extraction rate in those layers. This interaction between the layers can also be identified statistically in the pair plots of Figure 4.11.

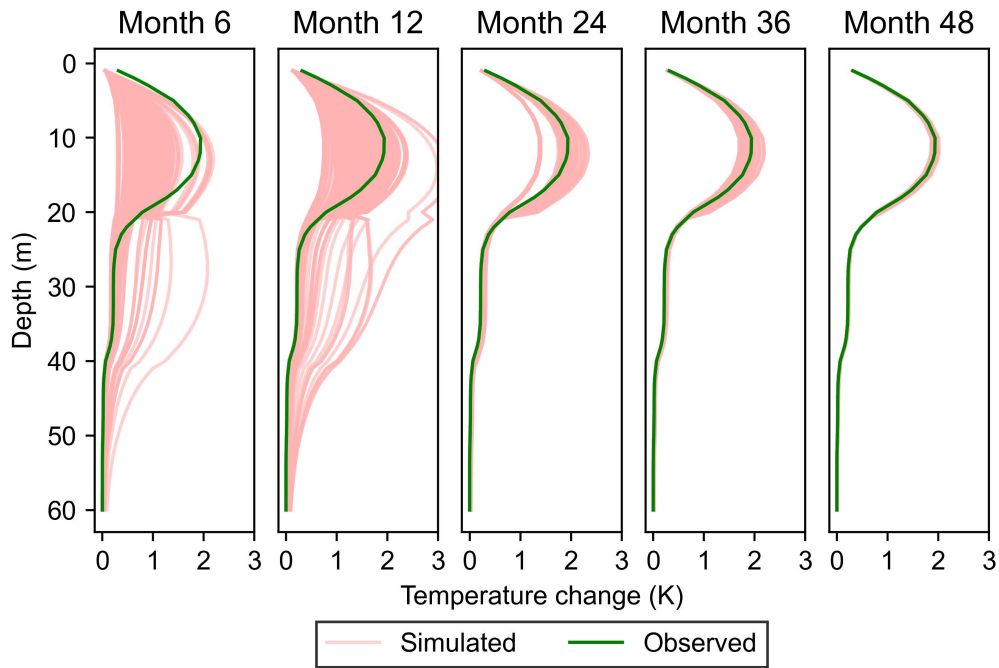


Figure 4.12: Comparison of simulated and observed temperature changes at month 60 over the depth, using inferred model parameters from months 6, 12, 24, 36, and 48.

4.3.3 Simulated temperature changes

So far, the generated samples using various statistical analyses have been discussed. However, the primary goal of this chapter is not merely to infer parameters, but to improve the prediction of thermal states in the field. Therefore, this section focuses on predicting temperature changes around the BHE in a stochastic manner, utilizing the measured temperatures from the inactive BHE over the operation time. As a first scenario, five time-steps at months 6, 12, 24, 36, and 48 are selected and at the end of each time-step, the measured temperatures are used within the Bayesian framework to infer a set of model parameters. These inferred parameters are then directly applied to predict temperature changes in the field across the layers after five years of operation. The results of these predictions, with a thinning factor of ten applied to the samples, are shown in Figure 4.12. It is revealed that over time, as more information is gathered, the uncertainty in the predictions is significantly reduced. Initially, most of the generated samples for the parameters in the first layer tend to underestimate the temperature, but as time progresses, the proposals are chosen more efficiently.

To better quantify the results shown in Figure 4.12, the root mean square error (RMSE) for temperature change predictions at month 60 is plotted in Figure 4.13. All sampled parameters from months 6, 12, 24, 36, and 48 are included in this analysis to predict the temperature change at the end of month 60 along the entire depth. It is observed that the maximum RMSE for predictions using samples from month 6 is 1.17 K, which decreases to 0.05 K with the consideration of samples from month 48. Similarly, the maximum range of temperature change predictions reduces from 1.91 K to 0.16 K as the month progresses from 6 to 48. This

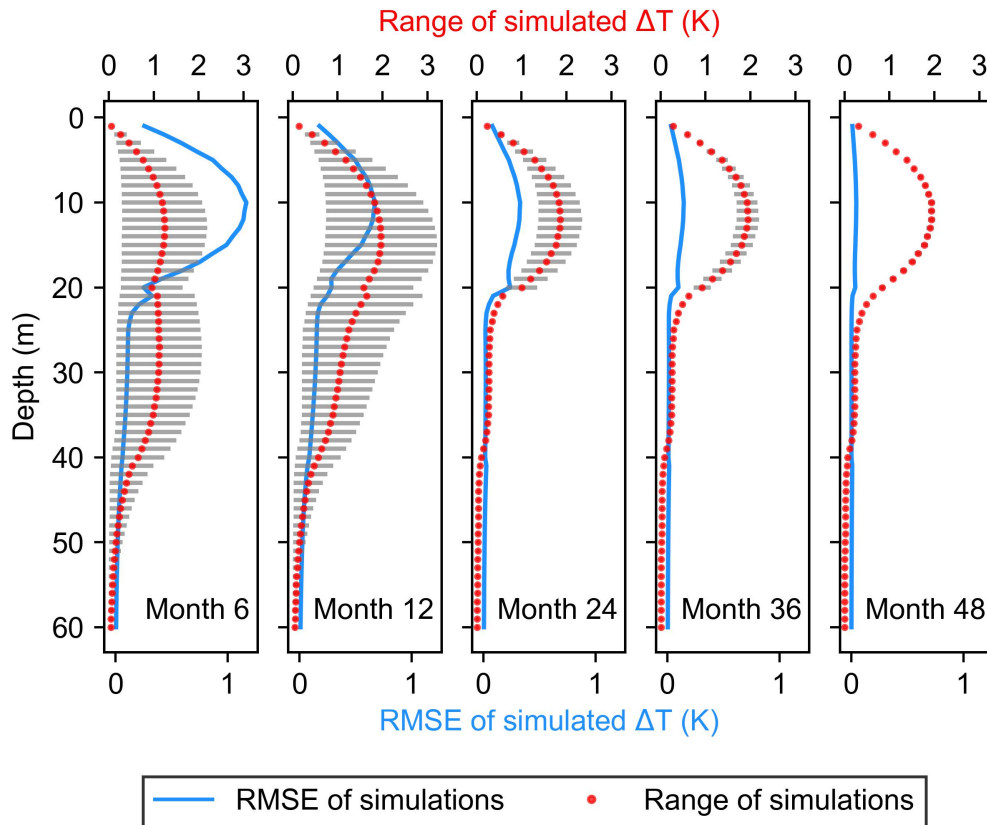


Figure 4.13: Comparison of the root mean square error (RMSE) and the range of temperature change predictions at month 60, based on the model samples from months 6, 12, 24, 36, and 48.

indicates that uncertainty in the temperature predictions for the final time-step reduces to 8% when inferred samples from month 48 are used. It should be noted that the faster dynamics of temperature change in the early months make capturing the correct behavior of temperature variation more challenging. However, if certain subsurface parameters, such as groundwater flow rate, or operational parameters, like the flow rate of the heat carrier fluid, change over time, fast temperature changes may also occur even in the later time-steps.

As expected from the statistical analysis, the first layer, due to low groundwater velocity and local cooling, is the main source of uncertainty for predicting temperatures. It is observed that predictions from layers 2 and 3 are more accurate, as they can more rapidly approach the true thermal state. This is because temperature signals in these layers reach a steady state more quickly, leading to smaller variations between time-steps. In the first case, the spatial predictability of the proposals across the entire depth is analyzed. As a further analysis, an examination of temperature changes within the first layer over entire time-steps is conducted. Therefore, the same five time-steps (months 6, 12, 24, 36, and 48) are selected, and based on the inferred parameters at each time-step, the simulated temperature change until the end of the operation is compared. The temperature change at a depth of 10 m is presented in Figure 4.14. This result clearly shows a reduction in temperature uncertainty over time.

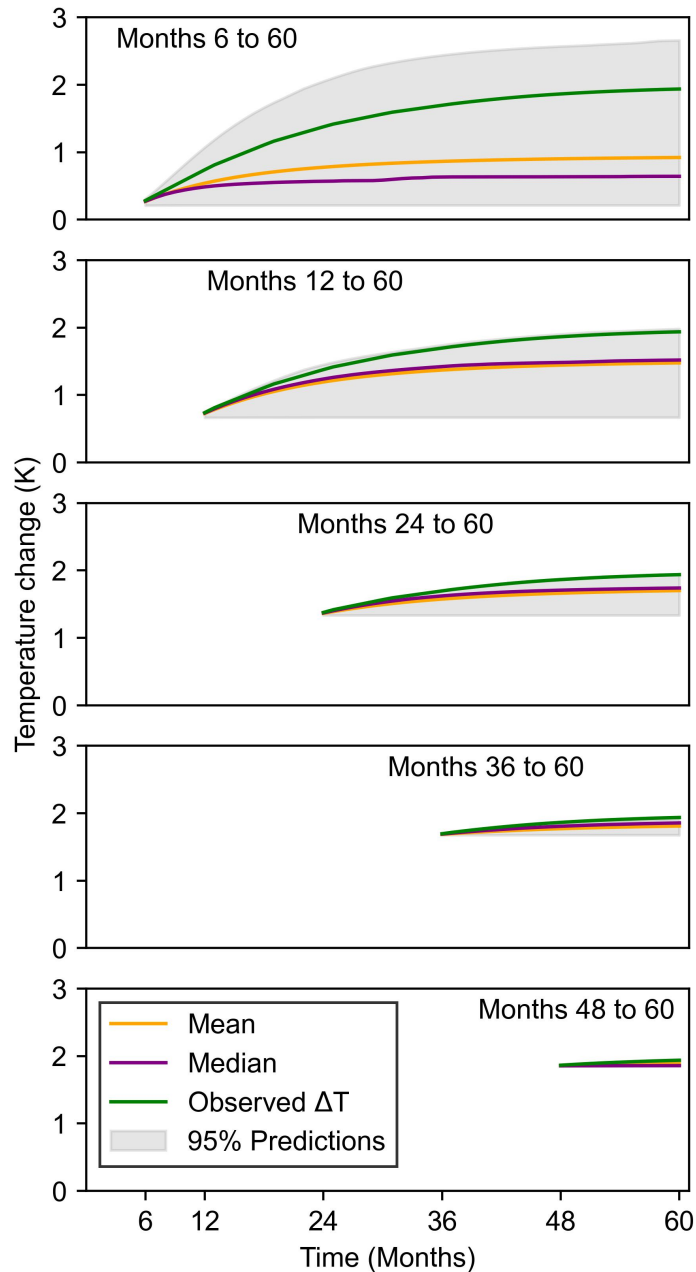


Figure 4.14: Comparison of the 95 % confidence interval, mean, and median of predicted temperature changes with observed temperature changes at a depth of 10 m, using inferred parameters from months 6, 12, 24, 36, and 48 until the end of the operation.

Similar to the previous case, predictions based on early inferred parameters cannot accurately reproduce the transient temperature evolution and tend to predict an earlier steady state for the subsurface system. For instance, by comparing the mean and median of predicted temperatures based on parameters from months 6 and 12, it is evident that predictions based on parameters from month 12 better follow the nonlinear transition from the transient phase to a quasi-steady state condition.

4.4 Conclusions and outlook

This chapter presents a probabilistic modeling framework for predicting long-term temperature changes in the subsurface surrounding BHE fields, accounting for multi-layer subsurface heterogeneity and groundwater flow. Leveraging a Bayesian approach, the newly developed framework infers the high-dimensional, correlated parameter space essential for accurately modeling heat transport in the subsurface caused by the operation of BHEs in fields with complex geological settings. To achieve this, the affine invariant ensemble sampler within a stochastic Bayesian method characterizes nine correlated parameters—such as heat extraction rate, thermal conductivity, and Darcy velocity—across three distinct subsurface layers. An efficient analytical forward solver, the MFLSA further enhances the framework's capacity to incorporate anisotropic conditions and groundwater flow.

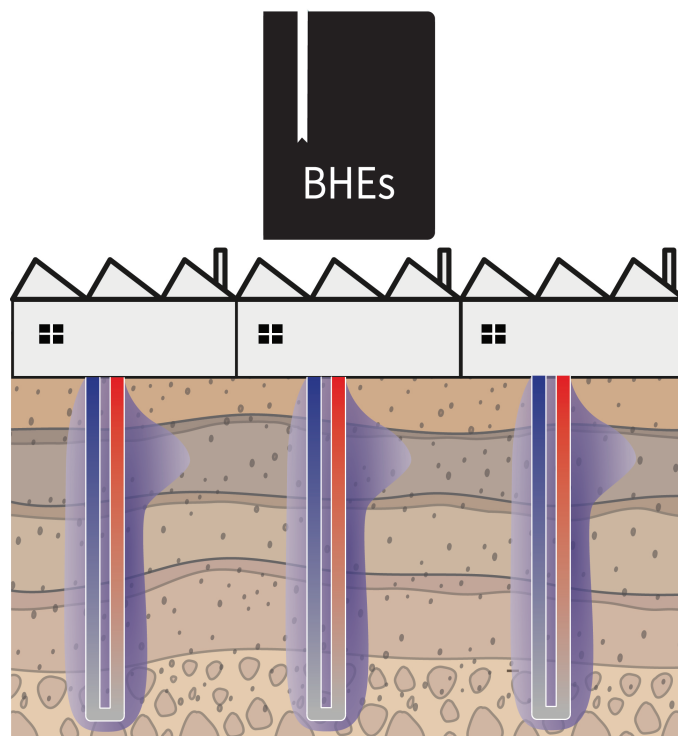
To demonstrate the framework's applicability, a synthetic five-year case study is conducted in COMSOL Multiphysics®, involving four active BHEs and one inactive BHE. Monthly simulated temperatures obtained at the inactive BHE by the numerical model are used as reference data for parameter estimation and to evaluate the framework's temperature change predictions. Comprehensive statistical analyses confirm the successful characterization of the parameter space, thereby achieving reliable spatial and temporal temperature predictions. Sequential application of the framework over 32 months shows a reduction in prediction uncertainty to 8% by the end of the five-year operation, underscoring the framework's effectiveness in managing long-term temperature predictions. However, the reduction in uncertainty may be less pronounced if operational conditions vary significantly over time.

Additionally, this framework extends the applicability of the MFLSA analytical model for realistic, heterogeneous subsurface scenarios by eliminating the need for a constant heat extraction rate across layers.

Future work will focus on applying this framework to real field data with extended, high-resolution measurements and exploring transient boundary conditions and variable operational parameters. Incorporating machine learning methods to further improve sampling efficiency, along with complementary data sources such as hydrogeological measurements and geophysical investigations, could refine the inversion process and enhance the reliability of inferred parameters.

Chapter 5

Conclusions and future work



5 Conclusions and futurework

5.1 Summary and conclusions

This dissertation presents a simulation-based optimization approach for adaptively managing load distribution among BHEs in a field, integrating an efficient optimization technique, analytical modeling tools, and a Bayesian data assimilation method. Adaptive management is essential due to uncertainties in both descriptive and predictive aspects, which make single-step planning for optimal load distributions impractical. This necessitates the development of novel methods that actively incorporate real-time information and adapt dynamically to temperature changes in BHE fields. In three interconnected chapters, this research addresses challenges such as managing uncertainties, accounting for complex subsurface geological conditions, incorporating coupled heat transfer processes, and adapting to fluctuations in heat demand. Each chapter builds upon insights or unresolved questions from the previous one, creating a cohesive methodology that enhances the reliability and adaptability of BHE system modeling and optimization.

Chapter 2 focuses on extending the existing concept of individual load distribution in BHE fields from a single-step approach to a sequential strategy that accommodates time-variant changes in the BHE field. This effort led to the development of sequential optimization—a dynamic approach that continuously updates optimal load distributions based on temperature measurements (Soltan Mohammadi et al., 2024a). By revisiting and refining the optimization process periodically, this method adjusts optimal load allocations to account for uncertainties in temperature change predictions and deviations in energy demand. The optimization process aims to minimize maximum subsurface temperature changes caused by BHE operations, ensuring optimal heat extraction and reducing local thermal anomalies. This is achieved by identifying critical BHEs in the field where temperature changes around them are most significant and redistributing loads among BHEs to avoid these extreme temperature changes. Constantly revisiting the BHEs and updating the thermal state in the subsurface as a new initial condition for simulation and optimization allows the algorithm to flexibly identify new critical BHE locations and sequentially revise the previous optimal plans. The applicability of this methodology is assessed through two case studies. Sequential optimization is applied to fields with five and 26 BHEs, resulting in significant reductions in maximum temperature changes—2.9 K and 8.9 K, respectively—over 15 years of operation, compared to a single-step optimization strategy. These findings validate the method's ability to dynamically adapt to new thermal and operational conditions, mitigate negative ecological impacts, and extend the sustainable lifespan of BHE field. Additionally, the role of underestimating and overestimating

heating demand on the deterioration of optimized patterns is investigated. In further analysis, sequential optimization demonstrates good performance in cases with fluctuating heating demand. In this case study, where fluctuations range from -50 % to +100 % of the planned loads within a stochastic analysis, sequential optimization achieves an average reduction of 2.7 K in maximum temperature changes.

The uncertainties discussed in Chapter 2 are not approached from a physics-based perspective, but are introduced as theoretical percentage deviations from temperature measurements at the location of BHEs. Chapter 3, employing the sequential optimization from the previous chapter, investigates the potential of this approach in a more realistic scenario where uncertainties arise from transient hydrogeological conditions in the BHE field (Soltan Mohammadi et al., 2024b). The focus shifts to incorporating advective heat transfer—a critical factor in subsurface thermal dynamics—into the sequential optimization framework.

To achieve this, the MFLS model (Molina-Giraldo et al., 2011) is adapted and rearranged to account for transient groundwater flow. This adaptation allowed the model to represent varying groundwater velocities using a superposition approach, enhancing its ability to capture transient thermal evolution in the BHE field. The revised MFLS model is validated against numerical models. The validation test cases cover diverse fluctuation patterns of groundwater velocity, including linear, nonlinear, periodic, increasing, decreasing, and noisy trends. These validation scenarios are applied to a case with one BHE and a field with ten BHEs. The results show mean absolute errors ranging from 0.05 to 0.18 K, well within the typical margins of common monitoring devices. This confirms the model's reliability in representing accurate thermal responses to transient groundwater flow.

The rearranged MFLS model is then integrated into the sequential optimization framework for the field with ten BHEs. This extended framework treats groundwater velocity as the primary source of uncertainty in subsurface temperature changes. An additional significant advancement is the introduction of dynamic parameter calibration into the optimization process. Unlike the previous chapter, which uses the current thermal condition as an updated initial state for the simulation of the upcoming months, the new approach in this chapter re-calibrates model parameters at monthly time-steps. This is done by formulating the problem as a nonlinear least-squares minimization, solved with the Trust-Region-Reflective algorithm (Byrd et al., 2000). The sequentially calibrated input model parameters ensure a more accurate description of the unknown or uncertain model parameters and help avoid cumulative errors in future simulations.

The results of Chapters 2 and 3 establish a solid foundation for extending optimization algorithms to dynamically control thermal anomalies in the subsurface. These chapters highlight the importance of predictive models capable of accurately describing heat transfer in subsurface settings that are often complex and subject to dynamic changes. Such changes typically manifest as transient boundary conditions within the modeling domain or as model parameters that are not fully characterized and subject to uncertainties.

Beyond the need for flexible and robust modeling tools, advancements in measurement technologies, such as distributed temperature sensing (DTS), which provides high-resolution

spatial and temporal data (Gebhardt et al., 2024; Heim et al., 2024b; Zhang et al., 2023a,b), inspire the development of a methodology that can more efficiently leverage the measured data.

In response, Chapter 4 introduces a novel Bayesian framework for modeling BHE fields (Soltan Mohammadi et al., 2025). This probabilistic framework is designed to improve the accuracy of long-term temperature predictions by assimilating real-time measurements to dynamically update the predictive model. This approach effectively characterizes high-dimensional and highly correlated parameter space that is critical for accurate heat transport modeling. In this chapter, these parameters include heat extraction rates, thermal conductivity, and Darcy velocity across multiple subsurface layers. By employing the AIES (Goodman and Weare, 2010), the framework overcomes challenges associated with sampling from the posterior distribution of nine correlated parameters. Additionally, the integration of the MFLSA (Erol and François, 2018) into the framework allows it to account for heterogeneous subsurface conditions and accurately describe heat transfer, while also considering groundwater flow effects across different layers.

To demonstrate its applicability, a synthetic case study involving four active BHEs is developed in this chapter. A numerical model is used to represent temperature measurements in the BHE field over five years of operation. The proposed Bayesian approach utilizes available measurements at monthly time-steps to infer a set of possible input parameters. The inferred parameter sets are then used to generate an ensemble of temperature predictions rather than a single deterministic forecast. This ensemble-based approach creates a reliability-driven and probabilistic framework for assessing temperature changes, providing insights into the likely range of temperature variations within each geological layer and the confidence level associated with the predictions. The sequential application of this framework in the demonstrated example over 32 months successfully reduces prediction uncertainty to 8% by the end of the operation period, highlighting its effectiveness in managing long-term temperature predictions. Furthermore, the framework eliminates the need to assume constant heat extraction rates across subsurface layers, offering a more realistic approach for modeling temperature changes in heterogeneous geological settings using analytical models.

In conclusion, this dissertation presents a set of comprehensive and innovative strategies for modeling and optimizing BHE field operations, aimed at managing uncertainties and adapting to the complexities of (hydro)geological systems, thus advancing the sustainable and efficient utilization of closed-loop geothermal systems.

5.2 Outlook

Although the advancements presented in this work have contributed to the modeling, optimization, and adaptive management of BHE fields, there remain several opportunities for further research and development.

The next step should focus on integrating the proposed Bayesian framework into optimization routines and applying the developed methodologies to real-world data from operational BHE

fields. Further analysis is needed to explore the potential of the Bayesian framework, particularly in models with transient boundary conditions and heterogeneous operational parameters, which are common in complex subsurface settings.

To enhance the efficiency of the Bayesian framework, improvements in sampling strategies could be made by incorporating a learning tool that continuously adapts the sampling process based on feedback from real-time measurements (Liang et al., 2011). This approach could focus on identifying and sampling the most relevant regions of the parameter space, thus accelerating the computational process and improving the precision of the results.

Another suggestion for improvement is the integration of additional data sources, such as geological logs or geophysical surveys. These complementary data sources could help constrain the inversion process, reduce implausible samples, and improve the geological realism of the results (Hermans et al., 2018, 2014; Thibaut et al., 2022).

While the optimization efforts in this thesis focused on minimizing temperature changes induced by BHE operations, expanding the scope of optimization to include heat pumps is a promising direction. By considering the efficiency and performance of the heat pumps in addition to the thermal anomalies in the subsurface, this extension would allow full system performance optimization (Kümpel et al., 2022). To support this, the modeling of BHEs should be expanded to account for temperature dynamics both inside and outside the borehole. Alternatively, a comprehensive sensitivity analysis might provide a viable approach to finding proxies for outlet temperatures based on other parameters, such as heat extraction rates and the thermal resistivity of the borehole. This could help further refine the optimization process and enhance the overall system's performance and sustainability.

Throughout this thesis, the time-steps for measurements, simulation, calibration and parameter inference were assumed to be monthly. However, a further parameter study is necessary to determine the optimal temporal resolution for calibration, parameter inference and optimization, particularly given the heat transfer dynamic in the subsurface, which is typically slow. Investigating the impact of higher-resolution measurements, such as weekly, daily, or hourly data, on the simulations and load proposal could provide insights into whether finer temporal data integration justifies the additional computational costs.

Another important consideration for future work is the potential impact of climate change on subsurface thermal regimes. As global temperatures rise, the thermal state of subsurface also changes, potentially affecting the long-term performance of BHE systems. Integrating climate change projections into the modeling framework will enable an assessment of whether the optimal load proposals remain valid under future climatic conditions or require adaptation. This extension could involve coupling the current framework with climate models to incorporate trends in subsurface temperature, groundwater temperature, and other relevant factors (Benz et al., 2024, 2022; Hemmerle et al., 2022).

As another avenue for future work, leveraging reduced-order models (ROM) and/or physics-informed machine learning techniques offers significant potential to address the computational challenges associated with modeling BHE systems in complex geological settings, an area that remains largely unexplored. While numerical methods are accurate, they are often prohibitively

computationally expensive when applied to large-scale BHE fields, making them unsuitable for fast simulations in the context of optimal control strategies. ROM techniques can mitigate these issues by simplifying high-dimensional models into a lower-order space that captures the essential physical characteristics of the system, significantly reducing computational demand (Cupeiro Figueroa et al., 2021; Menberg et al., 2020; Verhelst and Helsen, 2011). Additionally, the emerging paradigm of physics-informed machine learning (Karniadakis et al., 2021) combines data-driven algorithms with the physical principles governing heat transfer, enabling models to learn from existing data while ensuring that predictions remain physically plausible. These models can be trained on available data to approximate the behavior of the full system with much lower computational cost, making them particularly suitable for real-time simulations and optimal control of BHE systems in the field (Ahmed et al., 2023; Arroyo et al., 2022; Ishitsuka and Lin, 2023; Li et al., 2024).

Appendix

A. Supplementary material for Chapter 4

Validation of the forward solver over depth and time (30 years), using data and results from (Erol and François, 2018) for the (hydro)geological settings provided in Table 4.1.

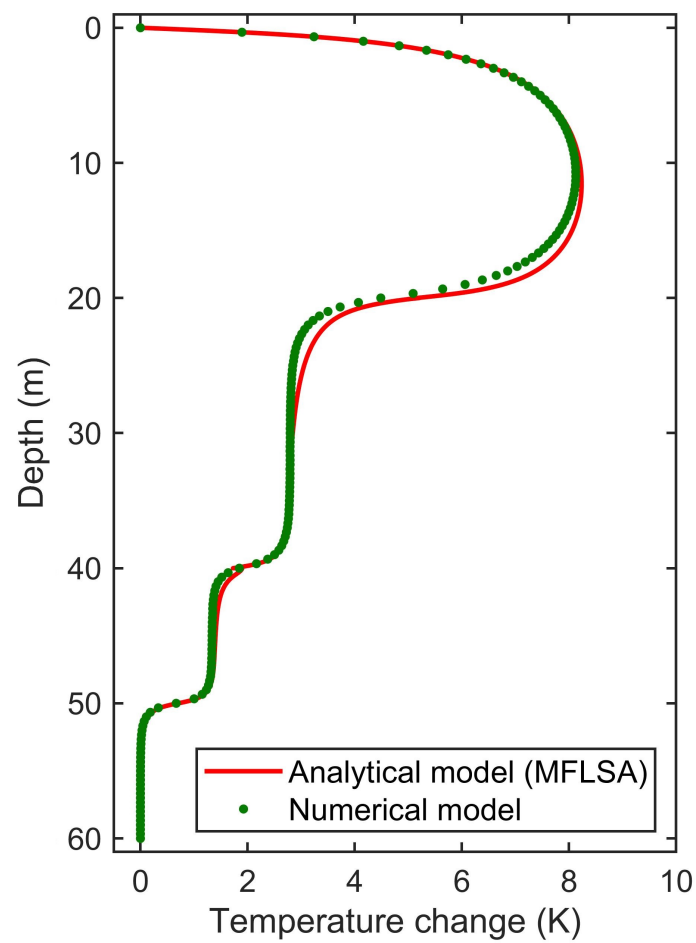


Figure A.1: Validation of the forward solver (MFLSA) with numerical results over depth.

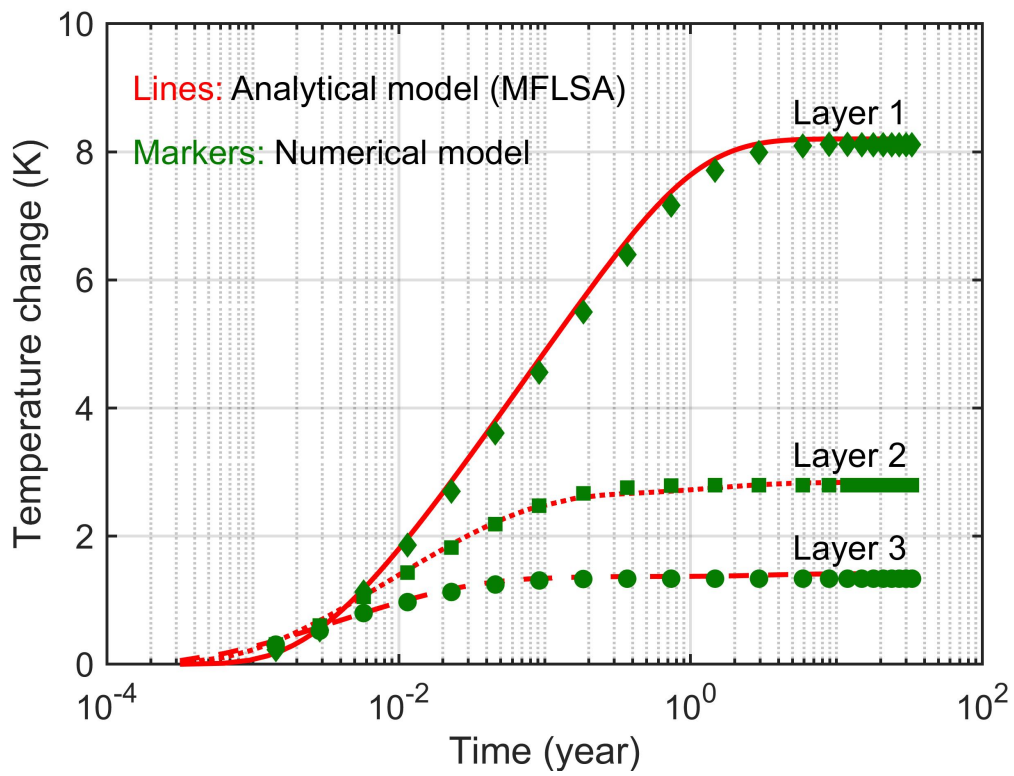


Figure A.2: Validation of the forward solver (MFLSA) with numerical results over time.

Pair plots for all nine parameters at different time-steps:

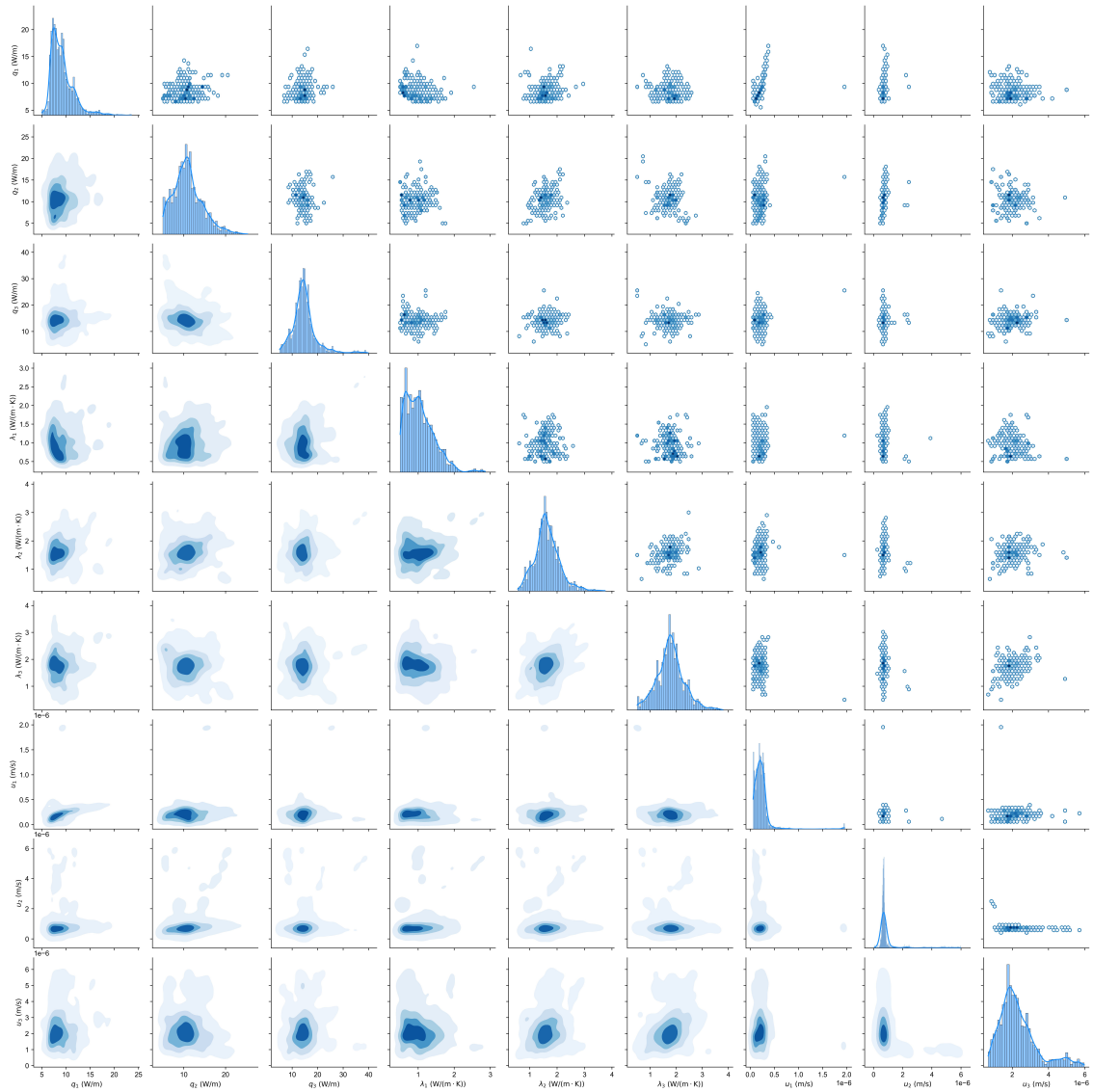


Figure A.3: Pair plots of all nine parameters at month 6.

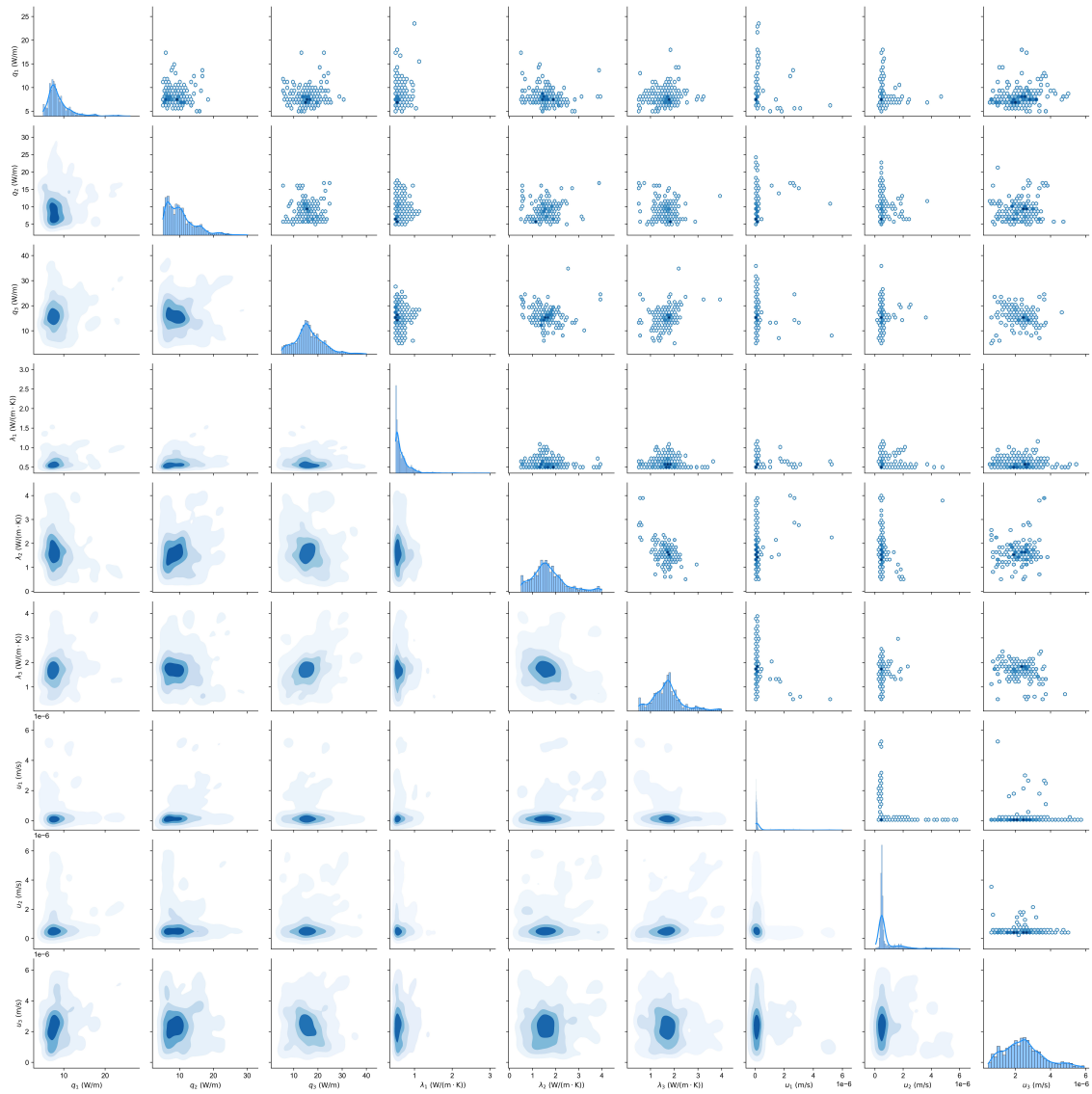


Figure A.4: Pair plots of all nine parameters at month 12.

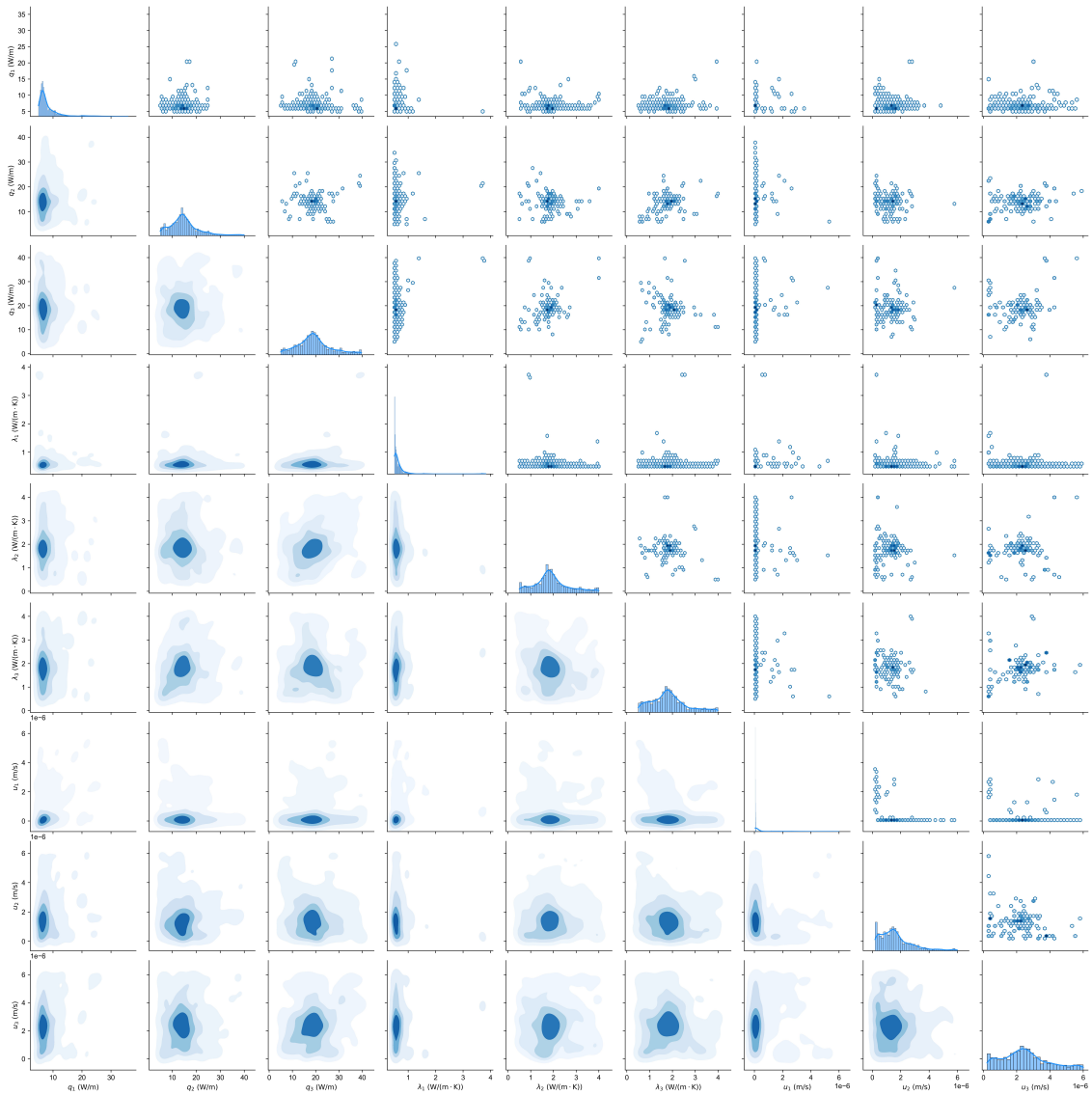


Figure A.5: Pair plots of all nine parameters at month 24.

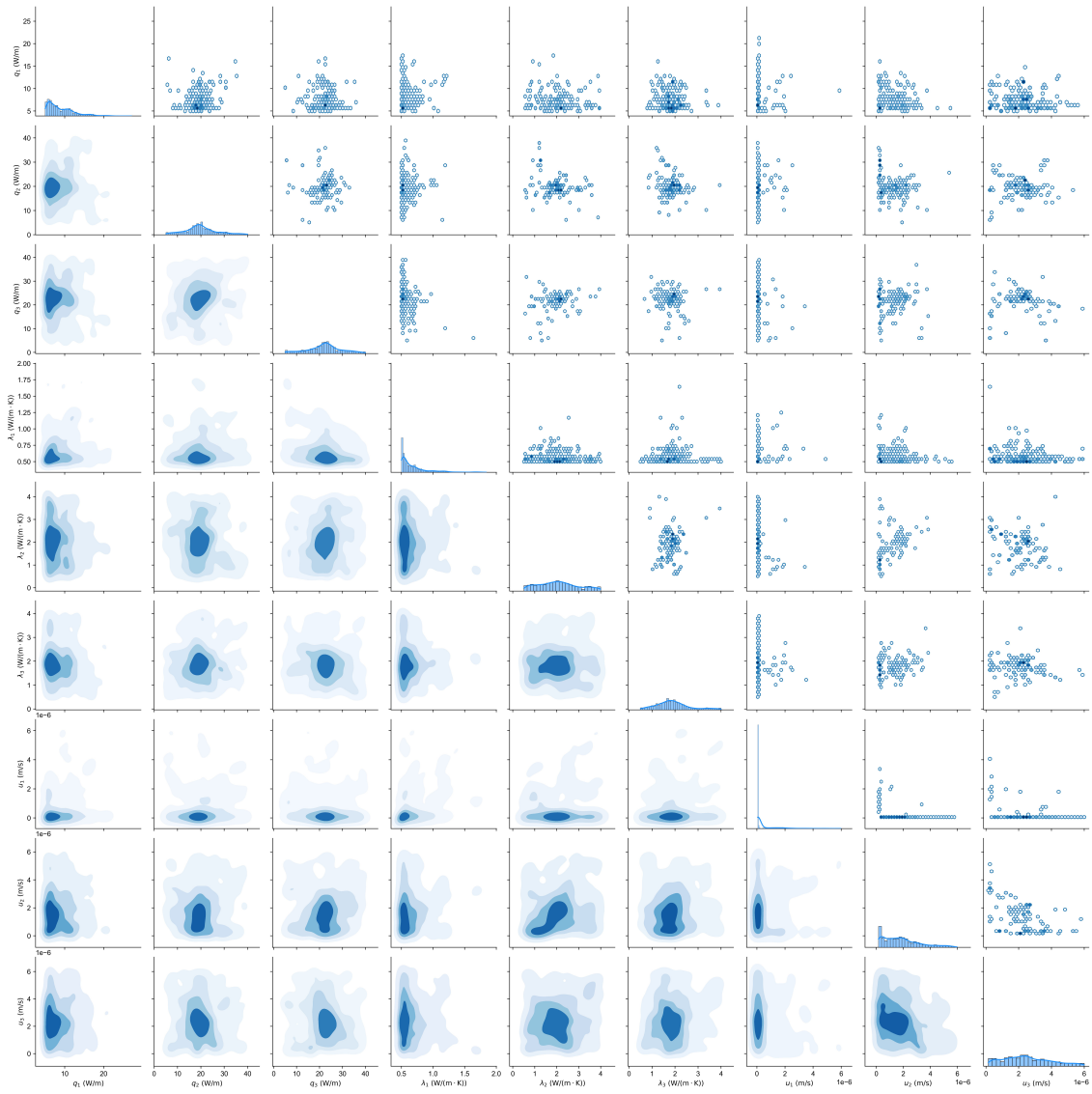


Figure A.6: Pair plots of all nine parameters at month 36.

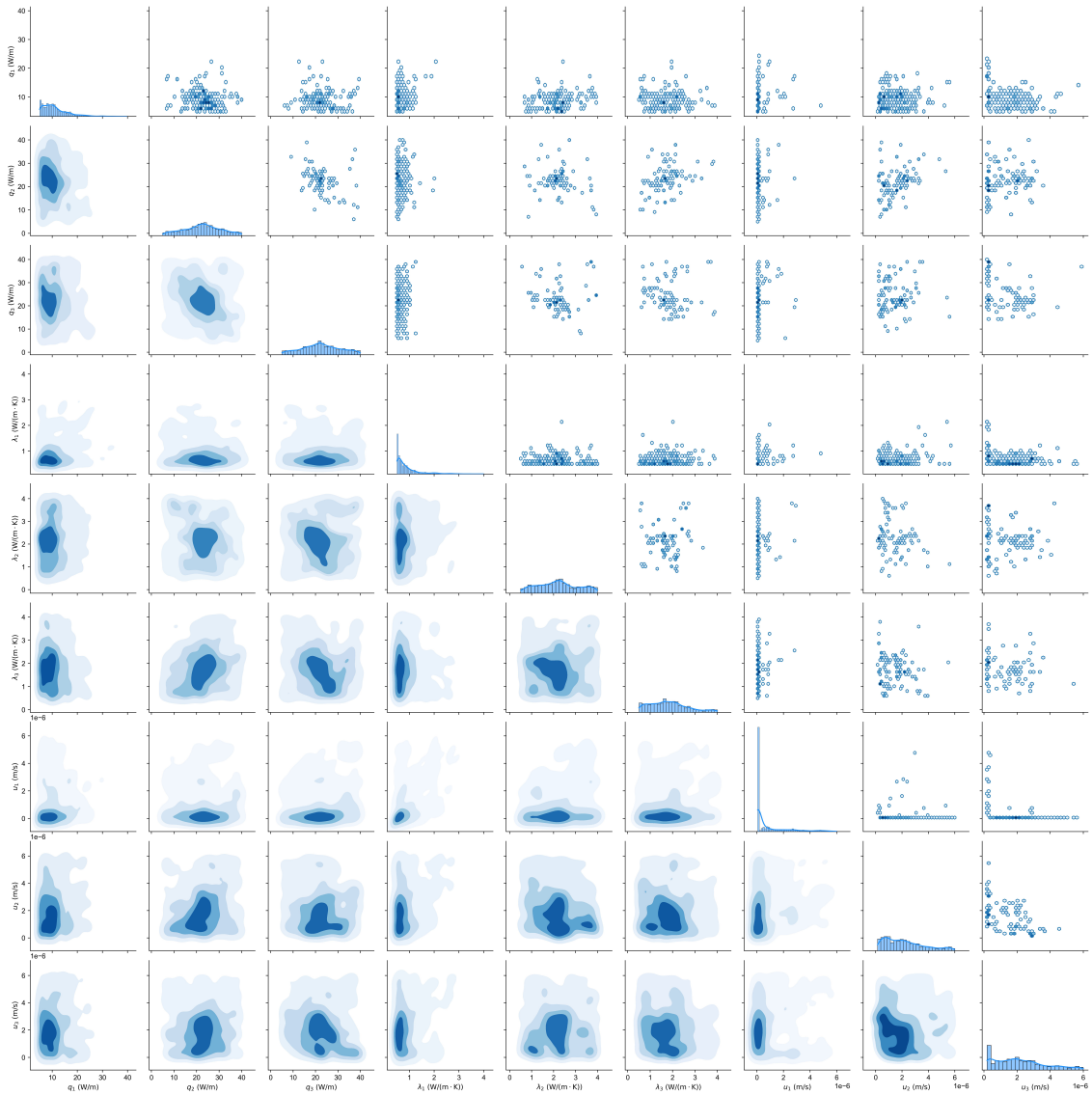


Figure A.7: Pair plots of all nine parameters at month 48.

References

- Abdelaziz, S., Ozudogru, T., Olgun, C., and Martin, J. (2014). Multilayer finite line source model for vertical heat exchangers. *Geothermics*, *51*, 406–416. <https://doi.org/10.1016/j.geothermics.2014.03.004>.
- Abesser, C., Schincariol, R. A., Raymond, J., García-Gil, A., Drysdale, R., Piatek, A., Giordano, N., Jaziri, N., and Molson, J. (2023). Case studies of geothermal system response to perturbations in groundwater flow and thermal regimes. *Groundwater*, *61*(2), 255–273. <https://doi.org/10.1111/gwat.13086>.
- Adebayo, P., Jathunge, C. B., Darbandi, A., Fry, N., Shor, R., Mohamad, A., Wemhöner, C., and Mwesigye, A. (2024). Development, modeling, and optimization of ground source heat pump systems for cold climates: A comprehensive review. *Energy and Buildings*, p. 114646. <https://doi.org/10.1016/j.enbuild.2024.114646>.
- Ahmed, N., Assadi, M., Ahmed, A. A., and Banihabib, R. (2023). Optimal design, operational controls, and data-driven machine learning in sustainable borehole heat exchanger coupled heat pumps: Key implementation challenges and advancement opportunities. *Energy for Sustainable Development*, *74*, 231–257. <https://doi.org/10.1016/j.esd.2023.04.004>.
- Al-Khoury, R. (2011). *Computational modeling of shallow geothermal systems*. CRC press.
- Albers, A., Steger, H., Zorn, R., and Blum, P. (2024). Evaluating an enhanced thermal response test (etrt) with high groundwater flow. *Geoth. Energy*, *12*, 1–22. <https://doi.org/10.1186/s40517-023-00278-y>.
- Antelmi, M., Turrin, F., Zille, A., and Fedrizzi, R. (2023). A new type in trnsys 18 for simulation of borehole heat exchangers affected by different groundwater flow velocities. *Energies*, *16*(3), 1288. <https://doi.org/10.3390/en16031288>.
- Aprianti, T., Tan, E., Diu, C., Sprivilis, B., Ryan, G., Srinivasan, K., and Chua, H. T. (2021). A comparison of ground and air source heat pump performance for domestic applications: A case study in perth, australia. *International Journal of Energy Research*, *45*(15), 20 686–20 699. <https://doi.org/10.1002/er.7133>.
- Aresti, L., Christodoulides, P., and Florides, G. (2018). A review of the design aspects of ground heat exchangers. *Renewable and Sustainable Energy Reviews*, *92*, 757–773. <https://doi.org/10.1016/j.rser.2018.04.053>.

- Arroyo, J., Manna, C., Spiessens, F., and Helsen, L. (2022). Reinforced model predictive control (rl-mpc) for building energy management. *Applied Energy*, 309, 118–346. <https://doi.org/10.1016/j.apenergy.2021.118346>.
- Atam, E., Patteeuw, D., Antonov, S., and Helsen, L. (2016). Optimal control approaches for analysis of energy use minimization of hybrid ground-coupled heat pump systems. *IEEE Transactions on Control Systems Technology*, 24, 525–540. <https://doi.org/10.1109/TCST.2015.2445851>.
- Banks, D. (2015). A review of the importance of regional groundwater advection for ground heat exchange. *Environ. Earth Sci.*, 73, 2555–2565. <https://doi.org/10.1007/s12665-014-3377-4>.
- Bayer, P., de Paly, M., and Beck, M. (2014). Strategic optimization of borehole heat exchanger field for seasonal geothermal heating and cooling. *Applied Energy*, 136, 445–453. <https://doi.org/10.1016/j.apenergy.2014.09.029>.
- Bayer, P., Attard, G., Blum, P., and Menberg, K. (2019). The geothermal potential of cities. *Renewable and Sustainable Energy Reviews*, 106, 17–30. <https://doi.org/10.1016/j.rser.2019.02.019>.
- Beck, M., Hecht-Méndez, J., De Paly, M., Bayer, P., Blum, P., and Zell, A. (2010). Optimization of the energy extraction of a shallow geothermal system. *2010 IEEE World Congress on Computational Intelligence (WCCI) - 2010 IEEE Congress on Evolutionary Computation (CEC)*, <https://doi.org/10.1109/CEC.2010.5585921>.
- Beck, M., Bayer, P., de Paly, M., Hecht-Méndez, J., and Zell, A. (2013). Geometric arrangement and operation mode adjustment in low-enthalpy geothermal borehole fields for heating. *Energy*, 49, 434–443. <https://doi.org/10.1016/j.energy.2012.10.060>.
- Benz, S., Menberg, K., Bayer, P., and Kurylyk, B. (2022). Shallow subsurface heat recycling is a sustainable global space heating alternative. *Nat. Commun.*, 13, 3962. <https://doi.org/10.1038/s41467-022-31624-6>.
- Benz, S. A., Irvine, D. J., Rau, G. C., Bayer, P., Menberg, K., Blum, P., Jamieson, R. C., Griebler, C., and Kurylyk, B. L. (2024). Global groundwater warming due to climate change. *Nature Geoscience*, pp. 1–7. <https://doi.org/10.1038/s41561-024-01453-x>.
- Bernier, M., Pinel, P., Labib, R., and Paillot, R. (2004). A multiple load aggregation algorithm for annual hourly simulations of gchp systems. *HVAC&R Research*, 10, 471–487. <https://doi.org/10.1080/10789669.2004.10391115>.
- Bidarmaghz, A., Narsilio, G., Johnston, I., and Colls, S. (2016). The importance of surface air temperature fluctuations on long-term performance of vertical ground heat exchangers. *Geomechanics for Energy and the Environment*, 6, 35–44. <https://doi.org/10.1016/j.gete.2016.02.003>.

- Biglarian, H., Abbaspour, M., and Saidi, M. H. (2017). A numerical model for transient simulation of borehole heat exchangers. *Renewable Energy*, 104, 224–237. <https://doi.org/10.1016/j.renene.2016.12.010>.
- Blum, P., Menberg, K., Koch, F., Benz, S., Tissen, C., Hemmerle, H., and Bayer, P. (2021). Is thermal use of groundwater a pollution? *Journal of Contaminant Hydrology*, 239, 103791. <https://doi.org/10.1016/j.jconhyd.2021.103791>.
- BniLam, N. and Al-Khoury, R. (2020). Parameter identification algorithm for ground source heat pump systems. *Applied Energy*, 264, 114712. <https://doi.org/10.1016/j.apenergy.2020.114712>.
- Boban, L., Soldo, V., and Fujii, H. (2020). Investigation of heat pump performance in heterogeneous ground. *Energy Conversion and Management*, 211, 112736. <https://doi.org/10.1016/j.enconman.2020.112736>.
- Bolstad, W. M. and Curran, J. M. (2016). *Introduction to Bayesian statistics*. John Wiley & Sons.
- Boockmeyer, A. and Bauer, S. (2016). Efficient simulation of multiple borehole heat exchanger storage sites. *Environmental Earth Sciences*, 75, 1–13. <https://doi.org/10.1007/s12665-016-5773-4>.
- Brand, A., Allen, L., Altman, M., Hlava, M., and Scott, J. (2015). Beyond authorship: Attribution, contribution, collaboration, and credit. *Learned Publishing*, 28(2). <https://doi.org/10.1087/20150211>.
- Brettschneider, A. L. and Perković, L. (2024). Theoretical analysis of using multiple borehole heat exchangers for production of heating and cooling energy in shallow geothermal reservoirs with underground water flow. *Applied thermal engineering*, 254, 123914. <https://doi.org/10.1016/j.applthermaleng.2024.123914>.
- Brooks, S., Gelman, A., Jones, G., and Meng, X.-L. (2011). *Handbook of markov chain monte carlo*. CRC press.
- Byrd, R., Gilbert, J., and Nocedal, J. (2000). A trust region method based on interior point techniques for nonlinear programming. *Math. Program.*, 89, 149–185. <https://doi.org/10.1007/PL00011391>.
- Cai, W., Wang, F., Chen, S., Chen, C., Zhang, Y., Kolditz, O., and Shao, H. (2022). Importance of long-term ground-loop temperature variation in performance optimization of ground source heat pump system. *Applied Thermal Engineering*, 204, 117945. <https://doi.org/10.1016/j.applthermaleng.2021.117945>.
- Casasso, A. and Sethi, R. (2014). Efficiency of closed loop geothermal heat pumps: a sensitivity analysis. *Renewable Energy*, 62, 737–746. <https://doi.org/10.1016/j.renene.2013.08.019>.

- Chen, K., Zheng, J., Li, J., Shao, J., and Zhang, Q. (2022). Numerical study on the heat performance of enhanced coaxial borehole heat exchanger and double u borehole heat exchanger. *Applied Thermal Engineering*, 203, 117916. <https://doi.org/10.1016/j.applthermaleng.2021.117916>.
- Chen, S., Witte, F., Kolditz, O., and Shao, H. (2020). Shifted thermal extraction rates in large borehole heat exchanger array—a numerical experiment. *Applied Thermal Engineering*, 167, 114750. <https://doi.org/10.1016/j.applthermaleng.2019.114750>.
- Chen, S., Cai, W., Witte, F., Wang, X., Wang, F., Kolditz, O., and Shao, H. (2021). Long-term thermal imbalance in large borehole heat exchangers array – a numerical study based on the leicester project. *Energy and Buildings*, 231, 110518. <https://doi.org/10.1016/j.enbuild.2020.110518>.
- Chiasson, A. and Elhashmi, R. (2017). Alternate approach to the calculation of thermal response factors for vertical borehole ground heat exchanger arrays using an incomplete bessel function. *Proceedings of the IGSHPA Technical/Research Conference and Expo*.
- Choi, W., Kikumoto, H., Choudhary, R., and Ooka, R. (2018a). Bayesian inference for thermal response test parameter estimation and uncertainty assessment. *Applied Energy*, 209, 306–321. <https://doi.org/10.1016/j.apenergy.2017.10.034>.
- Choi, W., Menberg, K., Kikumoto, H., Heo, Y., Choudhary, R., and Ooka, R. (2018b). Bayesian inference of structural error in inverse models of thermal response tests. *Applied Energy*, 228, 1473–1485. <https://doi.org/10.1016/j.apenergy.2018.06.147>.
- Choi, W., Kikumoto, H., and Ooka, R. (2022). Probabilistic uncertainty quantification of borehole thermal resistance in real-world scenarios. *Energy*, 254, 124400. <https://doi.org/10.1016/j.energy.2022.124400>.
- Christen, J. A. and Fox, C. (2010). A general purpose sampling algorithm for continuous distributions (the t-walk). *Bayesian Analysis*. <https://doi.org/10.1214/10-BA603>.
- Chwieduk, M. (2021). New global thermal numerical model of vertical u-tube ground heat exchanger. *Renewable Energy*, 168, 343–352. <https://doi.org/10.1016/j.renene.2020.12.069>.
- Cimmino, M. (2015). The effects of borehole thermal resistances and fluid flow rate on the g-functions of geothermal bore fields. *Int. J. Heat Mass Tran.*, 91, 1119–1127. <https://doi.org/10.1016/j.ijheatmasstransfer.2015.08.041>.
- Cimmino, M. (2016). Fluid and borehole wall temperature profiles in vertical geothermal boreholes with multiple u-tubes. *Renewable Energy*, 96, 137–147. <https://doi.org/10.1016/j.renene.2016.04.067>.

- Cimmino, M. and Bernier, M. (2014a). A semi-analytical method to generate g-functions for geothermal bore fields. *International Journal of Heat and Mass Transfer*, 70, 641–650. <https://doi.org/10.1016/j.ijheatmasstransfer.2013.11.037>.
- Cimmino, M. and Bernier, M. (2014b). Effects of unequal borehole spacing on the required borehole length. *ASHRAE Transactions*, 120, 158.
- Cimmino, M., Bernier, M., and Adams, F. (2013). A contribution towards the determination of g-functions using the finite line source. *Applied Thermal Engineering*, 51, 401–412. <https://doi.org/10.1016/j.applthermaleng.2012.07.044>.
- Claesson, J. and Javed, S. (2011). An analytical method to calculate borehole fluid temperatures for time-scales from minutes to decades. *ASHRAE Transactions*, 117, 279–288.
- Coen, T., François, B., and Gerard, P. (2021). Analytical solution for multi-borehole heat exchangers field including discontinuous and heterogeneous heat loads. *Energy and Buildings*, 253, 111520. <https://doi.org/10.1016/j.enbuild.2021.111520>.
- Cui, P., Yang, W., Zhang, W., Zhu, K., Spitler, J. D., and Yu, M. (2024). Advances in ground heat exchangers for space heating and cooling: Review and perspectives. *Energy and Built Environment*, 5(2), 255–269. <https://doi.org/10.1016/j.renene.2024.121436>.
- Cupeiro Figueroa, I., Cimmino, M., Drgoňa, J., and Helsen, L. (2021). Fluid temperature predictions of geothermal borefields using load estimations via state observers. *Journal of Building Performance Simulation*, 14(1), 1–19. <https://doi.org/10.1080/19401493.2020.1838612>.
- de Paly, M., Hecht-Méndez, J., Beck, M., Blum, P., Zell, A., and Bayer, P. (2012). Optimization of energy extraction for closed shallow geothermal systems using linear programming. *Geothermics*, 43, 57–65. <https://doi.org/10.1016/j.geothermics.2012.03.001>.
- De Ridder, F., Diehl, M., Mulder, G., Desmedt, J., and Van Bael, J. (2011). An optimal control algorithm for borehole thermal energy storage systems. *Energy Build*, 43, 2918–2925. <https://doi.org/10.1016/j.enbuild.2011.07.015>.
- Deng, F., Li, W., Pei, P., Wang, L., and Ren, Y. (2024). Study on design and calculation method of borehole heat exchangers based on seasonal patterns of groundwater. *Renew. Energy*, 220, 119711. <https://doi.org/10.1016/j.renene.2023.119711>.
- Dion, G., Pasquier, P., and Marcotte, D. (2022). Deconvolution of experimental thermal response test data to recover short-term g-function. *Geothermics*, 100, 102302. <https://doi.org/10.1016/j.geothermics.2021.102302>.
- Dion, G., Pasquier, P., and Marcotte, D. (2024a). Application of deconvolution to interpretation of distributed thermal response test (dtrt) and to determination of thermal conductivity profiles. *Applied Thermal Engineering*, 236, 121680. <https://doi.org/10.1016/j.applthermaleng.2023.121680>.

- Dion, G., Pasquier, P., Marcotte, D., and Beaudry, G. (2024b). Multi-deconvolution in non-stationary conditions applied to experimental thermal response test analysis to obtain short-term transfer functions. *Science and Technology for the Built Environment*, 30(3), 220–233. <https://doi.org/10.1080/23744731.2023.2217729>.
- Dube Kerme, E. and Fung, A. S. (2020). Transient heat transfer simulation, analysis and thermal performance study of double u-tube borehole heat exchanger based on numerical heat transfer model. *Applied Thermal Engineering*, 173, 115–189. <https://doi.org/10.1016/j.applthermaleng.2020.115189>.
- Egidi, N., Giacomini, J., and Maponi, P. (2023). Inverse heat conduction to model and optimise a geothermal field. *J. Comput. Appl. Math.*, 423, 114–1957. <https://doi.org/10.1016/j.cam.2022.114957>.
- Erol, S. and François, B. (2014). Efficiency of various grouting materials for borehole heat exchangers. *Appl. Therm. Eng.*, 70, 788–799. <https://doi.org/10.1016/j.applthermaleng.2014.05.034>.
- Erol, S. and François, B. (2018). Multilayer analytical model for vertical ground heat exchanger with groundwater flow. *Geothermics*, 71, 294–305. <https://doi.org/10.1016/j.geothermics.2017.09.008>.
- Erol, S., Hashemi, M., and François, B. (2015). Analytical solution of discontinuous heat extraction for sustainability and recovery aspects of borehole heat exchangers. *Int. J. Therm. Sci.*, 88, 47–58. <https://doi.org/10.1016/j.ijthermalsci.2014.09.007>.
- Eskilson, P. (1987). *Thermal analysis of heat extraction boreholes*. Lund Inst. of Tech.
- Fascì, M., Lazzarotto, A., Acuña, J., and Claesson, J. (2021). Simulation of thermal influence between independent geothermal boreholes in densely populated areas. *Appl. Therm. Eng.*, 196. <https://doi.org/10.1016/j.applthermaleng.2021.117241>.
- Fascì, M. L. (2023), Thermal interference between neighbouring ground-source heat pumps: Tools to calculate it and solutions to limit it, Ph.D. thesis, KTH Royal Institute of Technology.
- Fascì, M. L., Pallard, W. M., Lazzarotto, A., and Claesson, J. (2023). Temperature of energy boreholes accounting for climate change and the built environment—a new model for its estimation. *Renewable energy*, 202, 1479–1496. <https://doi.org/10.1016/j.renene.2022.12.023>.
- Figueira, J. S., Gil, A. G., Vieira, A., Michopoulos, A. K., Boon, D. P., Loveridge, F., Cecinato, F., Götzl, G., Epting, J., Zosseder, K., et al. (2024). Shallow geothermal energy systems for district heating and cooling networks: Review and technological progression through case studies. *Renewable Energy*, 236, 121–1436.

- Florides, G. A., Christodoulides, P., and Pouloupatis, P. (2013). Single and double u-tube ground heat exchangers in multiple-layer substrates. *Applied energy*, *102*, 364–373. <https://doi.org/10.1016/j.apenergy.2012.07.035>.
- Fossa, M. (2011). The temperature penalty approach to the design of borehole heat exchangers for heat pump applications. *Energy Build.*, *43*, 1473–1479. <https://doi.org/10.1016/j.enbuild.2011.02.020>.
- Gang, W., Wang, J., and Wang, S. (2014). Performance analysis of hybrid ground source heat pump systems based on ann predictive control. *Appl. Energy*, *136*, 1138–1144. <https://doi.org/10.1016/j.apenergy.2014.04.005>.
- Gebhardt, H., Soltan Mohammadi, H., Ebert, A., Bott, C., Visser, A., and Bayer, P. (2024). High-resolution monitoring and simulation of the temperatures in a borehole heat exchanger field over multiple years. *IGSHPA Research Congress*, <https://doi.org/10.22488/okstate.24.000019>.
- Gehlin, S. (2002), Thermal response test: method development and evaluation, Ph.D. thesis, Luleå tekniska universitet.
- Gheysari, A. F., Holländer, H. M., Maghoul, P., and Shalaby, A. (2021). Sustainability, climate resiliency, and mitigation capacity of geothermal heat pump systems in cold regions. *Geothermics*, *91*, 101979. <https://doi.org/10.1016/j.geothermics.2020.101979>.
- Gil, A. and Moreno, M. (2020). Current legal framework on shallow geothermal energy use in Spain. *J. Sustain. Res.*, *2*, 1–14. <https://doi.org/10.20900/jsr20200005>.
- Gil, A., Schneider, E., Moreno, M., and Cerezal, J. (2020). *Shallow Geothermal Energy: Theory and Application*. Springer Hydrogeology, <https://doi.org/10.1007/978-3-030-92258-0>.
- Gilks, W. R., Richardson, S., and Spiegelhalter, D. (1995). *Markov chain Monte Carlo in practice*. CRC press.
- Goodman, J. and Weare, J. (2010). Ensemble samplers with affine invariance. *Communications in applied mathematics and computational science*, *5*(1), 65–80. <https://doi.org/10.2140/camcos.2010.5.65>.
- Grinsted, A. (2018). *Affine Invariant Ensemble Markov Chain Monte Carlo Sampler*. <https://github.com/grinsted/gwmcmc>, accessed: 2025-01-03.
- Gultekin, A., Aydin, M., and Sisman, A. (2016). Thermal performance analysis of multiple borehole heat exchangers. *Energy Convers. Manag.*, *122*, 544–551. <https://doi.org/10.1016/j.enconman.2016.05.086>.
- Guo, Y., Huang, G., and Liu, W. (2023). A new semi-analytical solution addressing varying heat transfer rates for u-shaped vertical borehole heat exchangers in multilayered ground. *Energy*, *274*, 127373. <https://doi.org/10.1016/j.energy.2023.127373>.

- Guo, Y., Zhao, J., and Liu, W. (2024). A novel solution for vertical borehole heat exchangers in multilayered ground with the robin boundary condition. *Applied Thermal Engineering*, 255, 123 923. <https://doi.org/10.1016/j.applthermaleng.2024.123923>.
- Haehnlein, S., Bayer, P., and Blum, P. (2010). International legal status of the use of shallow geothermal energy. *Renew. Sustain. Energy Rev.*, 14, 2611–2625. <https://doi.org/10.1016/j.rser.2010.07.069>.
- Harris, B., Lightstone, M., Reitsma, S., and Cotton, J. (2024). A numerical study on the intermittent operation of u-tube and coaxial borehole heat exchangers. *Geothermics*, 121, 103 030. <https://doi.org/10.1016/j.geothermics.2024.103030>.
- He, Z., Zhou, N., Guo, C., and Liu, J. (2024). Study on configurational operation strategy of ground heat exchangers under the effect of groundwater flow. *Therm. Sci. Eng. Prog.*, 47, 102 302. <https://doi.org/10.1016/j.tsep.2023.102302>.
- Hecht-Méndez, J., De Paly, M., Beck, M., and Bayer, P. (2013). Optimization of energy extraction for vertical closed-loop geothermal systems considering groundwater flow. *Energy Convers. Manag.*, 66, 1–10. <https://doi.org/10.1016/j.enconman.2012.09.019>.
- Heim, E., Laska, M., Becker, R., and Klitzsch, N. (2022). Estimating the subsurface thermal conductivity and its uncertainty for shallow geothermal energy use—a workflow and geoportal based on publicly available data. *Energies*, 15, 3687. <https://doi.org/10.3390/en15103687>.
- Heim, E., Stoffel, P., Düber, S., Knapp, D., Kümpel, A., Müller, D., and Klitzsch, N. (2024a). Comparison of simulation tools for optimizing borehole heat exchanger field operation. *Geothermal Energy*, 24, 12–24. <https://doi.org/10.1186/s40517-024-00303-8>.
- Heim, E., Stoffel, P., Müller, D., and Klitzsch, N. (2024b). Six years of high-resolution monitoring data of 40 borehole heat exchangers. *Scientific Data*, 11(1), 1334. <https://doi.org/10.1038/s41597-024-04241-9>.
- Hein, P., Kolditz, O., Görke, U., Bucher, A., and Shao, H. (2016). A numerical study on the sustainability and efficiency of borehole heat exchanger coupled ground source heat pump systems. *Appl. Therm. Eng.*, 100, 421–433. <https://doi.org/10.1016/j.applthermaleng.2016.02.039>.
- Hemmerle, H., Ferguson, G., Blum, P., and Bayer, P. (2022). The evolution of the geothermal potential of a subsurface urban heat island. *Environmental Research Letters*, 17(8), 084 018. <https://doi.org/10.1088/1748-9326/ac7e60>.
- Hermans, T., Nguyen, F., Robert, T., and Revil, A. (2014). Geophysical methods for monitoring temperature changes in shallow low enthalpy geothermal systems. *Energies*, 7(7), 5083–5118. <https://doi.org/10.3390/en7085083>.

- Hermans, T., Nguyen, F., Klepikova, M., Dassargues, A., and Caers, J. (2018). Uncertainty quantification of medium-term heat storage from short-term geophysical experiments using bayesian evidential learning. *Water Resources Research*, 54(4), 2931–2948. <https://doi.org/10.1002/2017WR022135>.
- Huang, S., Li, J., Gao, H., Dong, J., and Jiang, Y. (2024). Thermal performance of medium-deep u-type borehole heat exchanger based on a novel numerical model considering ground-water seepage. *Renewable Energy*, 222, 119 988. <https://doi.org/10.1016/j.renene.2024.119988>.
- Häfner, F., Wagner, R., and Meusel, L. (2015). *Bau und Berechnung von Erdwärmeanlagen: Einführung mit praktischen Beispielen*. Springer-Verlag.
- Hähnlein, S., Bayer, P., Ferguson, G., and Blum, P. (2013). Sustainability and policy for the thermal use of shallow geothermal energy. *Energy Policy*, 59, 914–925. <https://doi.org/10.1016/j.enpol.2013.04.040>.
- Ikeda, S., Choi, W., and Ooka, R. (2017). Optimization method for multiple heat source operation including ground source heat pump considering dynamic variation in ground temperature. *Appl. Energy*, 193, 466–478. <https://doi.org/10.1016/j.apenergy.2017.02.047>.
- Ishitsuka, K. and Lin, W. (2023). Physics-informed neural network for inverse modeling of natural-state geothermal systems. *Applied Energy*, 337, 120 855. <https://doi.org/10.1016/j.apenergy.2023.120855>.
- Jahangir, M. H., Sarrafha, H., and Kasaeian, A. (2018). Numerical modeling of energy transfer in underground borehole heat exchanger within unsaturated soil. *Applied Thermal Engineering*, 132, 697–707. <https://doi.org/10.1016/j.applthermaleng.2018.01.020>.
- Javadi, H., Mousavi Ajarostaghi, S., Rosen, M., and Pourfallah, M. (2019). Performance of ground heat exchangers: a comprehensive review of recent advances. *Energy*, 178, 207–233. <https://doi.org/10.1016/j.energy.2019.04.094>.
- Karniadakis, G. E., Kevrekidis, I. G., Lu, L., Perdikaris, P., Wang, S., and Yang, L. (2021). Physics-informed machine learning. *Nature Reviews Physics*, 3(6), 422–440. <https://doi.org/10.1038/s42254-021-00314-5>.
- Kirschstein, X., Ohagen, M., Reber, J., Vardon, P. J., and Bishara, N. (2024). Regeneration of shallow borehole heat exchanger fields: a literature review. *Energy and Buildings*, p. 114381. <https://doi.org/10.1016/j.enbuild.2024.114381>.
- Koenigsdorff, R. and van Treeck, C. (2006). Einfluss variabler und unsicherer parameter auf den betrieb und die dimensionierung von erdwärmesondenanlagen. *BauSIM*.
- Kümpel, A., Stoffel, P., and Müller, D. (2022). Development of a long-term operational optimization model for a building energy system supplied by a geothermal field. *J. Therm. Sci.*, 31, 1293–1301. <https://doi.org/10.1007/s11630-022-1616-7>.

- Lamarche, L. (2011). Analytical g-function for inclined boreholes in ground-source heat pump systems. *Geothermics*, 40, 241–249. <https://doi.org/10.1016/j.geothermics.2011.07.006>.
- Lazzarotto, A. (2016). A methodology for the calculation of response functions for geothermal fields with arbitrarily oriented boreholes - part 1. *Renew. Energy*, 86, 1380–1393. <https://doi.org/10.1016/j.renene.2015.09.056>.
- Lazzarotto, A. and Björk, F. (2016). A methodology for the calculation of response functions for geothermal fields with arbitrarily oriented boreholes - part 2. *Renew. Energy*, 86, 1353–1361. <https://doi.org/10.1016/j.renene.2015.09.057>.
- Lee, C. (2011). Effects of multiple ground layers on thermal response test analysis and ground-source heat pump simulation. *Appl. Energy*, 88, 4405–4410. <https://doi.org/10.1016/j.apenergy.2011.05.023>.
- Lembcke, L., Roubinet, D., Gidel, F., Irving, J., Pehme, P., and Parker, B. (2016). Analytical analysis of borehole experiments for the estimation of subsurface thermal properties. *Advances in Water Resources*, 91, 88–103. <https://doi.org/10.1016/j.advwatres.2016.02.011>.
- Li, M. and Lai, A. (2015). Review of analytical models for heat transfer by vertical ground heat exchangers (ghes): A perspective of time and space scales. *Applied Energy*, 151, 178–191. <https://doi.org/10.1016/j.apenergy.2015.04.070>.
- Li, P., Guo, F., Li, Y., Yang, X., and Yang, X. (2024). Physics-informed neural network for real-time thermal modeling of large-scale borehole thermal energy storage systems. *Energy*, p. 134344. <https://doi.org/10.1016/j.energy.2024.134344>.
- Li, W., Li, X., Peng, Y., Wang, Y., and Tu, J. (2020). Experimental and numerical studies on the thermal performance of ground heat exchangers in a layered subsurface with groundwater. *Renew. Energy*, 147, 620–629. <https://doi.org/10.1016/j.renene.2019.09.008>.
- Liang, F., Liu, C., and Carroll, R. (2011). *Advanced Markov chain Monte Carlo methods: learning from past samples*. John Wiley & Sons.
- Liu, W., Chen, G., Yan, B., Zhou, Z., Du, H., and Zuo, J. (2015). Hourly operation strategy of a cchp system with gshp and thermal energy storage (tes) under variable loads: a case study. *Energy Build*, 93, 143–153. <https://doi.org/10.1016/j.enbuild.2015.02.030>.
- Lund, J. and Boyd, T. (2016). Direct utilization of geothermal energy 2015 worldwide review. *Geothermics*, 60, 66–93. <https://doi.org/10.1016/j.geothermics.2015.11.004>.
- Lund, J. and Toth, A. (2021). Direct utilization of geothermal energy 2020 worldwide review. *Geothermics*, 90, 101915. <https://doi.org/10.1016/j.geothermics.2020.101915>.
- Luo, J., Rohn, J., Bayer, M., Priess, A., and Xiang, W. (2014). Analysis on performance of borehole heat exchanger in a layered subsurface. *Appl. Energy*, 123, 55–65. <https://doi.org/10.1016/j.apenergy.2014.02.044>.

- Luo, J., Tuo, J., Huang, W., Zhu, Y., Jiao, Y., Xiang, W., and Rohn, J. (2018). Influence of groundwater levels on effective thermal conductivity of the ground and heat transfer rate of borehole heat exchangers. *Appl. Therm. Eng.*, *128*, 508–516. <https://doi.org/10.1016/j.applthermaleng.2017.08.148>.
- Ma, J., Jiang, Q., Zhang, Q., Xie, Y., Wang, Y., and Yi, F. (2021). Effect of groundwater forced seepage on heat transfer characteristics of borehole heat exchangers. *Geoth. Energy*, *9*, 1–23. <https://doi.org/10.1186/s40517-021-00192-1>.
- Ma, Z., Xia, L., Gong, X., Kokogiannakis, G., Wang, S., and Zhou, X. (2020). Recent advances and development in optimal design and control of ground source heat pump systems. *Renew. Sustain. Energy Rev.*, *131*. <https://doi.org/10.1016/j.rser.2020.110001>.
- Marcotte, D. and Pasquier, P. (2008). Fast fluid and ground temperature computation for geothermal ground-loop heat exchanger systems. *Geothermics*, *37*, 651–665. <https://doi.org/10.1016/j.geothermics.2008.08.003>.
- Marcotte, D., Pasquier, P., Sheriff, F., and Bernier, M. (2010). The importance of axial effects for borehole design of geothermal heat-pump systems. *Renew. Energy*, *35*, 763–770. <https://doi.org/10.1016/j.renene.2009.09.015>.
- Menberg, K., Heo, Y., and Choudhary, R. (2019). Influence of error terms in bayesian calibration of energy system models. *Journal of Building Performance Simulation*, *12*(1), 82–96. <https://doi.org/10.1080/19401493.2018.1475506>.
- Menberg, K., Bidarmaghz, A., Gregory, A., Choudhary, R., and Girolami, M. (2020). Multi-fidelity approach to bayesian parameter estimation in subsurface heat and fluid transport models. *Science of the Total Environment*, *745*, 140846. <https://doi.org/10.1016/j.scitotenv.2020.140846>.
- Michopoulos, A. and Kyriakis, N. (2009). A new energy analysis tool for ground source heat pump systems. *Energy Build*, *41*, 937–941. <https://doi.org/10.1016/j.enbuild.2009.03.017>.
- Molina-Giraldo, N., Blum, P., Zhu, K., Bayer, P., and Fang, Z. (2011). A moving finite line source model to simulate borehole heat exchangers with groundwater advection. *Int. J. Therm. Sci.*, *50*, 2506–2513. <https://doi.org/10.1016/j.ijthermalsci.2011.06.012>.
- Moreira, D., Macias, J., Hidalgo-Leon, R., Jarvis, F., and Soriano, G. (2022). Performance of a borehole heat exchanger: the influence of thermal properties estimation under tidal fluctuation. *Eng. Sci. Technol. an Int. J.*, *30*, 101057. <https://doi.org/10.1016/j.jestch.2021.09.003>.
- Nguyen, A., Pasquier, P., and Marcotte, D. (2017). Borehole thermal energy storage systems under the influence of groundwater flow and time-varying surface temperature. *Geothermics*, *66*, 110–118. <https://doi.org/10.1016/j.geothermics.2016.11.002>.

- Noel, A. and Cimmino, M. (2022). Development of a topology optimization method for the design of ground heat exchangers. *IGSHPA Research Track*, <https://doi.org/10.22488/okstate.22.000017>.
- Noethen, M., Hemmerle, H., and Bayer, P. (2023a). Sources, intensities, and implications of subsurface warming in times of climate change. *Crit. Rev. Environ. Sci. Technol.*, *53*, 700–722. <https://doi.org/10.1080/10643389.2022.2083899>.
- Noethen, M., Hemmerle, H., Menberg, K., Epting, J., Benz, S., Blum, P., and Bayer, P. (2023b). Thermal impact of underground car parks on urban groundwater. *Sci. Total Environ.*, *903*, 166 572. <https://doi.org/10.1016/j.scitotenv.2023.166572>.
- Noye, S., Martinez, R. M., Carnieletto, L., De Carli, M., and Aguirre, A. C. (2022). A review of advanced ground source heat pump control: Artificial intelligence for autonomous and adaptive control. *Renewable and Sustainable Energy Reviews*, *153*, 111 685. <https://doi.org/10.1016/j.rser.2021.111685>.
- Olabi, A. G., Mahmoud, M., Soudan, B., Wilberforce, T., and Ramadan, M. (2020). Geothermal based hybrid energy systems, toward eco-friendly energy approaches. *Renewable energy*, *147*, 2003–2012. <https://doi.org/10.1016/j.renene.2019.09.140>.
- Pasquier, P. and Lamarche, L. (2022). Analytic expressions for the moving infinite line source model. *Geothermics*, *103*, 102 413. <https://doi.org/10.1016/j.geothermics.2022.102413>.
- Pasquier, P. and Marcotte, D. (2020). Robust identification of volumetric heat capacity and analysis of thermal response tests by bayesian inference with correlated residuals. *Applied Energy*, *261*, 114 394. <https://doi.org/10.1016/j.apenergy.2019.114394>.
- Pasquier, P., Zarrella, A., and Marcotte, D. (2019). A multi-objective optimization strategy to reduce correlation and uncertainty for thermal response test analysis. *Geothermics*, *79*, 176–187. <https://doi.org/10.1016/j.geothermics.2019.02.003>.
- Perego, R., Dalla Santa, G., Galgaro, A., and Pera, S. (2022). Intensive thermal exploitation from closed and open shallow geothermal systems at urban scale: unmanaged conflicts and potential synergies. *Geothermics*, *103*, 102 417. <https://doi.org/10.1016/j.geothermics.2022.102417>.
- Previati, A. and Crosta, G. (2024). On groundwater flow and shallow geothermal potential: a surrogate model for regional scale analyses. *Sci. Total Environ.*, *912*, 169 046. <https://doi.org/10.1016/j.scitotenv.2023.169046>.
- Puttige, A. R., Andersson, S., Östin, R., and Olofsson, T. (2020). Improvement of borehole heat exchanger model performance by calibration using measured data. *Journal of Building Performance Simulation*, *13*(4), 430–442. <https://doi.org/10.1080/19401493.2020.1761451>.

- Raymond, J. and Lamarche, L. (2013). Simulation of thermal response tests in a layered subsurface. *Appl. Energy*, *109*, 293–301. <https://doi.org/10.1016/j.apenergy.2013.01.033>.
- Rees, S. (2016). *Advances in ground-source heat pump systems*. Woodhead Publishing.
- Rivera, J., Blum, P., and Bayer, P. (2017). Increased ground temperatures in urban areas: Estimation of the technical geothermal potential. *Renewable Energy*, *103*, 388–400. <https://doi.org/10.1016/j.renene.2016.11.005>.
- Rivera, J. A., Blum, P., and Bayer, P. (2015). Analytical simulation of groundwater flow and land surface effects on thermal plumes of borehole heat exchangers. *Applied energy*, *146*, 421–433. <https://doi.org/10.1016/j.apenergy.2015.02.035>.
- Robert, S., Pasquier, P., and Nguyen, A. (2022). Impact of layered heterogeneity on thermal response test interpretation performed on a standing column well operated without bleed. *Geothermics*, *101*, 102 353. <https://doi.org/10.1016/j.geothermics.2022.102353>.
- Roy, V. (2020). Convergence diagnostics for markov chain monte carlo. *Annual Review of Statistics and Its Application*, *7*(1), 387–412. <https://doi.org/10.1146/annurev-statistics-031219-041300>.
- Scheidt, C., Li, L., and Caers, J. (2018). *Quantifying uncertainty in subsurface systems*. vol. 236, John Wiley & Sons.
- Shah, M., Prajapati, M., Yadav, K., and Sircar, A. (2024). A comprehensive review of geothermal energy storage: Methods and applications. *Journal of Energy Storage*, *98*, 113 019. <https://doi.org/10.1016/j.est.2024.113019>.
- Shin, E., Kim, Y., Kim, Y.-S., Lee, S., and Choi, W. (2024). Dynamic management of ground thermal response uncertainty through temporal analysis of parameter sensitivity. *Applied Energy*, *376*, 124 267. <https://doi.org/10.1016/j.apenergy.2024.124267>.
- Shoji, Y., Katsura, T., and Nagano, K. (2023). Improvement of accuracy with uncertainty quantification in the simulation of a ground heat exchanger by combining model prediction and observation. *Geothermics*, *107*, 102 611. <https://doi.org/10.1016/j.geothermics.2022.102611>.
- Signorelli, S., Bassetti, S., Pahud, D., and Kohl, T. (2007). Numerical evaluation of thermal response tests. *Geothermics*, *36*, 141–166. <https://doi.org/10.1016/j.geothermics.2006.10.006>.
- Soltan Mohammadi, H., Ringel, L., and Bayer, P. (2023). Sequential simulation-optimization of a borehole heat exchanger field considering variability in heating demand and subsurface thermal responses. *Copernicus Meetings EGU23-3243*. <https://doi.org/10.5194/egusphere-egu23-3243>.

- Soltan Mohammadi, H., Ringel, L., de Paly, M., and Bayer, P. (2024a). Sequential long-term optimization of shallow geothermal systems under descriptive uncertainty and dynamic variation of heating demand. *Geothermics*, *121*, 103 021. <https://doi.org/10.1016/j.geothermics.2024.103021>.
- Soltan Mohammadi, H., Ringel, L. M., Bott, C., and Bayer, P. (2024b). Adaptive management of borehole heat exchanger fields under transient groundwater flow conditions. *Renewable Energy*, *234*, 121 060. <https://doi.org/10.1016/j.renene.2024.121060>.
- Soltan Mohammadi, H., Ringel, L. M., Bott, C., Erol, S., and Bayer, P. (2025). Bayesian uncertainty quantification in temperature simulation of borehole heat exchanger fields for geothermal energy supply. *Applied Thermal Engineering*, *265*, 125 210. <https://doi.org/10.1016/j.applthermaleng.2024.125210>.
- Soltani, M., Kashkooli, F. M., Souri, M., Rafiei, B., Jabarifar, M., Gharali, K., and Nathwani, J. S. (2021). Environmental, economic, and social impacts of geothermal energy systems. *Renewable and Sustainable Energy Reviews*, *140*, 110 750. <https://doi.org/10.1016/j.rser.2021.110750>.
- Song, W., Liu, X., Zheng, T., and Yang, J. (2020). A review of recharge and clogging in sandstone aquifer. *Geothermics*, *87*, 101 857. <https://doi.org/10.1016/j.geothermics.2020.101857>.
- Spitler, J. and Gehlin, S. (2015). Thermal response testing for ground source heat pump systems - an historical review. *Renew. Sustain. Energy Rev.*, *50*, 1125–1137. <https://doi.org/10.1016/j.rser.2015.05.061>.
- Spitler, J., Cook, J., and Liu, X. (2020). A preliminary investigation on the cost reduction potential of optimizing bore fields for commercial ground source heat pump systems. *45th Workshop on Geothermal Reservoir Engineering*.
- Spitler, J., West, T., and Liu, X. (2022). Ground heat exchanger design tool with rowwise placement of boreholes. *IGSHPA Research Track*, <https://doi.org/10.22488/okstate.22.000016>.
- Stauffer, F., Bayer, P., Blum, P., Giraldo, N., and Kinzelbach, W. (2013). *Thermal Use of Shallow Groundwater*. CRC Press.
- Stoffel, P., Kümpel, A., and Müller, D. (2022). Cloud-based optimal control of individual borehole heat exchangers in a geothermal field. *J. Therm. Sci.*, *31*, 1253–1265. <https://doi.org/10.1007/s11630-022-1639-0>.
- Stoffel, P., Maier, L., Kümpel, A., Schreiber, T., and Müller, D. (2023). Evaluation of advanced control strategies for building energy systems. *Energy Build.*, *280*, 112 709. <https://doi.org/10.1016/j.enbuild.2022.112709>.

- Thibaut, R., Compaire, N., Lesparre, N., Ramgraber, M., Laloy, E., and Hermans, T. (2022). Comparing well and geophysical data for temperature monitoring within a bayesian experimental design framework. *Water Resources Research*, *58*(11), e2022WR033045. <https://doi.org/10.1029/2022WR033045>.
- Tsagarakis, K., Efthymiou, L., Michopoulos, A., Mavragani, A., Anđelković, A., Antolini, F., Bacic, M., Bajare, D., Baralis, M., Bogusz, W., Burlon, S., Figueira, J., Genç, M., Javed, S., Jurelionis, A., Koca, K., Ryzynski, G., Urchueguia, J., and Zlender, B. (2020). A review of the legal framework in shallow geothermal energy in selected european countries: need for guidelines. *Renew. Energy*, *147*, 2556–2571. <https://doi.org/10.1016/j.renene.2018.10.007>.
- VDI (2001). *Thermal Use of the Underground. Part 2: Geothermal Heat Pump Systems: VDI 4640*. P. 43.
- Verhelst, C. and Helsen, L. (2011). Low-order state space models for borehole heat exchangers. *HVAC&R Research*, *17*(6), 928–947. <https://doi.org/10.1080/10789669.2011.617188>.
- Violante, A. C., Donato, F., Guidi, G., and Proposito, M. (2022). Comparative life cycle assessment of the ground source heat pump vs air source heat pump. *Renewable Energy*, *188*, 1029–1037. <https://doi.org/10.1016/j.renene.2022.02.075>.
- Wagner, V., Bayer, P., Kübert, M., and Blum, P. (2012). Numerical sensitivity study of thermal response tests. *Renew. Energy*, *41*, 245–253. <https://doi.org/10.1016/j.renene.2011.11.001>.
- Wagner, V., Bayer, P., Bisch, G., Kübert, M., and Blum, P. (2014). Hydraulic characterization of aquifers by thermal response testing: validation by large-scale tank and field experiments. *Water Resources Research*, *50*(1), 71–85. <https://doi.org/10.1002/2013WR013939>.
- Walch, A., Li, X., Chambers, J., Mohajeri, N., Yilmaz, S., Patel, M., and Scartezzini, J.-L. (2022). Shallow geothermal energy potential for heating and cooling of buildings with regeneration under climate change scenarios. *Energy*, *244*, 123086. <https://doi.org/10.1016/j.energy.2021.123086>.
- Yavuzturk, C. and Spitler, J. (2000). Comparative study of operating and control strategies for hybrid ground-source heat pump systems using a short time step simulation model. *Ashrae Trans.*, *106*, 192.
- Yoshioka, M., Shrestha, G., Widiatmojo, A., and Uchida, Y. (2022). Seasonal changes in thermal process based on thermal response test of borehole heat exchanger. *Geothermics*, *102*, 102390. <https://doi.org/10.1016/j.geothermics.2022.102390>.
- Yu, X., Li, H., Yao, S., Nielsen, V., and Heller, A. (2020). Development of an efficient numerical model and analysis of heat transfer performance for borehole heat exchanger. *Renewable Energy*, *152*, 189–197. <https://doi.org/10.1016/j.renene.2020.01.044>.

- Zanchini, E., Lazzari, S., and Priarone, A. (2012). Long-term performance of large borehole heat exchanger fields with unbalanced seasonal loads and groundwater flow. *Energy*, *38*, 66–77. <https://doi.org/10.1016/j.energy.2011.12.038>.
- Zeng, H., Diao, N., and Fang, Z. (2002). A finite line-source model for boreholes in geothermal heat exchangers. *Heat Transf. - Asian Res.*, *31*, 558–567. <https://doi.org/10.1002/htj.10057>.
- Zhang, B., Gu, K., Bayer, P., Qi, H., Shi, B., Wang, B., Jiang, Y., and Zhou, Q. (2023a). Estimation of groundwater flow rate by an actively heated fiber optics based thermal response test in a grouted borehole. *Water Resour. Res.*, *59*, e2022WR032672. <https://doi.org/10.1029/2022WR032672>.
- Zhang, B., Gu, K., Bayer, P., Xiang, F., Wei, Z., Wang, B., and Shi, B. (2023b). Estimation of vertical water flow in slopes from high-resolution temperature profiles. *Bulletin of Engineering Geology and the Environment*, *82*(1), 20. <https://doi.org/10.1007/s10064-022-03045-8>.
- Zhang, C., Lu, J., Wang, X., Xu, H., and Sun, S. (2022). Effect of geological stratification on estimated accuracy of ground thermal parameters in thermal response test. *Renew. Energy*, *186*, 585–595. <https://doi.org/10.1016/j.renene.2022.01.024>.
- Zhang, H., Han, Z., Ji, M., Li, G., Cheng, X., Yang, Z., and Yang, L. (2021). Analysis of influence of pipe group arrangement and heat exchanger type on operation performance of the ground source heat pump. *Geothermics*, *97*, 102–113. <https://doi.org/10.1016/j.geothermics.2021.102237>.
- Zhao, P., Li, X., Zhang, D., Lin, Y., Zhang, Y., and Ji, Y. (2023). Numerical investigation of vertical borehole heat exchanger heat transfer under coupled conditions of groundwater seepage and layered subsurface. *Geomechanics and Geophysics for Geo-Energy and Geo-Resources*, *9*(1), 33. <https://doi.org/10.1007/s40948-023-00571-x>.
- Zhao, Z., Lin, Y., Stumpf, A., and Wang, X. (2022). Assessing impacts of groundwater on geothermal heat exchangers: a review of methodology and modeling. *Renew. Energy*, *190*, 121–147. <https://doi.org/10.1016/j.renene.2022.03.089>.
- Zhou, Z., Wu, S., Du, T., Chen, G., Zhang, Z., Zuo, J., and He, Q. (2016). The energy-saving effects of ground-coupled heat pump system integrated with borehole free cooling: a study in china. *Appl. Energy*, *182*, 9–19. <https://doi.org/10.1016/j.apenergy.2016.07.124>.

Curriculum vitae

Personal information

- First name: Hesam
- Last name: Soltan Mohammadi
- Date of birth: [REDACTED]
- Place of birth: [REDACTED]

Professional experience

- 06/2020 – current: **Research Assistant**, Department of Applied Geology, Institute of Geosciences and Geography, MLU Halle-Wittenberg, Halle (Saale), Germany

Education

- 06/2020 – current: **Ph.D. Candidate**, Martin Luther University Halle-Wittenberg, Halle (Saale), Germany
- 09/2016 – 06/2019: **M.Sc. Mining Engineering, Mine and Environment**, University of Tehran, Tehran, Iran
Thesis: Improvement of multiple-point statistics (MPS) simulation algorithms for reconstruction of missing data in images and problems of environmental hydrogeology
- 09/2012 – 09/2016: **B.Sc. Mining Engineering**, University of Tehran, Tehran, Iran

List of publications

Peer-reviewed journal publications

Soltan Mohammadi, H., Ringel, L. M., Bott, C., Erol, S., and Bayer, P. (2025). Bayesian uncertainty quantification in temperature simulation of borehole heat exchanger fields for geothermal energy supply. *Applied Thermal Engineering* (265), 125210. <https://doi.org/10.1016/j.applthermaleng.2024.125210>.

Soltan Mohammadi, H., Ringel, L.M., Bott, C., and Bayer, P. (2024). Adaptive management of borehole heat exchanger fields under transient groundwater flow conditions. *Renewable Energy* (234), 121060. <https://doi.org/10.1016/j.renene.2024.121060>.

Soltan Mohammadi, H., Ringel, L.M., de Paly, M., and Bayer, P. (2024). Sequential long-term optimization of shallow geothermal systems under descriptive uncertainty and dynamic variation of heating demand. *Geothermics* (121), 103021. <https://doi.org/10.1016/j.geothermics.2024.103021>.

Soltan Mohammadi, H., Abdollahifard, M.J., and Doulati Ardejani, F. (2020). CHDS: conflict handling in direct sampling for stochastic simulation of spatial variables. *Stochastic Environmental Research and Risk Assessment* (34), 825-847. <https://doi.org/10.1007/s00477-020-01801-4>.

Abdollahifard, M.J., Mariétoz, G., and **Soltan Mohammadi, H.** (2020). Investigating extreme scenarios with multiple-point geostatistics and variance maximization. *Stochastic Environmental Research and Risk Assessment* (34), 67-85. <https://doi.org/10.1007/s00477-019-01759-y>.

International Conference contributions

Soltan Mohammadi, H., Ringel, L. M., Bott, C., and Bayer, P. (2024). Adaptive optimization of borehole heat exchanger fields in response to transient groundwater flow, *IAH - World Groundwater Congress 2024*, Davos, Switzerland, 08–13 September 2024.

Gebhardt, H., **Soltan Mohammadi, H.**, Ebert, A., Bott, C., Visser, A., and Bayer, P. (2024). High-resolution monitoring and simulation of the temperatures in a borehole heat exchanger field over multiple years, *IGSHPA Research Conference*, Montréal, Canada, 28–30 May 2024. <https://doi.org/10.22488/okstate.24.000019>

Soltan Mohammadi, H., Ringel, L. M., Bott, C. and Bayer, P. (2024). Tuning the performance of a borehole heat exchanger array in response to transient hydrogeological conditions, *EGU General Assembly 2024*, Vienna, Austria, 14–19 April 2024. <https://doi.org/10.5194/egusphere-egu24-5378>

Soltan Mohammadi, H., Ringel, L. M. and Bayer, P. (2023). Sequential simulation-optimization of a borehole heat exchanger field considering variability in heating demand and subsurface thermal responses, *EGU General Assembly 2023*, Vienna, Austria, 23–28 April 2023. <https://doi.org/10.5194/egusphere-egu23-3243>

Soltan Mohammadi, H., Mariéthoz, G. and Bayer, P. (2021). Image-based priors for probabilistic inversion of nonstationary hydrogeological fields through conflict-handling direct sampling, *IAH-World Groundwater Congress 2021*, Brussels, Belgium, 06–10 September, 2021.

(Signature)

Declaration

Ich erkläre an Eides statt, dass ich die Arbeit selbstständig und ohne fremde Hilfe verfasst, keine anderen als die von mir angegebenen Quellen und Hilfsmittel benutzt und die den benutzten Werken wörtlich oder inhaltlich entnommenen Stellen als solche kenntlich gemacht habe.

I declare under penalty of perjury that this thesis is my own work entirely and has been written without any help from other people. I used only the sources mentioned and included all the citations correctly both in word and content.

(Datum, Date)

(Unterschrift, Signature)